UNSW

School of Mechanical and Manufacturing Engineering

Analysis of bearing faults under variable speed conditions

Author:

Xavier de Chasteigner du Mée **z3285912**

Bachelor of Engineering (Mechanical)

NOVEMBER 2016

Supervisors:

Associate Professor Zhongxiao Peng
Dr Wade Smith

Statement of Originality

I, Xavier de Chasteigner du Mee, hereby declare that this submission is my own work and to the best of my knowledge it contains no materials previously published or written by another person, or substantial proportions of material which have been accepted for the award of any other degree or diploma at UNSW or any other educational institution, except where due acknowledgement is made in the thesis. Any contribution made to the research by others, with whom I have worked at UNSW or elsewhere, is explicitly acknowledged in the thesis. I also declare that the intellectual content of this thesis is the product of my own work, except to the extent that assistance from others in the project's design and conception or in style, presentation and linguistic expression is acknowledged.

Signed:

Dated:

Acknowledgements

I would like to thank my supervisors Wade Smith and Zhongxiao Peng for their tremendous help throughout the year. I really enjoyed the nature of this thesis and I am thankful I was given the opportunity to work on this topic with your guidance. I have certainly learned a lot.

I would also like to thank Xihao Zhang, Dikang Peng and Chongqing Hu. Without them I would have never been able to operate the experimental rigs, understand the codes and obtain useful data for this thesis. I am truly thankful. Thank you to Bo Peng and Omear Saeed who were always great company in the laboratory.

To Robert Randall, thank you for taking the time out of your schedule to meet with us regularly and continue to enlighten us.

I would like to thank my family and friends for their support during my entire university career. I appreciate everything you have done for me.

Abstract

The widespread use of bearings in rotating machinery make them an important component, for their failure and subsequent machine breakdown can be accompanied by significant costs. A timely diagnosis would prevent catastrophic failure and costs and as such, vibration analysis of bearing faults has been extensively studied thus far. While the majority of research on bearing diagnostics consists of constant speed applications, this thesis explores and analyses the application of constant speed techniques in variable speed conditions. Variable speed conditions pose problems on currently used techniques because a variation in speed means the impulses caused by bearing defects no longer repeat at constant intervals.

Experiments were carried out on two different experimental rigs: a spur gearbox and a planetary gearbox. The spur gearbox featured a defective gear and bearing, and the analysis of both constant and variable speed profiles proved inconclusive in part due to suspected electromagnetic interference. Another important consideration found during these tests was the insignificant load on the bearing to force the rolling elements to interact with the fault. The Fast Kurtogram (FK) and Power Spectral Density (PSD) – two commonly used methods to select the most promising frequency band for analysis - both failed to reveal the bearing fault.

The experiments carried out on the planetary gearbox were successful at constant speed, where a clear indication of the bearing fault was revealed through envelope analysis. The FK was limited in these experiments and the PSD was used instead to locate other resonance peaks for filtering. The variable speed analysis worked well by following the procedure of bandpass filtering, then order tracking followed by discrete/random separation and finally using envelope analysis. The clarity of the fault was reduced in the variable speed analyses however this was attributed to the reduction in load experienced at changing speeds. Though the variable speed analysis procedure worked well, a number of recommendations were given for future improvements, one being the development of an improved band selection method, because the widely-used Fast Kurtogram proved unsuitable for this application.

Table of Contents

List of Figures

List of Tables

Nomenclature

$BPFO$ = ball passing frequency outer race

$BPFI$ = ball passing frequency inner race

FTF = fundamental train frequency

BSF = ball spin frequency

f_r = shaft speed

f_o = planet gear speed

f_i = carrier speed

n = number of rolling elements

ϕ = angle of the load from the radial plane

d = rolling element diameter

D = pitch circle diameter of bearing

Chapter 1: Introduction

1.1 Background and Project Aims

Rolling element bearings are extensively used in rotating machinery and their operation is critical in the machinery's performance. Their failure has been cited to be one of the most common causes of machine breakdown [1]. Harsh operating conditions or manufacturing defects often accelerate bearing failure. A timely diagnosis of an incipient fault can avoid significant costs associated with the machinery's breakdown, particularly in manufacturing or production plants where machine breakdown invariably results in loss of production. It is advantageous to thus determine techniques that will provide a robust diagnosis ahead of time to enable replacing the bearing before catastrophic failure. The widespread research in bearing diagnostics has primarily focused on the vibration analysis for constant speed applications. The vibration analysis involves firstly diagnosing faults, then observing their development in vibration signals acquired from the operating machinery. However much of the machinery in industry operates under variable speed conditions with multiple components, such as gears, which complicates the vibration signals used for processing as they too may be defective. This has the potential to make a diagnosis more difficult.

The aim of this thesis is to expand the use of currently available techniques developed for rolling element bearings under variable speed applications to establish reliable techniques that can be used for these conditions. This will assist and contribute to the current research undertaken for bearing diagnostics under variable speed conditions by assessing the suitability of the techniques and their limitations for this application.

1.2 Thesis Layout

This section presents the layout of the thesis, including a brief description of each chapter:

Chapter 1: Introduction presents a background of the project and its aims with a layout of the thesis.

Chapter 2: Literature Review presents a review of literature relevant to rolling element bearing fault diagnosis using vibration analysis and current challenges associated with bearings in variable speed applications.

Chapter 3: Methodology details the experiments carried out for the project and includes a description of the rig and setup with the data acquisition equipment. A post-processing plan is included.

Chapter 4: Results and Discussions details the findings of the experiments carried out and a comparison of various applicable techniques.

Chapter 5: Conclusion concludes the thesis and the findings obtained from the experiments.

Chapter 6: Future Work uses the conclusion and findings to determine the next course of action in experimentation and analysis.

Chapter 2: Literature Review

This chapter provides the important knowledge and concepts used throughout this thesis. Components of bearings are introduced and common bearing faults are discussed. Established diagnostic methods are introduced and where they fall short for variable speed conditions. Significant papers are reviewed and analysed to determine previous findings and the current gaps in knowledge with respect to bearing diagnostics under variable speed conditions.

2.1 Rolling Element Bearings

Rolling element bearings are widely used in rotating machinery. Their failure is one of the most common reasons of machine breakdown [1]. As a result, their reliability is vital to a machine's operation. The term rolling element bearing is used to describe the class of bearing that transfer the main loads through rolling contact as opposed to sliding contact [2]. Many types and configurations of bearings exist, the most common being the deep groove ball bearing. These bearings are capable of taking radial loading as well as some thrust loading [2]. Figure 1 [3] outlines the 4 main characteristics of a deep-groove ball bearing. It consists of an outer race, inner race, a cage (or retainer) and rolling elements positioned within the cage between the inner and outer races. Some bearings also include a cover to shield the cage and rolling elements.

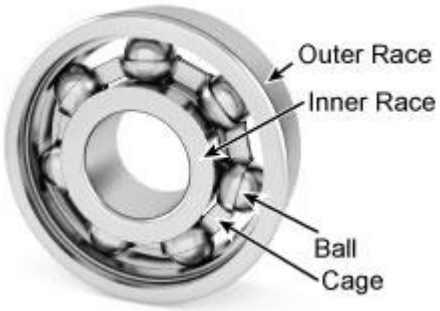

Figure 1: Deep groove ball bearing – common components of bearings [3]

In the majority of cases, this type of bearing has the inner race mounted on a rotating shaft while the outer race is attached to a stationary housing [4]. The balls (rolling elements) transfer loads over a small surface in contrast to rollers that transfer load via a contact line. Under radial loads with the presence of a defect, the balls are forced into the defect and

increase the effect of this impact which makes detection more likely in contrast to having minimal radial loading. The vibration signals generated by defects and faults in bearings have well established diagnostic techniques as they have been widely studied [1]. The next section outlines the common bearing faults and their vibration signals.

2.2 Common Bearing Faults and Their Signals

Despite bearings being manufactured using high precision machining tools [5], they have the potential to develop defects during the manufacturing stage and during their usage life. Bearing faults be classed in two categories: distributed or local. Distributed defects are caused by manufacturing errors and may include improper surface roughness, inadequate rolling element size or a misaligned race or cage [6]. Local defects include spalls on the rolling surfaces, cracks and pits. Spalling of the races or the rolling elements is the primary cause of rolling element bearing failure as fatigue cracks begin below the surface of the metal and propagate towards the surface until a small pit or spall is made [6].

Figure 2 [7] below illustrates the various stages of equipment operating life and the corresponding failure rates. In the run-in (or wear-in) stage, there is a decreasing failure rate with operating life. The failures in this stage can be caused by improper design, any manufacturing defects or a problem in the installation or assembly of the equipment.

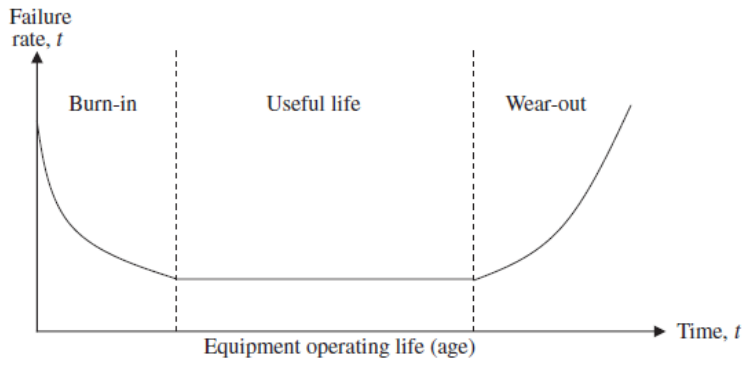

Figure 2: Bathtub curve [7]

The operating conditions and the environment in which bearings can be subject to can also contribute to defect development beyond the wear-in stage, where harsh operating conditions will likely accelerate fault development. Studying the vibration response of these defects,

both distributed and local, are important for quality inspection as well as condition monitoring to be able to determine the defect origin [6].

Bearing signals are considered pseudo-cyclostationary, meaning they are not periodic functions of time, but have the appearance that its statistical characteristics vary periodically with time [1] due to the nature of the impacts caused by the rolling elements. Some fault types may be treated as cyclostationary. Bearing signals are a series of high-frequency bursts as the resonance frequencies are excited by these near-periodic impacts [1]. The faults generally start as small spalls or pits and generate sharp impulses that cover a wide frequency range. There are some faults, however, that do not give rise to these sharp impulses, one of which is brinelling. Brinelling, where either race is indented by the rolling elements, causes a permanent deformation rather than a spall or pits which do not result in the same sharp impacts [1]. In this case the frequency range excited would not be so wide. It is possible for faults to remain undetected as the spalls become smoothed by wear. Figure 3 [1] illustrates the common bearing signals that result from local faults in each component of the bearing and their typical modulation patterns.

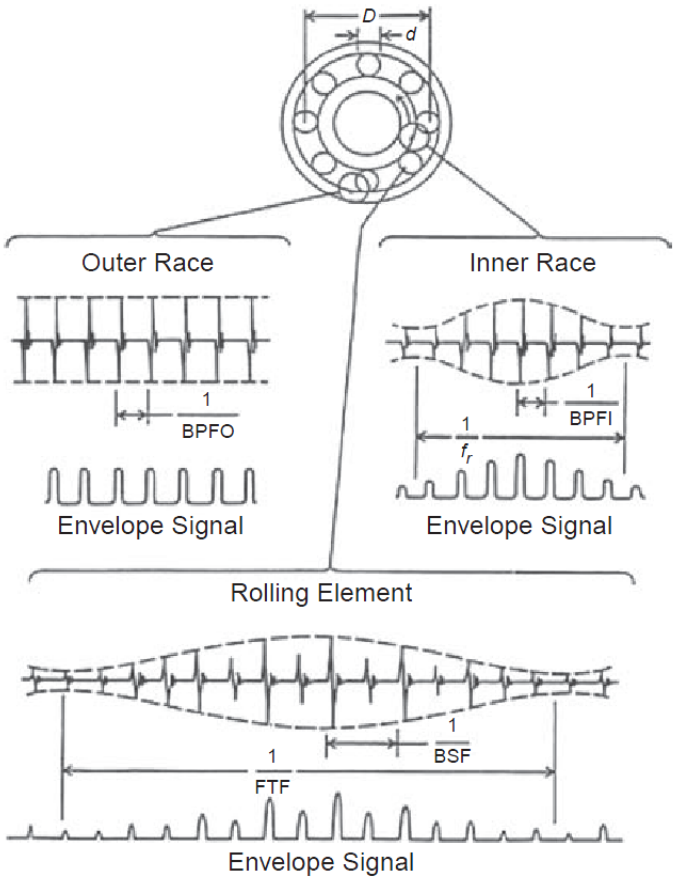

Figure 3: Common bearing fault signals [1]

The next section outlines the various techniques that have been developed and widely studied in the field of bearing diagnostics.

2.3 Bearing Diagnostic Methods

The vibration signals that result from bearing faults have been widely studied and there exist a number of techniques available for bearing fault diagnostics. These techniques range from simple time-domain analysis to kurtogram and its variations. These techniques, however, need not be used independently; in many cases they are used to complement one another [6].

2.3.1 Basic Diagnostic Techniques

2.3.1.1 Root Mean Squared

The simplest time-domain analysis is the root mean square (RMS) value.

$$\text{RMS} = \sqrt{\frac{1}{N}\left[\sum_{i=1}^{N}(x_i - \bar{x})^2\right]} \tag{1}$$

As the name suggests, it is purely the square root of the signal's mean of the squared values. This parameter describes the power content of the vibration signal [8]. RMS has been used as a trending indicator due to its simplicity, however the overall vibration levels often only increases in the later stages of fault development and as a result, the RMS offers a late warning of failure [8].

2.3.1.2 Crest Factor

Crest factor is another simple parameter which is the ratio of the signal's peak value to its RMS.

$$Crest\ factor = \frac{x_{peak}}{RMS} \tag{2}$$

Rather than look at the power content of the signal, it gives an indication to how strong the peaks are in the signal. As the bearing fault develops, the peak of the signal generated increases at faster rate than its RMS from the increase in impulsiveness [8]. The crest factor subsequently increases and provides earlier warning of bearing failure as compared to the RMS of the signal but decreases towards failure.

2.3.1.3 Kurtosis

Kurtosis is the fourth moment normalised by the square of the mean square of the vibration signal waveform [8]:

$$K = \frac{\frac{1}{N}\sum_{i=1}^{N}(x_i - \bar{x})^4}{RMS^4} \tag{3}$$

For an undamaged bearing, the kurtosis value is said to be close to 3 [6]. A value greater than 3 is said to indicate approaching failure, however in the later stages of fault development the kurtosis value decreases to the level of an undamaged bearing. This disadvantage works against using this method for fault detection.

2.3.1.4 Spectrum and Envelope Spectrum Analysis

The time-domain analyses only give an indication of bearing failure but no information about the location of the defect. A vibration signal can be represented in terms of its frequency content rather than its time-domain content. They usually consist of a large number of frequencies that occur at the same time and are not necessarily noticeable from the time-domain signal. By measuring the signal over a wide frequency band, it is possible to reveal the distinct frequency components that make up the signal in this wide frequency band and perform a frequency (or spectral) analysis. This is achieved by using a fast Fourier transform (FFT). The resulting representation of the signal becomes a frequency spectrum plot with the x-axis as the frequency and the y-axis as the amplitude of displacement, velocity or acceleration [9]. The raw signal is dominated by excited resonances; however, the envelope of the signal contains more diagnostic information on repetition frequencies and modulation.

From Figure 3, the various frequencies from local faults in rolling element bearings can be found using the following formulae [1]:

$$BPFO = \frac{nf_r}{2}\left\{1 - \frac{d}{D}cos\phi\right\} \quad (4)$$

$$BPFI = \frac{nf_r}{2}\left\{1 + \frac{d}{D}cos\phi\right\} \quad (5)$$

$$FTF = \frac{f_r}{2}\left\{1 - \frac{d}{D}cos\phi\right\} \quad (6)$$

$$BSF = \frac{f_r D}{2d}\left\{1 - \left(\frac{d}{D}cos\phi\right)^2\right\} \quad (7)$$

These equations assume that there is no slip in the rolling element bearings. In reality, however, there is approximately 1-2% slip [1] which results in a change in the character of the signal. Figure 4 [1] below reveals the effect of this slip on the raw signal, frequency spectrum and envelope spectrum of a bearing with an outer race fault:

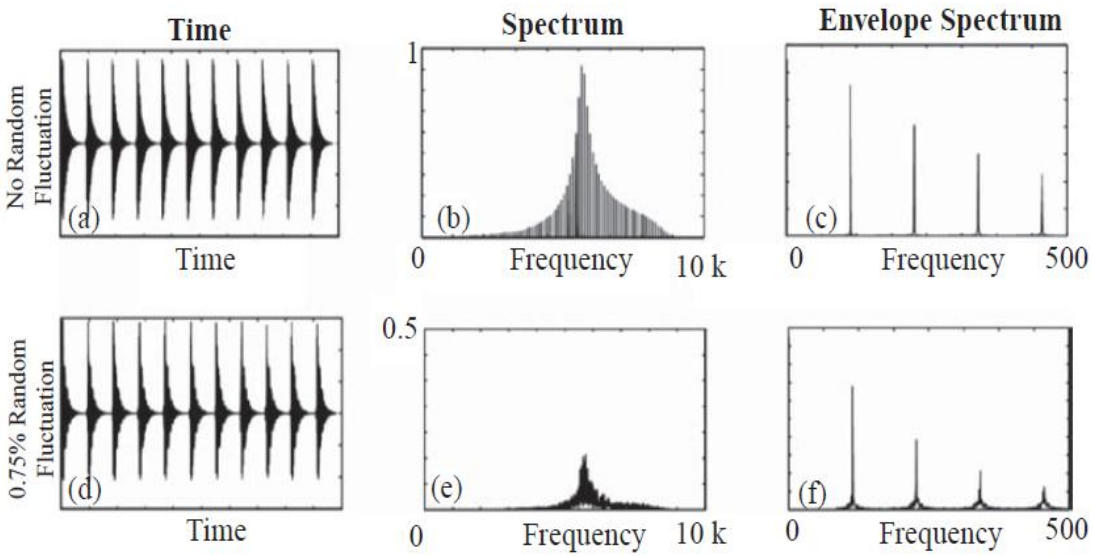

Figure 4: Signals with and without slip: (a, d) time signal; (b, e) raw spectra; (c, f) envelope spectra [1]

As can be seen, the information on periodicity is removed from the raw spectrum with the introduction of a small amount of random variation. However, despite slight smearing in the higher harmonics, periodicity is still evident in the envelope spectrum [1]. For cases of an outer race fault, the envelope spectrum is dominated by harmonics of $BPFO$. For inner race faults, the envelope spectrum would have harmonics of $BPFI$ and for rolling element faults harmonics of BSF. Even harmonics of BSF are often dominant. Should sidebands be present at shaft or cage speed around the harmonics, this would indicate modulation.

Using equations (4) – (7) and analysing the envelope spectrum, it is possible to determine if a fault is present and where it is located within the bearing. This method becomes problematic with noise and other machine components within the raw signal recorded by the transducer [1].

2.3.2 Fault Signal Enhancement

Vibration signals are generally measured externally on machines and are distorted by the transmission path from the source of the vibration to the transducer [1]. This is problematic for impulsive-type signals that result from sharp impacts, e.g. from local spalls in bearings, as successful diagnosis depends on extracting the information from the signal. A number of diagnostic methods rely on the ability to identify these impulsive signals for analysis. This is only possible, however, if the impulse response function (IRF) are shorter than the spacing between other impulse responses. The signal can be masked by noise and other components of the machine being monitored depending on the location of the sensor and therefore require enhancement.

2.3.2.1 Minimum Entropy Deconvolution (MED)

The MED assumes that the original signal source is impulsive and attempts to reduce the spread of IRFs. It works by finding an inverse filter that will counteract the effect of the transmission path by assuming the original excitation is impulsive and has high kurtosis [1].

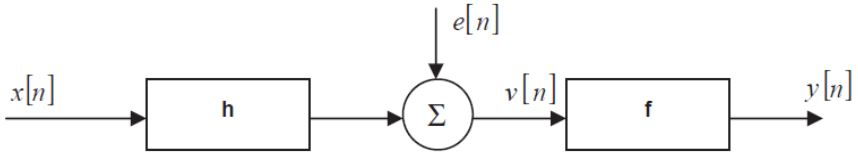

Figure 5: Inverse filtering (deconvolution) process for MED

Figure 5 above illustrates the basic process where a signal $x[n]$ is passed through a filter h whose output is mixed with noise $e[n]$ to give a measured output, $v[n]$. The inverse filter f produces an output $y[n]$ which must be as close as possible to the original signal $x[n]$ [1].

Figure 6 provides an example of this process after discrete frequency components were removed from the time signal using an autoregressive (AR) model of linear prediction and enhanced with MED to reveal a bearing signal with an inner race fault in a high-speed bearing. The kurtosis was improved marginally with AR when compared to the improvement seen with the application of MED. With every shaft rotation, a clear impulse is not detectable for correct diagnosis of the fault and its location. The MED minimises the entropy of the signal through deconvolution to maximise the kurtosis of the signal [10].

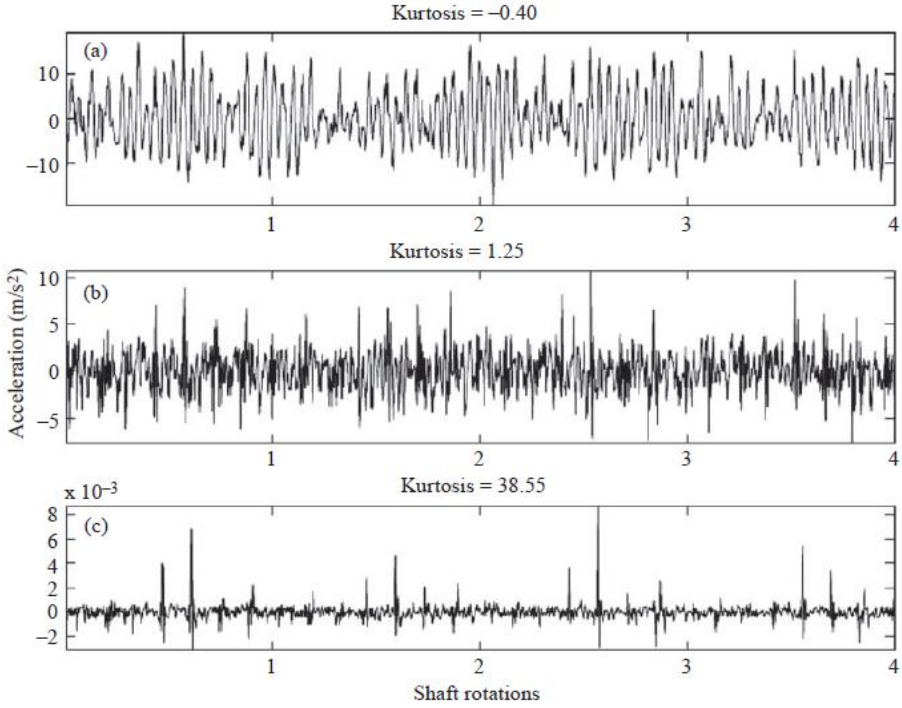

Figure 6: AR and MED filtering of bearing signal with inner race fault: (a) original time signal; (b) after AR filtering; (c) after MED filtering [1]

2.3.2.2 Wavelet Denoising

The primary use of wavelets, which are decomposed signals that have fixed shape but can be shifted and dilated in time [1]. The formula for finding the wavelet transform is a convolution, in which the wavelets can be considered to be a set of impulse responses of filters which have constant percentage bandwidth properties [1]. Wavelets are useful for detecting local events in a signal as they give a better time localisation at high frequencies.

2.3.2.3 Time Synchronous Averaging (TSA)

TSA can be used to remove background noise from a periodic signal, ultimately enhancing the signal. It has been commonly used in particular to extract vibration signals that correspond to a particular gear. Section 2.3.3.2 discusses this technique further as it is used as a separating technique to remove gear signal components to obtain a clear bearing vibration signal.

2.3.3 Discrete-Random Separation Techniques

Gears are commonly used to transmit power between shafts and used in conjunction with bearings. They are a major source of masking the relatively weak bearing signals [11]. The vibration signals generated from gears tend to be deterministic as the same tooth profiles mesh in the same manner every time, however randomness is introduced from speed fluctuations or random loads. Much like bearings, faults in gears can develop due to manufacturing defects or from the operating conditions and environment. With both gears and bearings contributing to vibrations, it becomes more difficult to detect a fault from either component – gear or bearing – however a means of separating the two is possible due to the difference in the nature of the signal. It was said that bearings can be considered cyclostationary while gears tend to be deterministic. When signals are made up of several components that also include changes in machine speed, the signal becomes more difficult to analyse. In machines running at constant speed, signals phase locked to shaft speed are not entirely deterministic unless speed variations are removed [1], and this is achieved by the use of order tracking.

2.3.3.1 Order Tracking

Under variable speed conditions, the separation of the signals cannot be performed before order tracking. The vibration becomes non-stationary and the fixed time sampling cannot cope with the changing rotational frequency and it ultimately results in increased leakage error and smearing in the envelope spectrum [12]. Order tracking works by angular resampling that is performed digitally by software using a tachometer signal to interpolate data [13]. The difference then is that the signal is sampled at constant angular increments as opposed to constant time intervals and the frequency analysis performed is now in terms of

orders, i.e. multiples of the referenced shaft speed, rather than absolute frequencies. This aids in decreasing leakage error and smearing in the envelope spectrum to allow envelope analysis (discussed in Section 2.3.4.4) to be carried out and to be effective to determine the local fault in a bearing. If there is leakage and smearing, envelope analysis is not effective therefore order tracking plays an important role in the diagnosis.

Stander and Heyns [14] noticed in their experiment that while the excitations remained perfectly synchronous to shaft rotation, there was a delay and amplification caused in the response by the transfer function of the mechanical system. Because of the varying speed, they found that the behaviour of the transfer function varied over time because of its excitation at different frequencies at different times. This poses problems to order tracking and significantly affects the quality of the discrete-random separation (DRS) as seen by Borghesani et al [13].

2.3.3.2 Time Synchronous Averaging (TSA)

TSA is a way of separating periodic signals from background noise, as well as everything else that is not periodic with a fundamental frequency [1]. It is commonly used to extract vibration signals corresponding to a gear from a gearbox. Gear signals are deterministic while bearing signals are considered cyclostationary. These characteristics allow this technique to separate the signals from each other. This is accomplished by averaging signal segments that correspond to one period of a synchronising signal [1]:

$$y_a(t) = \frac{1}{N}\sum_{n=0}^{N-1} y(t + nT) \tag{8}$$

The above formula can be modelled as the convolution of $y(t)$ with a train of N delta functions displaced by integer multiples of the periodic time T, which corresponds in the frequency domain to multiplication by Fourier Transform of the signal given by the expression [1]:

$$C(f) = (1/N)\sin(N\pi Tf)/\sin(\pi Tf) \tag{9}$$

For this technique to be effective, Randall [1] suggests synchronising the signals to correspond exactly with the samples of the signal to be averaged. He also recommends to sample the signal using a sampling frequency that has been derived from a tacho signal (i.e. to carry out order tracking).

2.3.3.3 Linear Prediction

Linear prediction obtains a model of deterministic (i.e. 'predictable') part of a vibration signal using a certain number of samples from the immediate past to predict the next value in the series [1]. The residual part of the signal left is then subtracted from the raw signal value. The following equation describes the autoregressive (AR) model used for linear prediction [1]:

$$\hat{x}(n) = -\sum_{k=1}^{p} a(k)x(n-k) \tag{10}$$

where the predicted value is $\hat{x}(n)$ and is obtained from the weighted sum of the previous p values. The $a(k)$ term is the weighting coefficient obtained from linear operation of the autocorrelation function $r_{xx}(n)$ of $x(n)$. The actual value is given by summing the predicted term and a noise term:

$$x(n) = \hat{x}(n) + e(n) \tag{11}$$

Figure 6 (b) reveals the use of AR to remove the toothmesh signal of gears to reveal a bearing signal with an inner race defect.

2.3.3.4 Self-adaptive Noise Cancellation SANC

The SANC adaptive filter can separate gear and bearing vibration signals by using the fact that gear vibrations are more discrete in characteristic as compared to bearing vibrations [15]. This method of separating the signal works off using a reference signal, which is the delayed version of the primary signal, and will cause the bearing component in the reference signal to be decorrelated from those in the primary signal input. Figure 7 below illustrates this concept as a schematic:

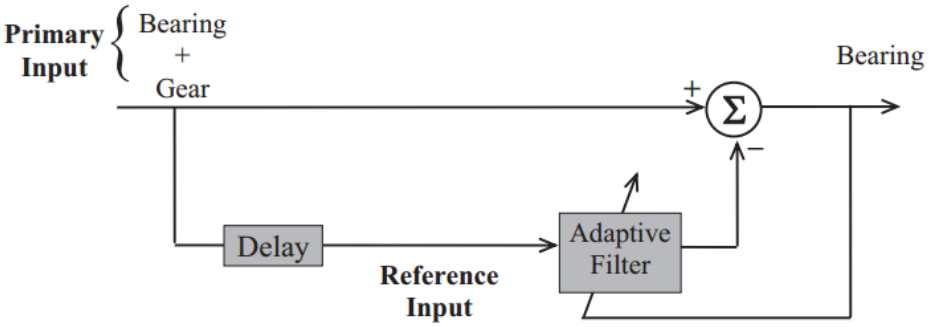

Figure 7: SANC schematic diagram [1]

The adaptive filter in the figure refers to a recursive filter which updates at every step which allows the process to cope with slow changes to the signal or the system properties [1]. Antoni and Randall [16] point out that prior knowledge of the signal being analysed and conducting many trials is required to obtain the "best" solution. They also found that applying this method to an actual signal requires a filter length that is long enough to resolve a number of harmonics that are in high level of noise. This can lead to convergence problems if not tuned properly.

2.3.3.5 Discrete/Random Separation DRS

This method was proposed by Antoni and Randall in [17] and achieves the same results as SANC but more efficiently as it is based in the frequency domain using the advantage of FFT. This method works by obtaining the transfer function between the signal and a delayed version [1]. As opposed to the SANC method, it does not require adaptation as the filter used to remove the discrete frequency component is found first and then applied to the data, however it does cause a significant loss in frequency resolution [1, 17]. Because of this, it requires that the discrete frequency components be stable and the use of order tracking is a recommended pre-processing step.

For the separation of gear and bearing signals, Randall [1] advises the best choice is to generally use DRS because it results in reduced problems with parameter choice.

2.3.4 Frequency Band Selection Techniques

Frequency band selection techniques are an important step in fault diagnosis as they determine the demodulation frequency utilised for further processing. A number of techniques have been developed each with their own advantage and limitation.

2.3.4.1 Spectral Kurtosis

Spectral Kurtosis (SK) is a technique used to determine the frequency band that contains the maximum impulsivity of a signal and how it varies with frequency [18]. Using kurtosis, the impulse response due to a fault in a bearing would increase, however SK can be used to determine the frequency band at which this occurs. SK has a value of zero for a Gaussian random signal and -1 for a sinusoid. It takes large positive values at the frequencies in which transients occur. This allows the use of SK as a filter to capture the parts of a signal with the highest impulsiveness. It has been shown that the ideal matched filter is a narrowband filter at the maximum value of SK [19]. From [18-20], SK was concluded to be a useful tool in reducing background noise and improving the impulse visibility of bearing signals obtained from defective bearings. It was also stated that it can be used to indicate the best frequency band for demodulation to conduct envelope analysis without the need for historical data [18]. This is because the frequency band showing the highest kurtosis value would be a region with the highest signal to noise ratio and as such should be selected as a demodulation band (bandwidth and central frequency) for envelope analysis.

The drawback of this analysis is that while it allows the detection of faults, it does not provide information on the nature of the fault itself [19]. Moreover, in the case where the demodulation bandwidth is infinitely small, i.e. infinite resolution, SK would be zero from the Central Limit Theorem, however if it is too large, i.e. coarse resolution, SK would not detect a narrowband transient signal within stationary broadband noise [21]. To maximise the ability to determine the optimal combination of central frequency and frequency resolution which maximises SK, the concept of the kurtogram was developed.

2.3.4.2 Kurtogram

The kurtogram is an extension of SK and is based on using Short Time Fourier Transform (STFT) to map how SK varies with the central frequency and bandwidth of the filter. While the kurtogram is a valuable tool to explore this relationship, it comes at a cost [1] and is not justifiable in industry. It is a fourth order spectral analysis tool that detects and characterises non-stationarities in a signal [21]. Lei et al [22] state that more precise filters are required to be incorporated into this method so as to overcome the shortcomings and to enhance the accuracy with which it can be used to detect faults as the STFT or FIR filters limit its accuracy in extracting transient characteristics.

2.3.4.3 Fast Kurtogram

Antoni [21] proposed and presented a more efficient alternative called the fast kurtogram. Rather than operating with STFT, a series of digital filters are used to increase the computational speed to decrease calculation speed of the results. The basic principle is that the frequency range is split into bands that are half the width of the previous stage – a so called binary tree [11]. The recommended version from [1] is to use the 1/3 binary tree where the split includes divisions of 1/3 so that the division sequence is 1/2, 1/3, 1/4, 1/6, 1/8, 1/12 and so on. Figure 7 [1] illustrates the comparison between the fast kurtogram of a signal from loose parts in a nuclear plant with a full kurtogram:

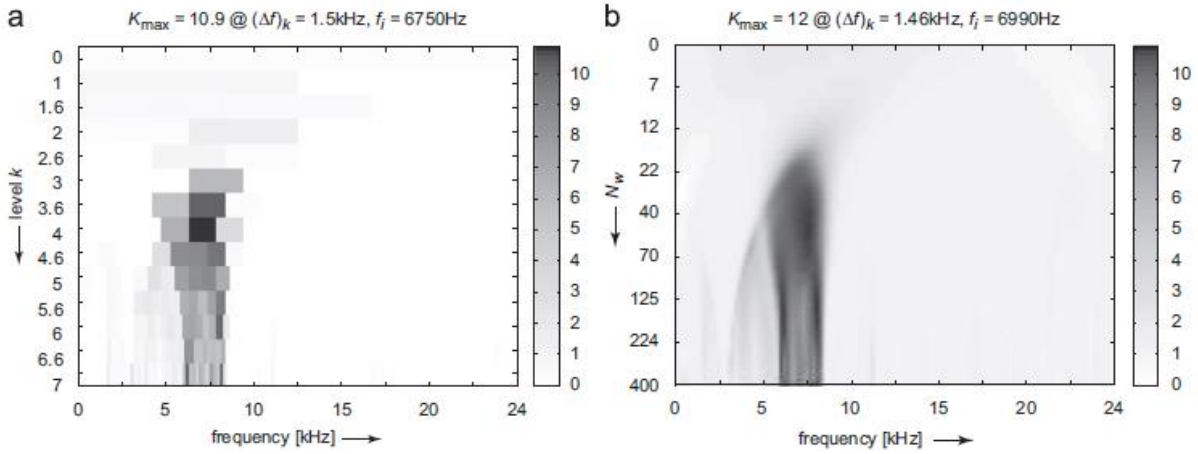

Figure 8: Fast kurtogram (a) comparison with full kurtogram (b) for impulsive signal from loose part monitoring [1]

This type of result enables identification of the band that corresponds to the maximum kurtosis of the signal. The resulting maximum kurtosis from both analyses is comparable. From [22], the results of the experiments performed validated this proposed method compared to the original kurtogram for extracting weak characteristics and diagnosing faults in rolling element bearings.

2.3.4.4 Envelope Analysis

It was mentioned in Section 2.3.1.4 that the raw spectrum of a defective signal contains little to no diagnostic information, however by using the envelope analysis, there is more information about the repetition frequencies and modulation. A well-established benchmark has been set with this diagnostic method. In this analysis, the signal is bandpass filtered in a high-frequency band where impulses are being amplified by structural resonance caused [1]. Performing an amplitude demodulation using the Hilbert Transform, Figure 8 [11] below outlines the procedure for envelope analysis.

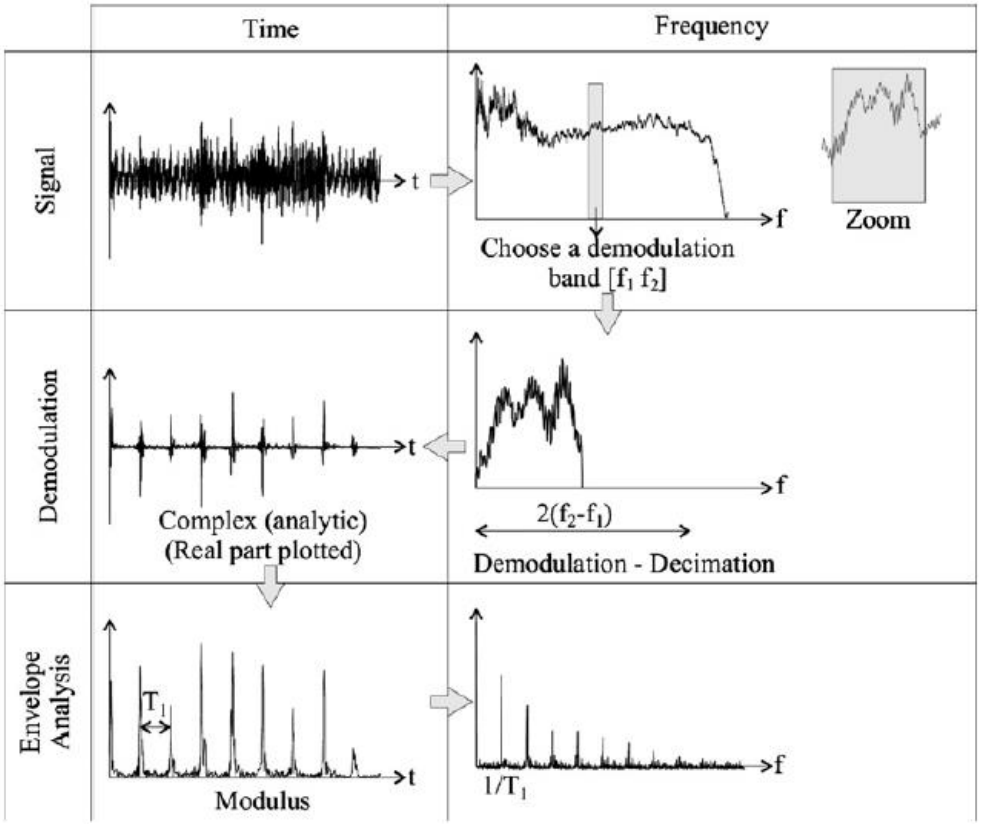

Figure 9: Procedure for envelope analysis [11]

The above process shows that the raw signal is bandpass filtered in a high frequency band to effectively remove the low-frequency signals associated with imbalance and misalignment and eliminating random noise [4]. This bandwidth selection can be accomplished using the aforementioned kurtogram or fast kurtogram to determine the frequency band containing the maximum kurtosis. The filtered signal is then amplitude demodulated using the Hilbert transform technique. After this, the positive frequencies of the spectrum is transformed back into the time domain by using the inverse fast Fourier transform [11]. The amplitude of the complex time signal is squared, giving the square envelope signal. This is done to avoid aliasing issues that may arise from rectifying the signal [11]. The final step is to conduct a fast Fourier transform on the square envelope signal to obtain the square envelope spectrum. In this spectrum there is better signal-to-noise ratio obtained which further helps identifying bearing faults. This is because the peaks are now more observable at the bearing harmonics.

2.4 Planetary Gearbox

Planetary gearboxes offer the advantages of large transmission ratios and strong load-bearing capacities and are widely used in helicopters, wind turbines and heavy trucks [23]. In these applications, it can be said they operate in harsh working conditions and as a result, the gears and bearings, being the primary components of the system, are subject to damage during their service life. Figure 10 [23] below illustrates a planetary gearbox configuration. It is comprised of a sun gear at the centre, a ring gear on the outside, and planet gears in between.

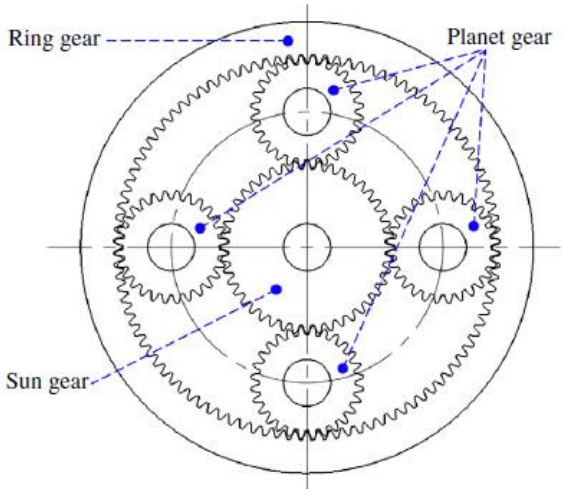

Figure 10: Planetary gearbox gear configuration [23]

Because of this unique configuration, the outer race of the planetary bearings rotates at the speed of the planet gear. The inner race is not stationary and rotates in the opposite direction of the planet gear but has fixed orientation with respect to the load [24]. This results in inner race faults to not being modulated but rather the outer race faults are modulated by the frequency at which the outer race fault passes through the load zone [1]. The characteristic defect frequencies because of this are [24]:

$$BPFO = \frac{n}{2}\left\{(f_i - f_o)\left(1 - \frac{d}{D}cos\phi\right)\right\} \tag{12}$$

$$BPFI = \frac{n}{2}\left\{(f_i - f_o)\left(1 + \frac{d}{D}cos\phi\right)\right\} \tag{13}$$

$$FTF = \frac{1}{2}\left\{(f_i - f_o)\left(1 + \frac{d}{D}cos\phi\right)\right\} \tag{14}$$

$$BSF = \frac{D(f_i - f_o)}{2d}\left\{1 - \left(\frac{d}{D}cos\phi\right)^2\right\} \tag{15}$$

where $f_o$and f_i are the planet bearing outer and inner race speeds, planet gear and carrier speeds respectively. All vibration based diagnostic techniques aforementioned are applicable to this gearbox.

2.5 Variable Speed Applications

This section discusses the challenges and the current techniques used in variable speed diagnostics.

2.5.1 Challenges Arising from Variable Speed

It has become an area of interest in vibration analysis and condition monitoring to develop techniques useable for machine operating under variable speeds, such as wind turbines. Much of the diagnostic methods aforementioned were developed for constant speed machinery and require speed fluctuations be removed in order to conduct an effective analysis on defective bearings [13]. The varying speed affects the frequency and the amplitude of the vibration signals. In terms of frequency, the impulse caused by the defect does not repeat at constant intervals therefore using the demodulated resonance technique and other techniques operating under the assumption of constant speed no longer applies [25]. Vibration signals depend on

the load and speed fluctuations [26] therefore much of the currently available techniques have difficulty overcoming the characteristics obtained from the signal due to varying load and speed. In the time-domain under constant speed conditions, the signal exhibits cyclostationarity and components in the signal that relate to the speed change their characteristic frequency with speed variations [26]. The modulation signal under variable speed then becomes non-deterministic in the time-domain. Angular resampling (i.e. order tracking) is required to make the modulation signal stationary. The natural frequencies however do not depend on the varying speed so their values do not change.

Bearing faults may show up more dominantly at certain speeds during machine run-up or run-down and as such provides a reason of performing analyses over a wide speed range [27]. Current diagnostic methods make the use of equal time interval digital sampling as much of the existing techniques were developed for constant speed machinery. This poses a considerable problem for diagnostics of bearing faults in machinery that operate under variable speeds as the use of equal time interval sampling causes leakage error and smearing in the envelope spectrum [12]. Order tracking then becomes necessary to obtain sampling that produces a frequency base in terms of harmonic order and shaft speed rather than absolute frequencies. The need for a tachometer for resampling adds cost and effort into the procedure to obtain the required reference signal to enable order tracking.

Beyond these, Stander and Heyns [14] found that the fluctuating speed cause the transfer function of the mechanical system to be excited at different frequencies at different times which varies its behaviour over time. This was said to significantly affect the capabilities of order tracking which further influences the quality of DRS. If the process of order tracking does not accurately reflect and pass on the correct data then diagnostic of a defect becomes more challenging with the use of further techniques, such as envelope analysis.

2.5.2 Techniques Used in Variable Speed Diagnostics

Sawalhi and Randall [28] have proposed an analysis procedure illustrated in Figure 11, applicable to constant speed machinery. Randall [1] states this procedure to be semi-automated as only a small number of parameters need adjusting.

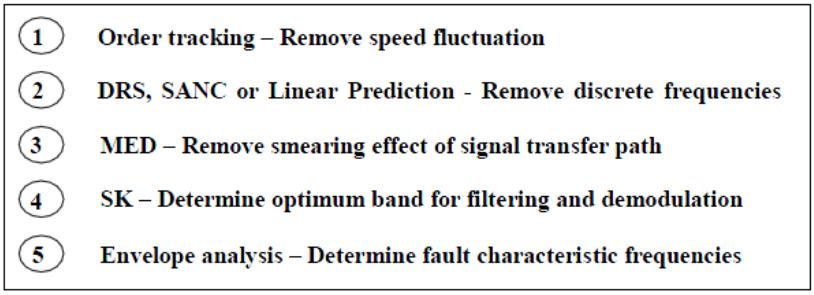

Figure 11: Proposed constant speed analysis procedure [24]

The first step is to remove speed fluctuations by order tracking as the second step involves the removal of discrete frequency components. The case where bearing faults are being analysed which are coupled with gears transmitting power between shafts, the second step is to use a discrete-random separation technique, i.e. DRS, SANC or linear prediction. This is possible due to the slight random nature of bearing signals that are caused by slip which allows them to be separated from gear signals [28]. Randall [1] states the best choice in this step is to generally use DRS because it results in reduced problems for parameter choice. DRS method is a more efficient way of achieving the same results from SANC as the advantage of FFT is used. From there, the next step is to enhance the fault signal using MED which removes the effects of the transmission path from the source of the signal to the transducer for a better representation of the source signal. The fourth step uses SK to determine a suitable frequency band for filtering and demodulation to perform the final step: envelope analysis. It is with envelope analysis that the repetition frequencies stand out to determine fault characteristic frequencies.

Randall et al [27] advised treating the bearing fault signals in the time-domain as many of its characteristics are related to the resonance frequencies. The resonance frequencies are constant in the time/frequency domains as opposed to the order (or shaft speed). With signal enhancement, order tracking is used to allow a diagnosis using envelope analysis. They concluded their techniques worked well for the situation but noted the data was straight forward to diagnose and gave good results with the simple methods. For cases of variable speed machinery, the techniques that are based on resonance frequencies are to be carried first (i.e. kurtogram or MED) as opposed to order tracking and DRS.

Urbanek et al [26] proposed a method of extracting second-order cyclostationary (i.e. bearing signals) components of a vibration signal using an algorithm that allows the estimation of the

amount of energy of each cyclic component of interest in the time-frequency domain. This method thus results in a representation that contains only the selected second-order cyclostationary component which is manifested from a number of carrier frequencies that are modulated by the harmonic signal of the selected frequency. They state the advantage of this technique allows the extraction of the desired component of the vibration signal for machinery that is operating under variable speed and load. The technique combines the application of average instantaneous power spectrum (AIPS) and information from a squared filterbank output of the signal, where the novelty of the technique lies in the ability to extract the component of interest while preserving the influence of the variable load (which changes with speed) [26]. Their technique requires the use of order tracking.

Borghesani et al [29] proposed a technique called reversed sequenced squared envelope spectrum (RS-SES) which is based on order tracking the envelope signal and was proven to be successful in both numerical simulation and experimental data. The authors suggest that demodulation should be performed in the time domain and the order tracking applied later to carry out an envelope analysis. The drawback to RS-SES is that there is more complexity in removing the first-order cyclostationary component and as such can partially compromise the quality of the analysis [29]. Their results showed that there is possibility to expand on this application of the squared envelope spectrum (SES) to most industrial applications.

2.6 Summary

From the above literature review, it is evident that the field of rolling element bearing vibration analysis has been thoroughly researched and studied which has led to well-established methods that have been widely applied. While much of these techniques were developed and used for constant speed machinery, research is now focused on developing or adapting current methods for variable speed conditions which are more applicable to industrial applications. The ability to perform analyses on variable speed machinery could possible increase the likelihood of diagnosing a bearing defect as bearing vibrations change in behaviour with changes in speed. By being able to do this, signals from machine run-up or run-down could be used to identify a fault. It was seen that the variable speed of the machinery causes considerable issues as the transmission path causes distortion and further problems with the recorded signal. This then influences the accuracy of order tracking and thus discrete frequency separation technique used thereon.

Chapter 3: Methodology

This thesis asses the suitability of current diagnostic techniques for bearing faults in multiple component machinery operating under variable speed conditions. To achieve this aim, vibration signals captured by accelerometers will be analysed using multiple techniques aforementioned to determine the most effective method. This section will discuss the details of the tests that were undertaken and post-processing plans for the captured data. It is important to understand the experimental setup and the components being used so as to gain a better understanding of the signals involved in the analysis. Experiments were carried out on two different test rigs for reasons discussed in Section 4.3.

3.1 Equipment and Setup – Spur Gearbox

A spur gearbox setup for utilised for testing in this thesis. This section details the equipment and setup of the spur gearbox experimental test rig.

3.1.1 Rig

This test rig was comprised on components shown in Figure 12 below. An induction motor is used and connected to the input shaft via couplings. Two spur gears mesh and transmit rotary motion to the output shaft which then powers a pump that recycles water in a water tank.

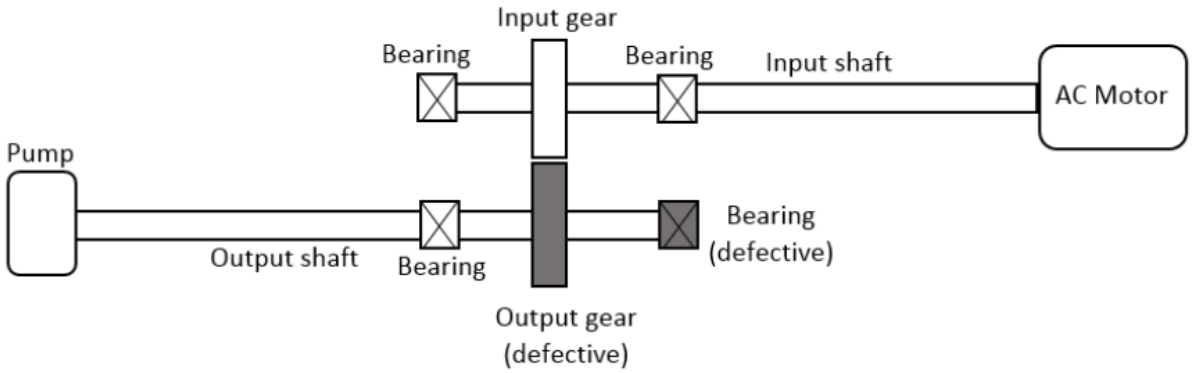

Figure 12: Spur gearbox rig - top view layout

Two sets of bearings are used on the input shaft and another two on the output shaft, all located in bearing housings. Two gears are used to step the power between shafts. The

bearings and gears are housed within the gearbox. The rotating speed of the input shaft is adjustable by the induction motor and its control system. Figure 13 [30] provides a side view of the experimental rig.

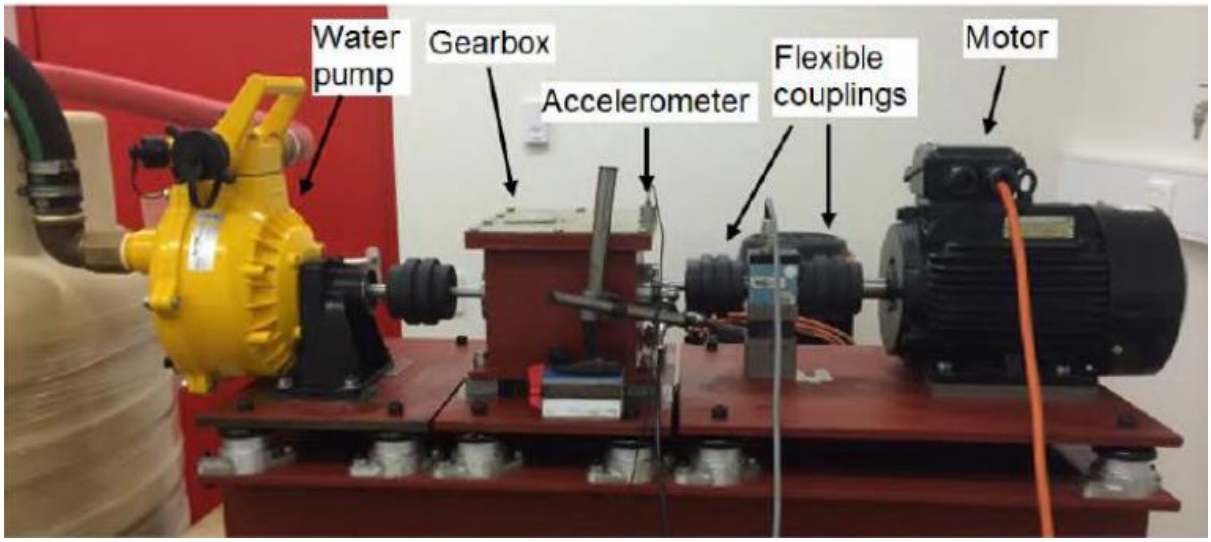

Figure 13: Side-view of spur gearbox rig [30]

A tachometer was installed to measure the angular speed of the output shaft. Two accelerometers were used, one placed on the pump side of the output shaft housing and the other closer to the defective bearing on the gearbox. The following table provides an overview of the components used:

Table 1: Spur gearbox component breakdown

Component	**Detail**
Motor	3 Phase four-pole induction motor, rated 2.2 kW
Pump	Davey bare shaft 5 blade 5150P
Bearings	SKF W6002 Deep groove ball bearing Defective bearing: inner race fault 0.8 mm
Gears	Input gear: 46 teeth SS2-46 (healthy) Output gear: 25 teeth SS2-25 (defective – half tooth root crack)
Coupling	SKF FRC 90
Torque Meter	Kirstler torque sensor 4502S 200RA

3.1.2 Bearings

With the aim of detecting and diagnosing bearing faults, one of the four SKF W6002 deep groove ball bearings used in the testing rig was artificially seeded. The fault is a notch with a

width of $0.8\,mm$ spanning across the entire inner race of the bearing as illustrated in Figure 14 and located as shown in Figure 12 in Section 3.1.1.

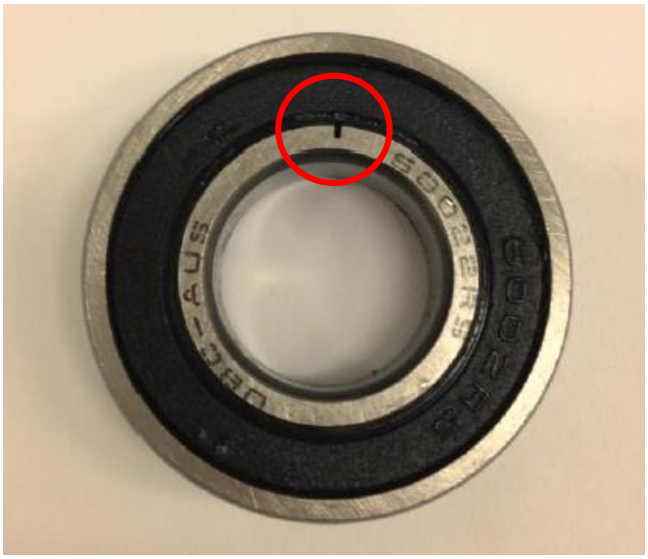

Figure 14: Defective bearing - inner race fault

The table below outlines the pertinent dimensions of the bearing.

Table 2: Bearing dimensions - spur gearbox

Component	**Value**
Number of ball rollers, n	9
Ball roller diameter, d	$5\,mm$
Bearing pitch diameter, D	$23.6\,mm$
Load angle, ϕ	0°

The pitch diameter was approximated based on measurements as bearing manufacturers do not publish this dimension. The load angle was also assumed to be 0°, however, this may not have been the case during the experiment. As a result, these will have a small influence on the frequency calculated.

3.1.3 Gears

To increase the complexity of the analysis, the output gear was also artificially seeded. The output gear featured a half tooth root crack as shown in Figure 15 below. This added to the complexity of the vibration signal collected in the course of the experiment to further test the

separation techniques and final outcome of the diagnosis based on well-established techniques.

Figure 15: Defective gear - output gear

3.1.4 Data Collection Instrument

Three sets of signals were collected; a tacho signal and two accelerometer signals. A National Instrument (NI) data acquisition system was used to measure the vibrations generated from the rig. It features a 4-channel acceleration measurement module that is used to synchronise the vibration signal with the tacho signal measured simultaneously. One accelerometer was positioned on the gearbox above the bearing housing of the defective bearing. The second accelerometer was positioned on the gearbox on the other bearing housing of the output shaft (closer to the pump).

3.2 Test Details of Spur Gearbox

Two sets of tests were to be conducted for this thesis. In all cases, the same bearing and gear faults were used. The first set of tests consisted of four simple shaft run-up speed profiles with varying accelerations. The second set of tests consisted of undulating speed profiles with two varying ranges of nominal input shaft speeds. This section details all the tests carried out for both sets. It is important to note that the changes in frequency were carried out by the use

of a linear potentiometer that was installed into the VFD control box. As a result, the actual frequencies deviated slightly from the targeted frequencies.

3.2.1 Test Set 1

Test Set 1 featured four simple input shaft run-up speed profiles with varying acceleration. The starting and ending speeds of the test remained the same for each acceleration profile. The first and last 20 seconds of the test were conducted at constant speed to allow the signal at constant speed to be used for comparison with the variable speed signal obtained. The starting constant nominal input shaft speed for these tests was set to $15\ Hz$ (30 on the variable speed drive due to the four-pole motor). The concluding constant nominal input shaft speed was set to $23\ Hz$ (46 on the VFD). The run-up stage of the tests varied in time-intervals from a total of 20 seconds down to 5 seconds. This is summarised in the table below:

Table 3: Test Set 1 – Nominal input shaft speeds

Start speed (nominal input shaft – Hz)	15
Ramp up times (s)	$20, 10, 5$
End speed (nominal input shaft – Hz)	23

3.2.2 Test Set 2

Test Set 2 consisted of the same speed profile for 2 different nominal input shaft mean speeds. The nominal input shaft speed varied by a maximum of $\pm 20\%$ around 2 means: 15 and $23\ Hz$ (30 and 46 on the VFD respectively). The test was to last approximately one minute, where a sinusoidal speed profile begun after 10 seconds of constant speed data covering 2 complete cycles over approximately 40 seconds and the last 10 seconds at constant speed. The test set is summarised below:

Table 4: Test Set 2 - Nominal input shaft speeds

Mean 1	$15\ Hz\ \pm 20\%\ (12 - 18\ Hz)$ $(24 - 36\ on\ VFD) for\ 2\ cycles\ over\ 40s$
Mean 2	$23\ Hz\ \pm 20\%\ (18 - 27\ Hz)$ $(36 - 54\ on\ VFD) for\ 2\ cycles\ over\ 40s$

3.3 Equipment and Setup – Planetary Gearbox

When considering industrial applications of vibration diagnostic techniques, rarely are simple spur gearbox configurations used in critical machinery. As such, this thesis aimed to include the analysis of a more complex gearbox to provide a comparison in the results and analysis gained from the spur gearbox. This section details the equipment and setup of the planetary gearbox experimental test rig.

3.3.1 Rig

The test rig is shown in Figure 16 [24] and 17 below. An induction motor provides the input shaft with torque that is transmitted and a hydraulic system provides a resistance torque to the gearbox. An external accelerometer is used to measure the vibration signal generated by running the rig with a defective bearing.

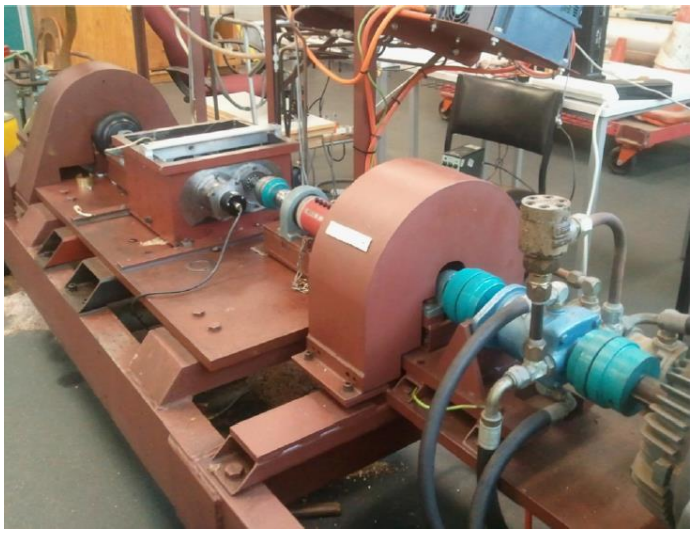

Figure 16: Planetary gearbox test rig [24]

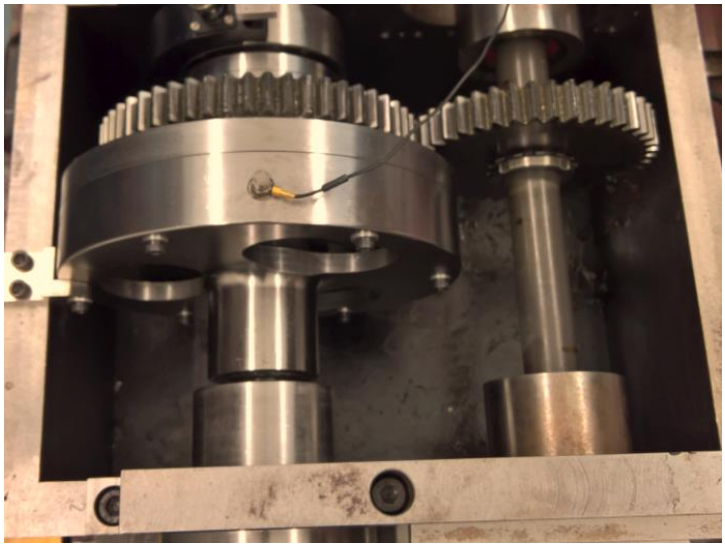

Figure 17: Close up of the gearbox and external accelerometer

Table 5 below reveals the gear tooth numbers of each gear type used in the experiment. This allows the calculation of gear ratios and frequencies for later analysis.

Table 5: Gear tooth numbers

Gear type	Number of teeth
Planet N_P	23
Sun N_S	34
Ring N_R	80
Spur N_{spur}	55
Pinion N_{pinion}	42

3.3.2 Defective Bearing

The defective bearing used in this experiment is an IKO radial cylindrical roller bearing (needle roller bearing) with designation RNAF 162812. The table below outlines the pertinent dimensions of the bearing.

Table 6: Bearing dimensions -planetary gearbox

Component	Value
Number of needle rollers, n	11
Needle roller diameter, d	3 mm
Bearing pitch diameter, D	19 mm
Load angle ϕ	0°

Figure 18 and 19 illustrate the defective bearing used on one of the planet gears in the test rig. The outer race fault can clearly be seen and measures 1.6 mm in width.

Figure 18: Outer race fault (1.6 mm)

Figure 19: Assembled defective bearing

3.3.3 Data Collection Instrument

Two sets of signals were collected; a tacho signal and an external accelerometer signal. A National Instrument (NI) data acquisition system was used to measure the vibrations generated from the rig. It features a 3-channel acceleration measurement module that is used to synchronise the vibration signal with the tacho signal measured simultaneously. The external accelerometer was positioned on the gearbox above the planetary gears of the defective bearing.

3.4 Test Details of Planetary Gearbox

Three tests were conducted for this thesis. In all cases, the same bearing fault was used. The first 2 tests consisted of 2 simple shaft run-up speed profiles with varying accelerations. The third test consisted of an undulating speed profile with varying range of nominal input shaft speeds. This section details all the tests carried out for all test sets. It is important to note that the changes in frequency were carried out by the use of an input signal created by MATLAB into the VFD control box. As a result, the actual frequencies were exact as compared to the targeted frequencies.

3.4.1 Test 1

Test 1 featured 1 simple input shaft run-up speed profile. The starting and ending speeds of the test remained the same for each acceleration profile. The gearbox was started and brought to speed with constant acceleration for the first constant speed section of the test. 20 seconds of constant speed data allows preliminary analysis and determines whether the fault is diagnosable. The speed proceeds to increase with constant acceleration over 30 seconds, followed by 20 seconds of constant speed at a higher frequency. The first and last 20 seconds of constant speed were used for comparison with the variable speed signal obtained. The starting constant nominal input shaft frequency for these tests was set to 3.935 Hz (15.74 Hz on the variable frequency drive due to the eight-pole motor). The concluding constant nominal input shaft frequency was set to 5.750 Hz (23.00 Hz on the VFD). The load condition was such that 60 $N.m$ was experienced at the highest shaft frequency, i.e. at 5.750 Hz input shaft frequency.

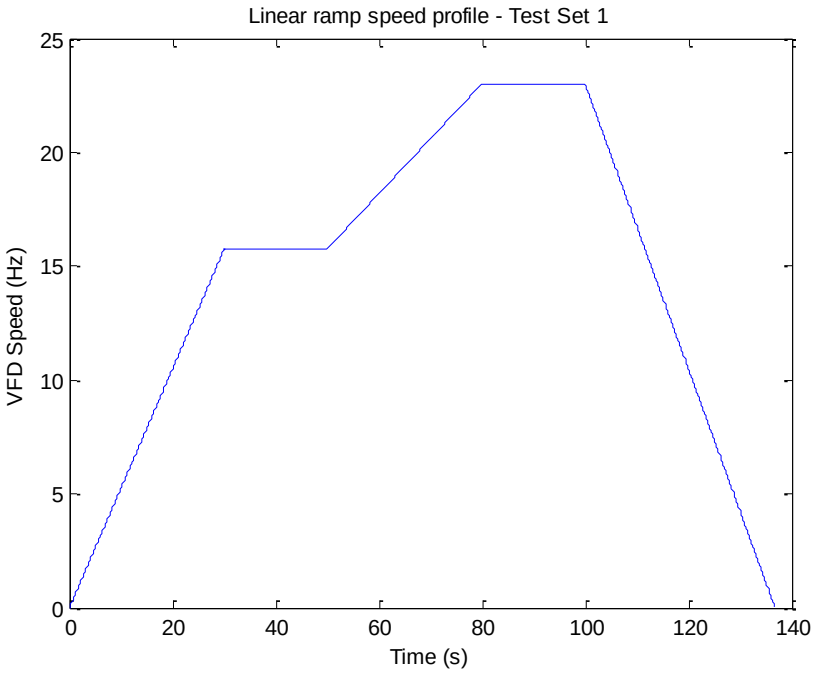

Figure 20: Test 1 speed profile

3.4.2 Test 2

Test 2 consisted of a constant acceleration speed profile as in Test 1. The constant acceleration took place over 20 seconds (as opposed to 30) for comparison with different acceleration. This test set was carried out under the same load case as Test 1.

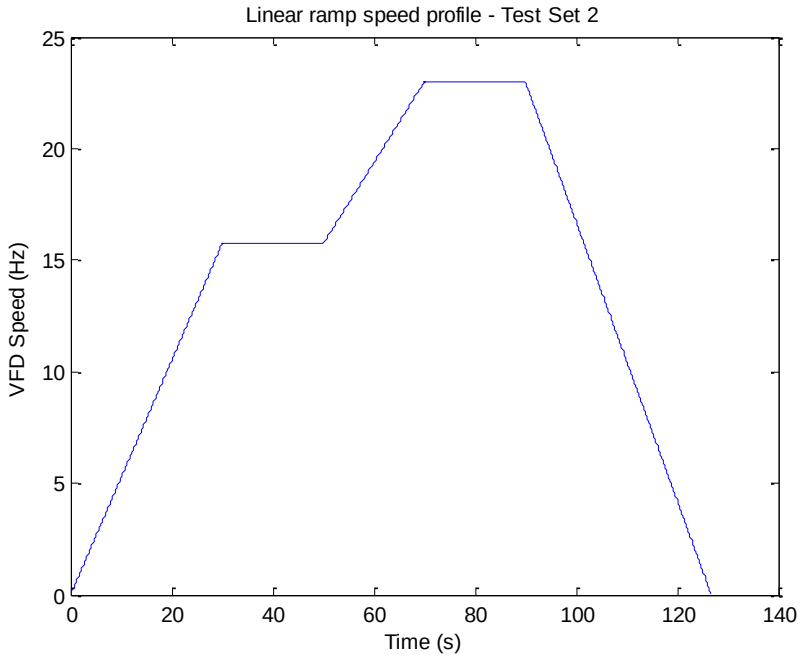

Figure 21: Test 2 speed profile

Table 2 below breaks down Test 1 and 2:

Table 7: Test 1 & 2 breakdown

Start speed (nominal input shaft)	$3.935\ Hz$
Ramp-up times	$30s, 20s$
End speed (nominal input shaft)	$5.750\ Hz$
Load condition	$60\ N.m$

3.4.3 Test 3

Test 3 consisted of an undulating speed profile. The planetary gearbox was accelerated to $15\ Hz$ on the VFD and from there proceeded to vary by $\pm 20\%$ around a mean of $15\ Hz$. Five cycles were completed over approximately 100 seconds. The speed profile is shown in the figure below. A maximum frequency of $18\ Hz$ occurred with a load of $60\ N.m$ and the minimum frequency was $15\ Hz$.

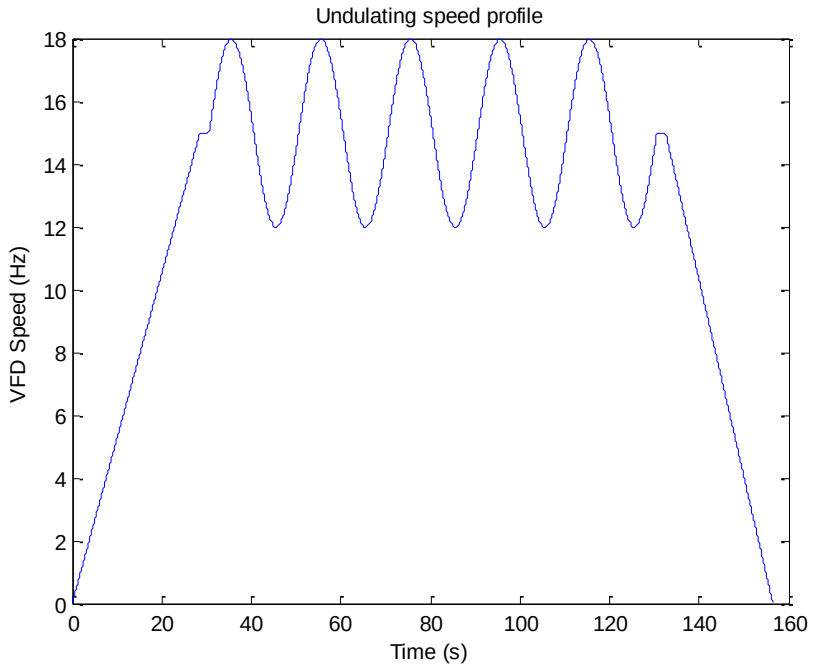

Figure 22: Test Set 3 speed profile

3.5 Processing and Analysis

The processing and analysis of the experimental data involves the implementation of various techniques to establish a diagnosis from the acquired data. Software program MATLAB was used extensively to process and analyse the data acquired from the experiment. The steps involved in the processing and analysis uses some of the techniques described in Section 2. Briefly, the steps used for constant speed data analysis follow a similar procedure to that discussed in Section 2.5.2 Figure 11. To remove speed fluctuations, order tracking was carried out, then DRS was used to remove discrete frequencies, followed by determining band for filtering and demodulation and finally using envelope analysis. The post-processing order for variable speed analysis was dissimilar in order, although used the same techniques. The steps used for variable speed analysis were:

1. Choosing demodulation frequency band (Fast Kurtogram)
2. Order tracking (obtaining frequency in 'orders' of shaft speed)
3. Denoising and separation of signal (DRS)
4. Envelope analysis.

For each test and their respective data processing, the same techniques were used to achieve the same outcome to establish a comparison between. As pointed out in Section 2.3.3, the variable speed condition affects the signal such that there is leakage and smearing in the frequency domain. Order tracking becomes an important step in the processing of the data to obtain a clear signal that can be used from envelope analysis.

To begin, a demodulation frequency band must be established, where a number of techniques can be used, i.e. SK, Kurtogram and Fast Kurtogram. In the post-processing carried out for this thesis, FK was used extensively for this step. Order tracking is then used, which resamples the signal in terms of 'orders' of shaft speed, removing speed variations to allow further processing. Denoising and separation of the signal is required to remove the gear component of the vibration as they are more dominant compared to the vibration signals caused by bearing faults, this is carried out using DRS. This provides a signal ready to use the advantages of envelope analysis to determine the nature of the bearing fault. Impulsive signals generated by the faults may be lost from the source as the sensor was placed on the testing rig external and thus require enhancement. In this thesis, enhancement was not carried out to determine suitability of the chosen techniques for diagnostic purposes.

Chapter 4: Results and Discussion

This chapter provides a detailed analysis of the vibration data that was obtained from the experimental rig. The data sets were obtained as per the methodology outlined in Chapter 3. Each test set included a sufficient amount of time to allow a baseline analysis at constant speed to establish if the bearing fault is diagnosable. The first section of this chapter provides an overview of the results and basic analysis of the constant speed data to establish the faults and ability to find the known faults in the experimental rig.

4.1 Preliminary Analysis of Spur Gearbox

4.1.1 Theoretical Frequencies

The frequency that is relevant for this experiment is the Ball Pass Frequency for an Inner Race fault. The formula is given by equation (5):

$$BPFI = \frac{nf_r}{2}\left\{1 + \frac{d}{D}cos\phi\right\}$$

The bearing dimensions are known and listed in Table 2 (Section 3.1.2). Substituting the values into equation (5) yields:

$$BPFI = \frac{9 \times f_r}{2}\left\{1 + \frac{5}{23.6}\cos(0°)\right\}$$

$$BPFI = 5.4534 \times f_r$$

The bearing fault frequency can be calculated using the above formula with the output shaft frequency f_r as this is the shaft on which the defective bearing is located. Note: the pitch diameter was approximated based on measurement therefore this value varies slightly. The AC motor used is 4 pole therefore the input speed on the VFD must be divided by 2 to further obtain f_r.

The gear mesh frequency can be calculated by multiplying the input shaft frequency by the number of teeth located on the input shaft gear, i.e.:

$$GM = f_{input} \times 46$$

The half tooth root crack on one of the teeth of the output gear would give rise to a shaft speed modulation of the gearmesh frequency. Its modulation effect should be seen in the envelope spectrum. This is because the defect will come into contact with the input gear once per revolution of the output shaft. The output shaft speed is calculated from the ratio of the teeth on the gears as follows:

$$f_r = f_{input} \times \frac{input\ gear\ teeth}{output\ gear\ teeth} = f_{input} \times \frac{46}{25} = 1.84 \times f_{input}$$

With these frequencies calculated in terms of input shaft frequencies, preliminary analysis can be carried out on the constant speed sections of the data obtain to determine whether the fault is diagnosable.

4.2.2 Constant Speed Data

The constant speed portion of the first test in Test Set 1 was carried out using the procedure outlined in Section 3.5. The input shaft frequency of the constant speed portion of the signal was 15 Hz. The following frequencies are expected to be found after processing:

$$f_r = 1.84 \times 15 = 27.6\ Hz$$

$$BPFI = 5.4534 \times (27.6) = 150.51 Hz$$

$$GM = 15 \times 46 = 690\ Hz$$

The average torque recorded during this portion of the signal was $8\ N.m$. The following figure illustrates the waveform of the signal at constant speed.

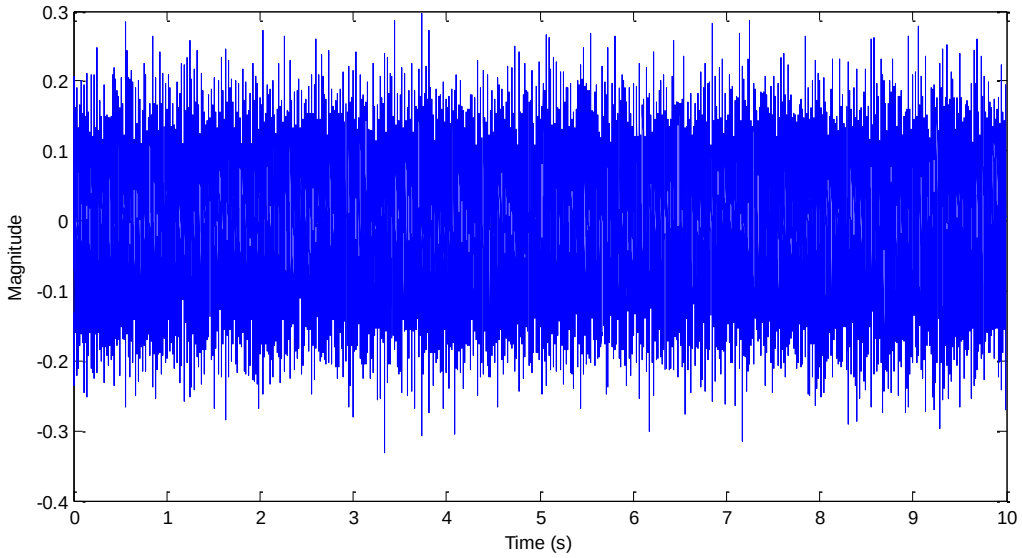

Figure 23: Waveform of constant speed signal

Impulsiveness is not clearly evident in the signal. The raw spectrum of this signal is shown below:

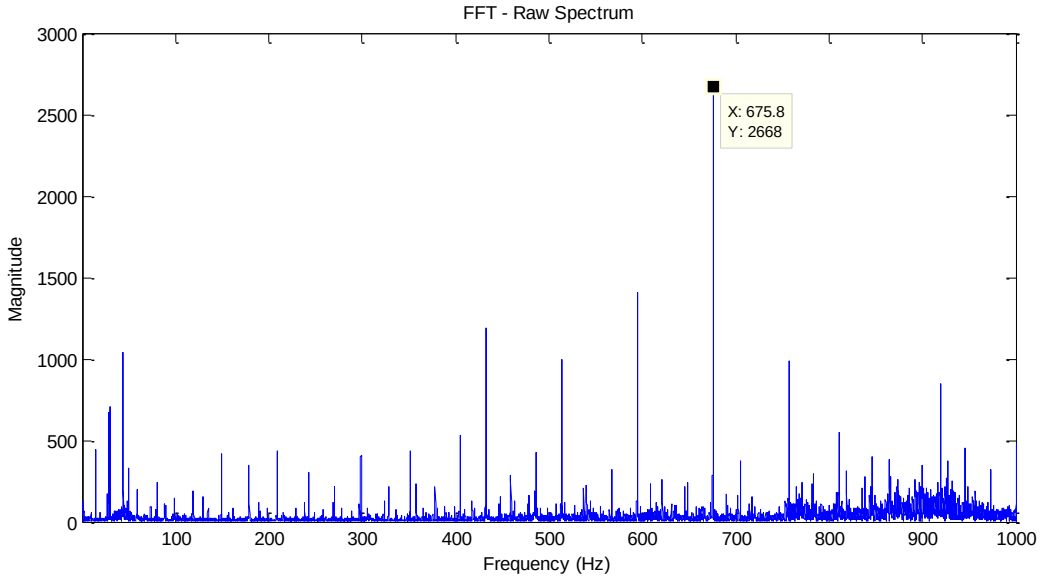

Figure 24: Raw spectrum of constant speed signal

A clear peak is evident, which is the gearmesh frequency. The expected value was calculated to be 690 Hz, however there exists slip in the induction motor therefore the actual input shaft speed is lower because of this. The actual shaft speed can be found by working backwards from this known frequency:

$$f_{input} = \frac{675.8}{46} = 14.7\ Hz$$

Therefore, the output shaft speed and BPFI become:

$$f_r = 14.7 \times 1.84 = 27.05\ Hz$$

$$BPFI = 147.51\ Hz$$

An envelope spectrum of the raw signal and the full band is shown below:

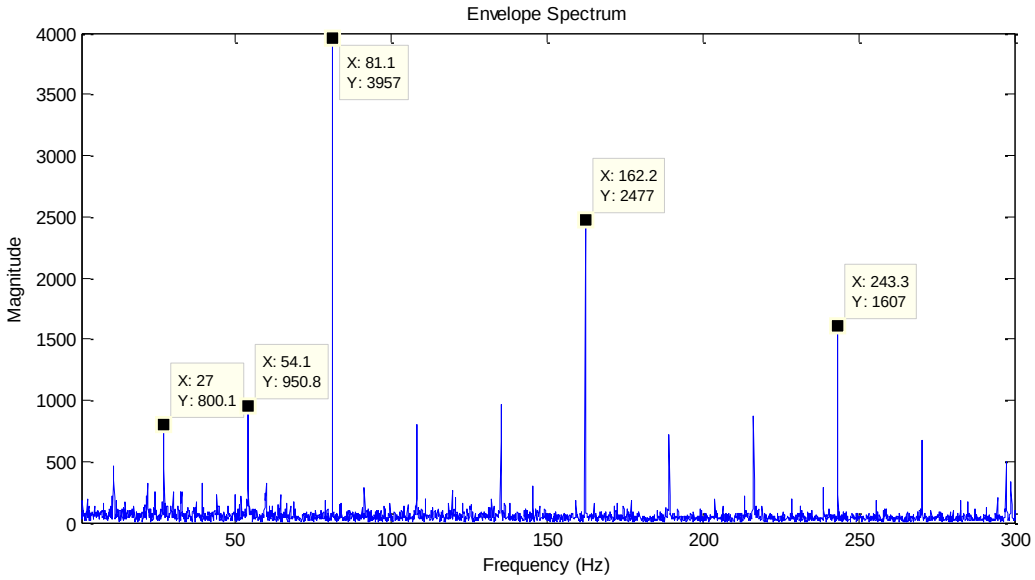

Figure 25: Envelope spectrum of constant speed signal, full band

There are strong peaks evident, however these peaks are occurring every $3 \times f_r$ (3 times output shaft speed). There is a small spike at the expected frequency however is not convincing, and could be masked by the gear vibrations and noise. The gearmesh frequency of the defective gear occurs at output shaft frequency therefore this fault may be dominating the signal and masking the bearing fault. This therefore requires further processing. Using a procedure similar to that outlined in Section 3.5 for constant speed data, order tracking is carried out, followed by TSA. The figure below illustrates the envelope spectrum of the residual signal extracted after the above processing was carried out.

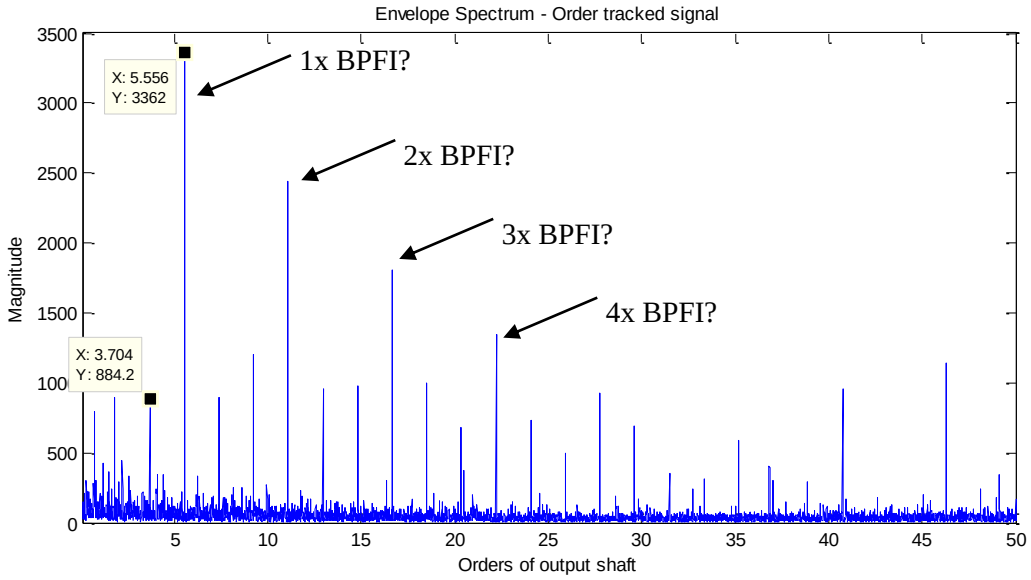

Figure 26: Envelope spectrum without bandpass filtering at constant speed

The above envelope spectrum without bandpass filtering reveals harmonics of what can be assumed to be BPFI clearly starting with 5.556 times output shaft order and all harmonics with smaller peaks either side spaced at 1.852 orders of output shaft frequency (data tips on the plots shown for clarity). Theory dictates that for this set up, the sidebands should be spaced at exactly one order of output shaft since this is the rate at which the fault passes through the load zone. This modulation is not subject to slip, i.e. it should be exactly one unless the inner race is slipping on the shaft, in which case it would indicate a design problem. 1.852 orders of output shaft frequency multiplied by output frequency of $27\,Hz$ results in $50\,Hz$ which is the electrical supply frequency. This raises the possibility that electromagnetic interference is affecting the signal. This possibility can be made more clear with further analysis as the remaining data obtained during the experiments are yet to be analysed.

The difference in envelope spectra obtained from following the post-processing procedure outlines the importance of separating gear and bearing signals as the preliminary envelope spectrum only revealed the faulty gear frequency and no trace of the defective bearing. Even though the clear harmonics may not be the result of the bearing fault, there is information not previously seen from the preliminary observation. Gear vibrations tend to mask bearing faults therefore to identify the possibility of a bearing fault, it is essential to consider further processing to ensure the diagnosis does not miss a faulty bearing should one exist. The

deviation of approximately 2% from the calculated BPFI (if the results do in fact reveal BPFI) can be attributed to slip in the bearing, the difference in the exact and approximation of the pitch diameter for the bearing used and the load angle experienced.

For comparison, Fast Kurtogram and power spectral density (PSD) are shown below.

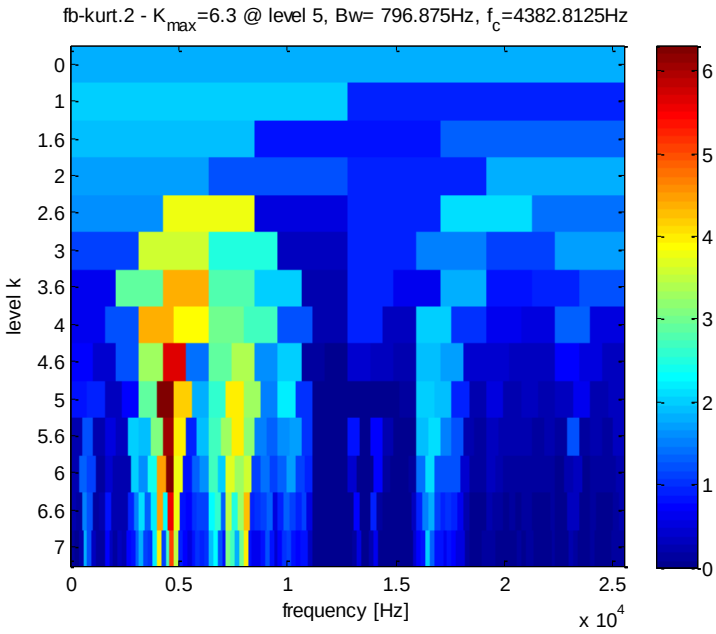

Figure 27: FK for band selection at constant speed

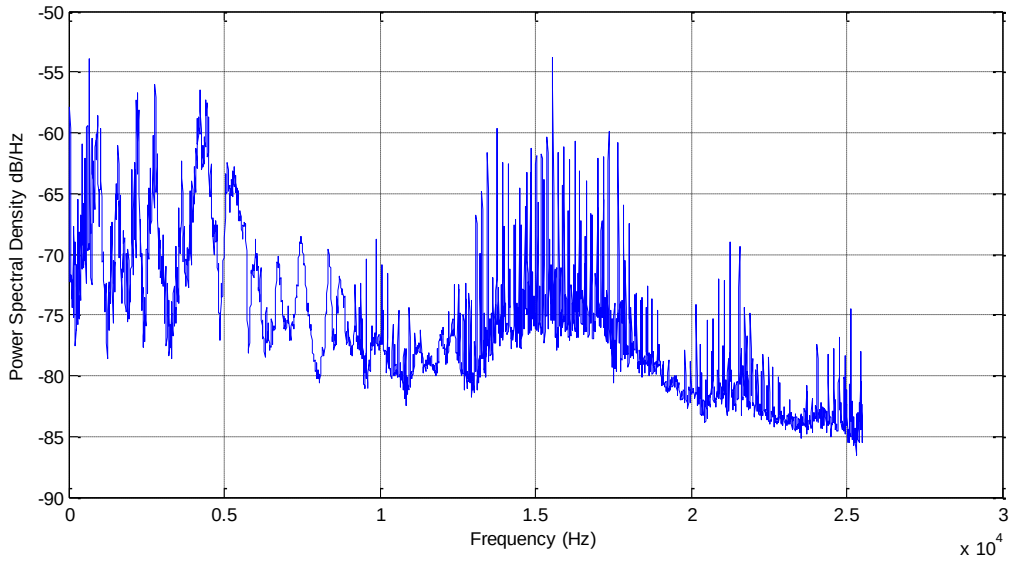

Figure 28: PSD of constant speed data

The PSD shows a large number of discrete frequencies at $\sim 15\ kHz$ which may be caused by electromagnetic interference. FK suggests bandpass filtering around centre frequency $f_c = 4{,}382\ Hz$ with a bandwidth of $Bw = 797\ Hz$. A comparison with the PSD reveals another peak next to the band suggested by FK that may also be suitable (shown in Figure 29).

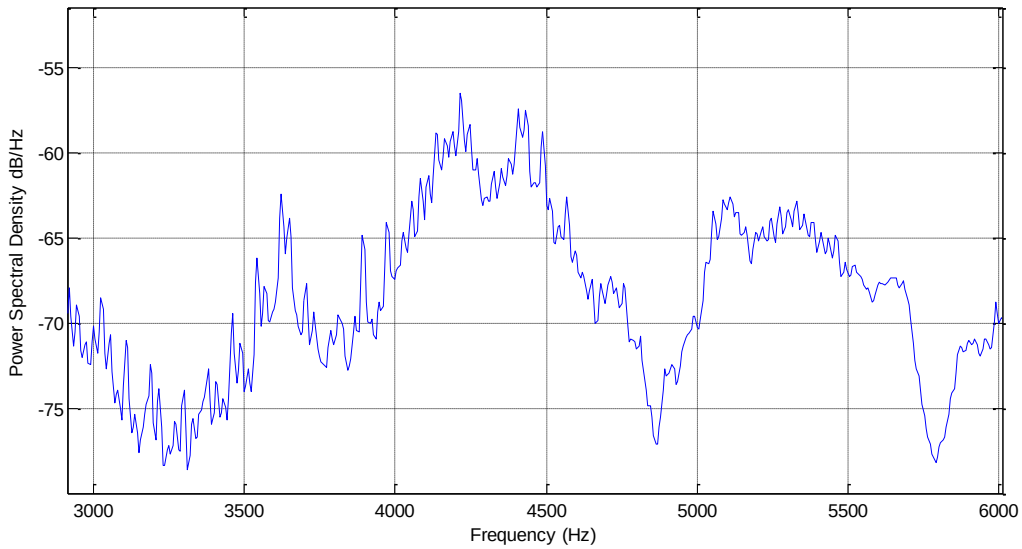

Figure 29: PSD of constant speed data - zoomed

The signal was filtered with the band suggested by FK and is illustrated below.

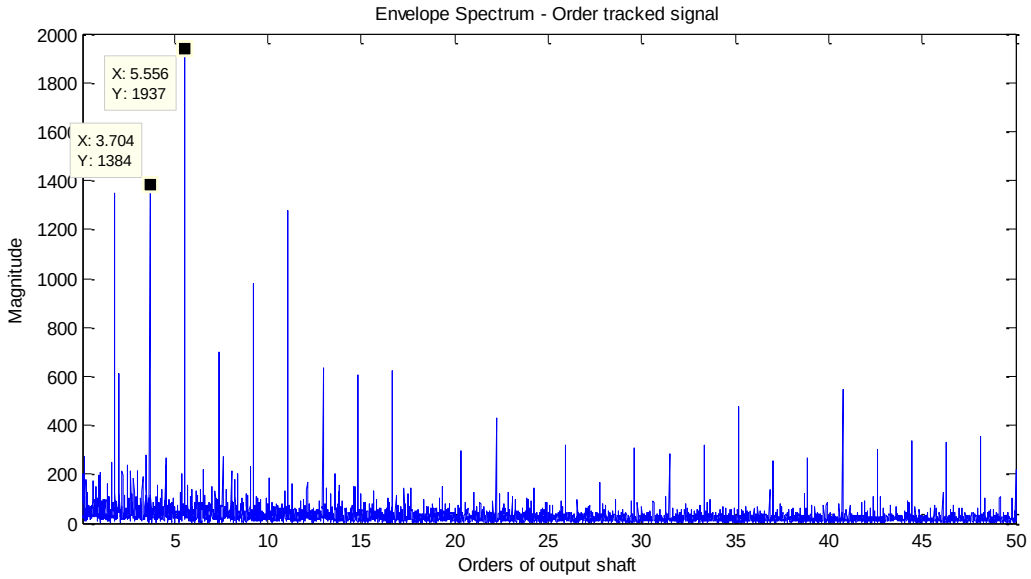

Figure 30: Envelope spectrum after bandpass filtering

The peaks are less prominent as compared with Figure 26, however the suspected fault is more clear in the higher harmonics. The sideband spacing is unchanged. The impulsiveness found by FK may have been attributed to another component in the test rig, possibly an electrical interference.

The next constant speed section at higher input shaft frequency ($23\ Hz$) was also analysed in the same fashion. After order tracking and carrying out TSA, the envelope spectrum of residual signal was expected to be similar. Because the previous signal analysed did not require bandpass filtering, this data set was not filtered for comparison. The envelope spectrum is shown below.

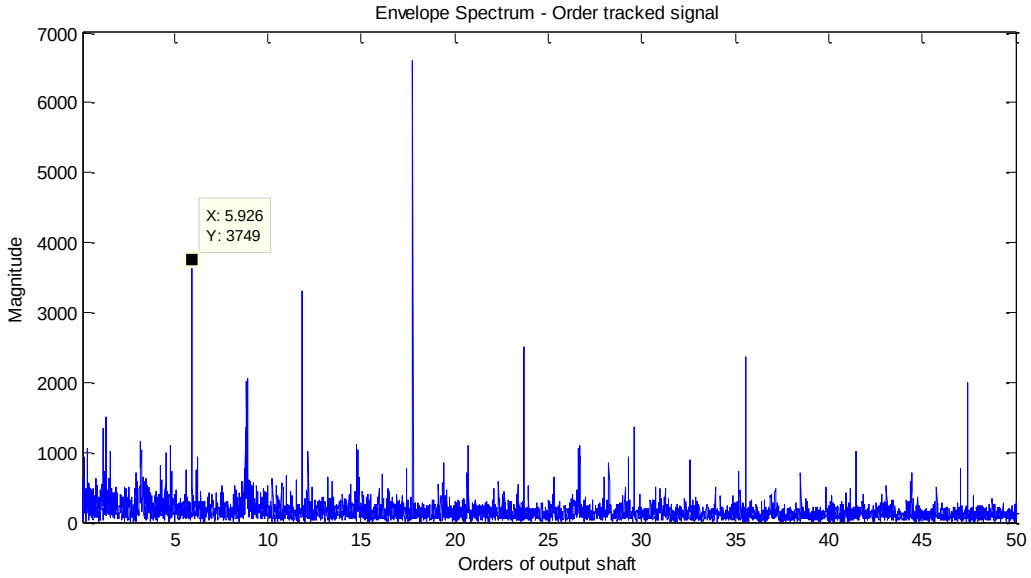

Figure 31: Envelope spectrum before bandpass filtering (higher constant speed)

The resulting envelope spectrum is not as uniform as the previous case and the clear sidebands that were present are no longer apparent. It should also be noted that the order of output shaft speed attributed to possible evidence of bearing fault has changed slightly and may be caused by a change in load on the bearing. After this result, it is difficult to use this as evidence of a bearing fault as the order of output shaft speed results in harmonics is just above $244\ Hz$ which is a 8.67% deviation from the calculated value of BPFI at this frequency ($23\ Hz$ input shaft speed). Another FK and PSD comparison is made below to determine the suitability of the band suggested by FK.

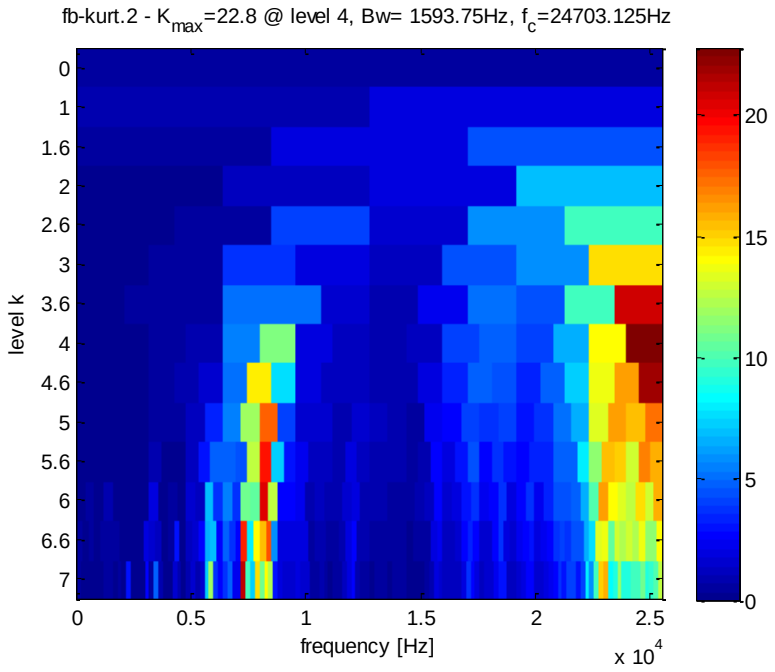

Figure 32: FK for band selection at higher constant speed

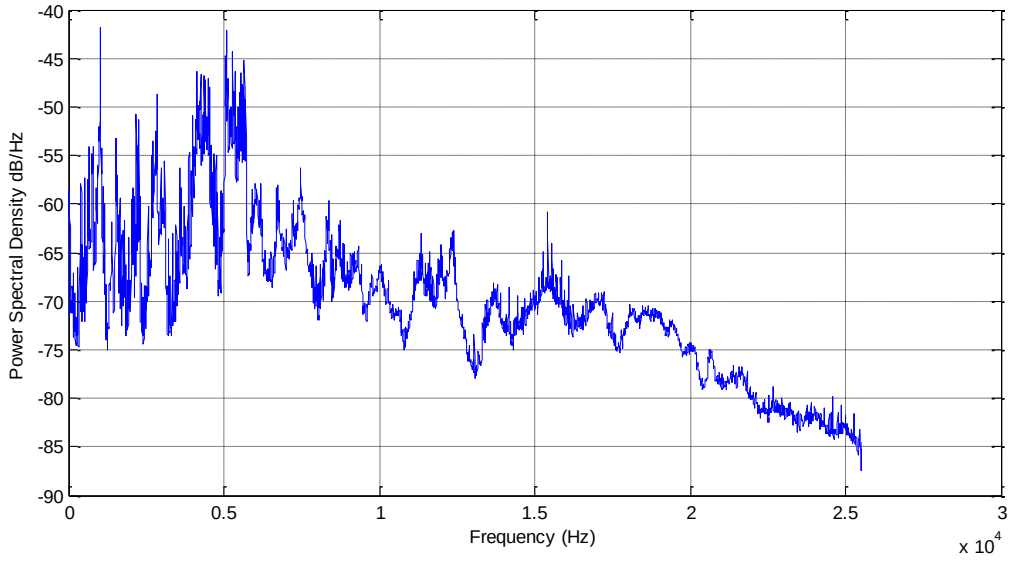

Figure 33: PSD of constant speed data at higher speed

FK revealed two impulsive bands, unlike the slower output shaft frequency. The most impulsive was found at a centre frequency of $f_c = 24{,}703\,Hz$ with a bandwidth of $Bw = 1{,}594\,Hz$, and the second at approximately $f_c = 7{,}275\,Hz$ with a bandwidth of $Bw = 185\,Hz$. The envelope spectrum of the filtered signal using the most impulsive frequency band revealed the following result:

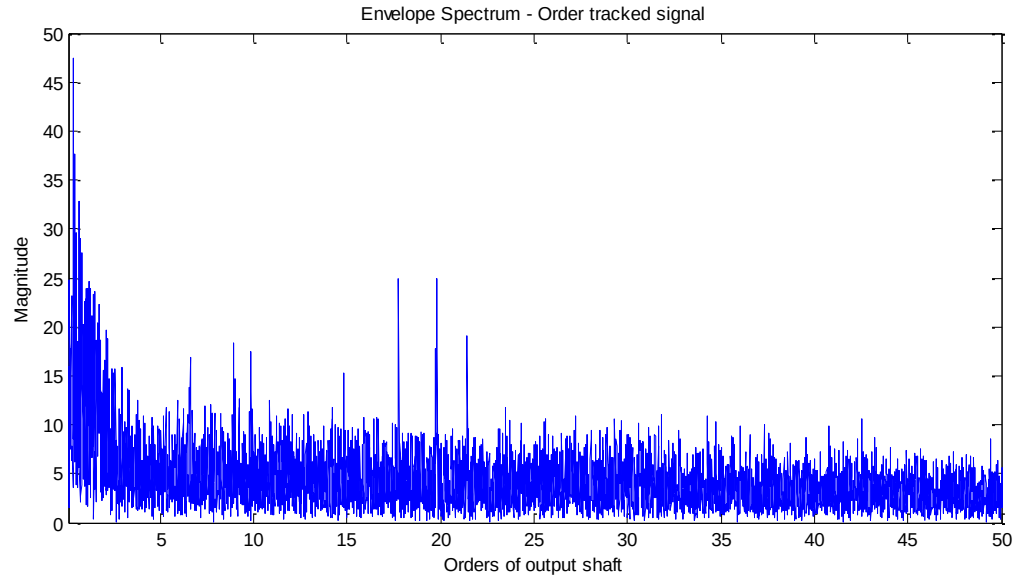

Figure 34: Envelope spectrum after bandpass filtering 1 (higher constant speed)

The fault is no longer clear in the above figure which suggests the most impulsive band selected was not a result of the bearing fault. The second impulsive band was used and resulted in the following envelope spectrum:

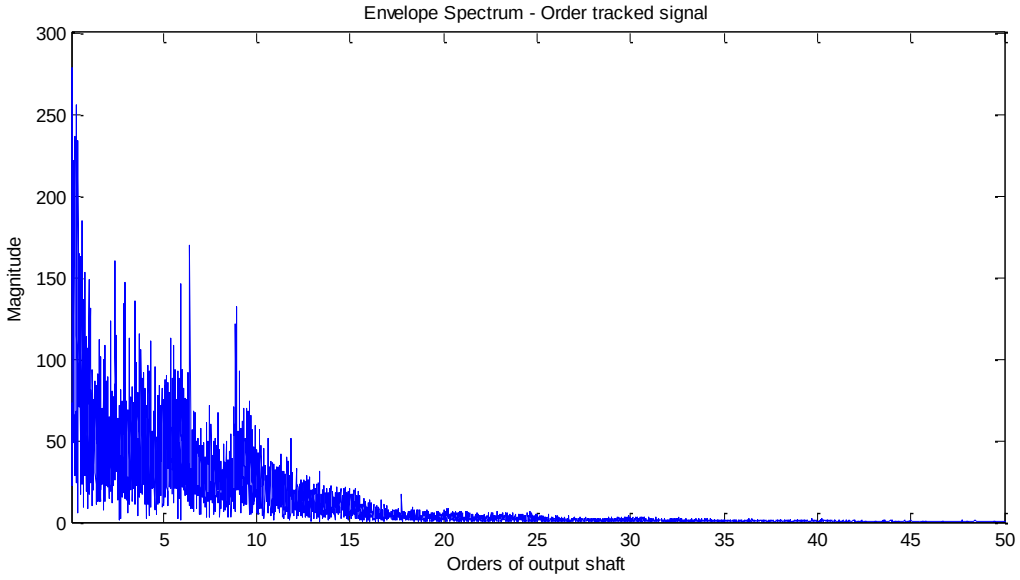

Figure 35: Envelope spectrum after bandpass filtering 2 (higher constant speed)

The selected band did not reveal the bearing fault in this case either. This may suggest that another component in the rig was responsible for this vibration. The Fast Kurtogram did not effectively allow a successful band selection under constant speed based on the obtained results therefore, it remains to be seen if the bearing fault can be found in the variable speed

portion of the recorded signal using FK. Selecting a band from visual inspection of the PSD was briefly explored below to determine the extent of the FK short-coming. The band between 5,012 and 5,715 Hz was selected to filter the signal (as seen in Figure 36). The envelope spectrum can be seen in Figure 37.

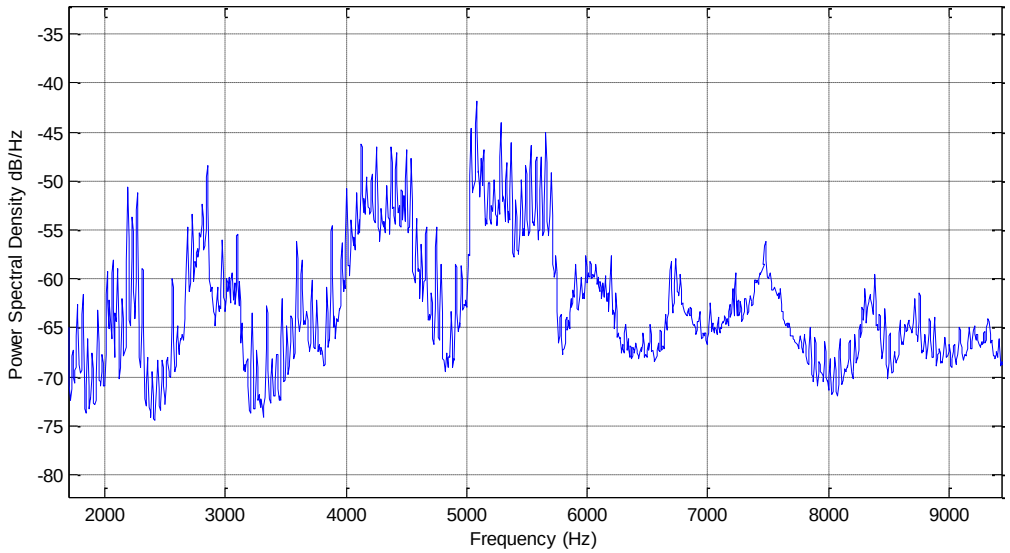

Figure 36: PSD of constant speed data at higher speed - zoom

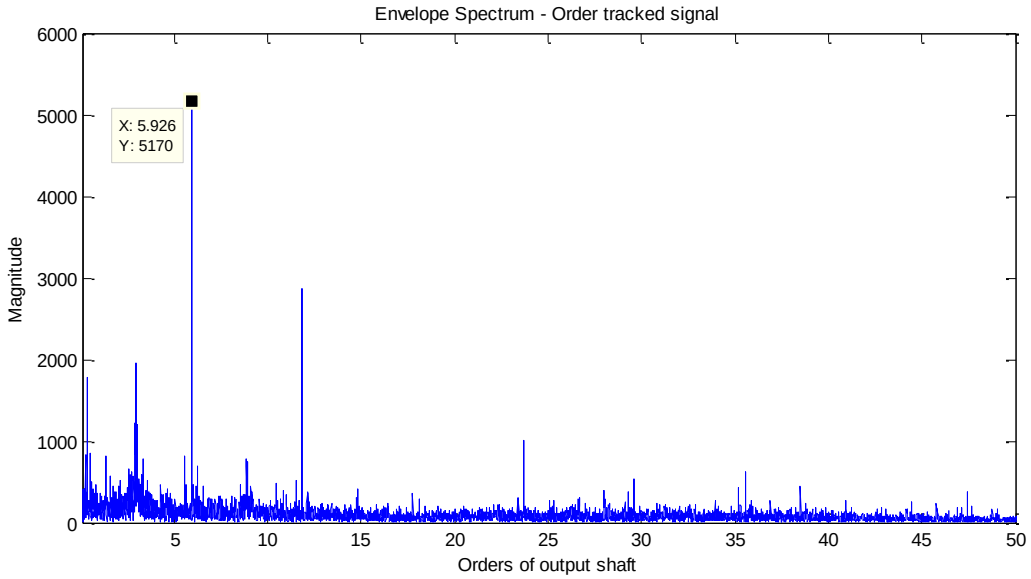

Figure 37: Envelope spectrum with manual bandpass filtering

If the dominant component is in fact the bearing fault, it represents more slip than usual (1-2% typically) which is not convincing. Manual selection of the band for filtering revealed this dominant component more so than FK in this case. The constant speed results are further discussed in Section 4.3.

4.2 Variable Speed Analysis of Spur Gearbox

This section analyses the variable speed portions of the signals obtained during experiments on the spur gearbox. It should be noted the frequency of the motor was controlled by a linear potentiometer which was connected to the variable frequency drive. The potentiometer was manually operated and therefore gave rise to deviations from the frequency ($\sim \pm 1\ Hz$) and timing ($\sim \pm 1\ s$) of all the experiments carried out under variable speed.

4.2.1 Test Set 1

In this section, the different ramp up speeds are analysed and discussed.

4.2.1.1 Linear ramp-up over 20 seconds

The first test in this Test Set was a linear ramp up in frequency from $15\ Hz$ to $23\ Hz$ over 20 seconds. The figure below reveals the gradual increase in magnitude of the vibration over the 20 second extract from the linear increase in shaft frequency.

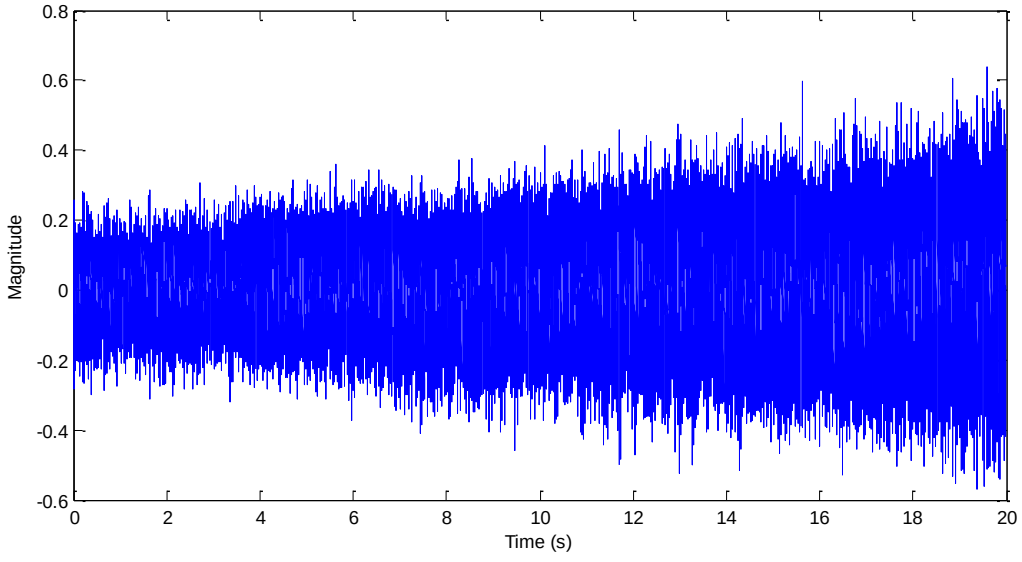

Figure 38: Waveform of variable speed

Much like the constant speed waveform, the variable speed waveform does not provide clear impulsiveness. There is a clear increase in magnitude with time. The raw spectrum is illustrated in the next figure:

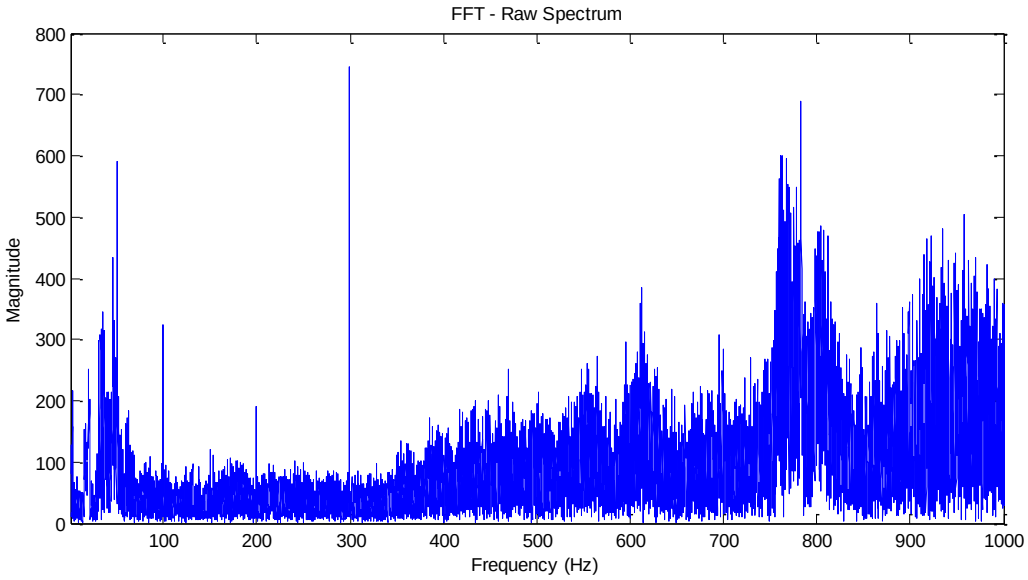

Figure 39: Raw spectrum of variable speed

The frequencies are smeared due to the variable speed and as previously discussed, makes analysis more difficult requiring a different order of data processing.

The clear peaks at $50, 100, 200$ and $300\ Hz$ that do not appear smeared are a result of electromagnetic interference from the supply frequency of $50\ Hz$ since this is constant in time as opposed to the mechanical and VFD frequencies changing with time. This may be the cause of the harmonics in the envelope spectra.

The envelope spectrum of the full band without order tracking and TSA need not be shown as it does not yield useful results. The variable speed analysis followed the procedure outlined in Section 3.5, i.e. performing FK for bandpass filtering, followed by order tracking and TSA to finally use the envelope analysis.

The constant speed analysis in Section 4.2.2 indicated that FK may be revealing impulsive bands in the signal that did not seem to be attributed to the bearing fault and that there may be electromagnetic interference, which is evident in the raw spectrum in this case. The figure below reveals the envelope spectrum without bandpass filtering for this variable speed condition.

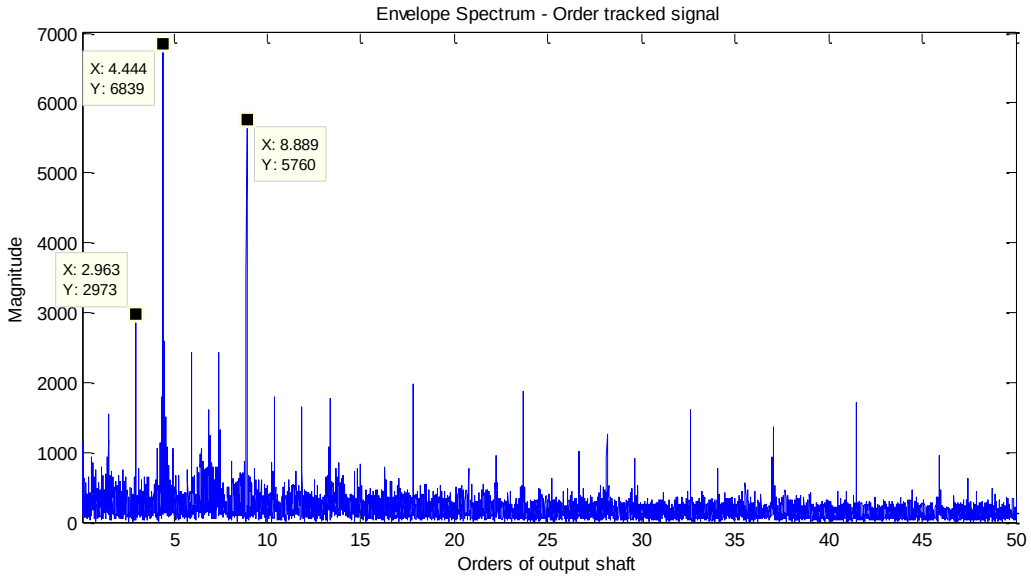

Figure 40: Envelope spectrum without bandpass filtering at variable speed (20 second ramp)

The first two harmonics of 4.444 orders of output shaft are clearly seen from the envelope spectrum without bandpass filtering. A closer look at the fundamental bearing fault frequencies (equations $4-7$) revealed the possibility that these harmonics were very close to BSF. There is a possibility that the rolling elements of the healthy bearings were damaged as they did not have seals protecting the cage and rolling elements, however this is very unlikely. The component at 5.926 orders and its harmonics are clear but not as prominent as the other peaks aforementioned.

Deep groove ball bearings are designed to have some clearance in an unloaded condition, which suggests there may be some axial loading in this condition. This can result in a change in the load angle and therefore a deviation from BPFI (and BSF if a fault was present). The load experienced by the bearing could be considered low at an average recorded torque value of $8\ N.m$, which was calculated as a load of approximately $100\ N$ on each bearing, not much more than the gravitational load. The dynamic load rating of the bearing is $5.85\ kN$. The load angle could have changed during the acceleration period, and this would have affected BPFI such that an increase in load angle from $0°$ would have caused the value of BPFI in terms of orders of output shaft to decrease. It is unclear these harmonics are due to the bearing fault in the system and if they are, the significant deviation from the calculated BPFI may be a result of a large amount of slip during the acceleration.

The following figure reveals the variable speed FK and PSD of the variable speed condition for bandpass filtering:

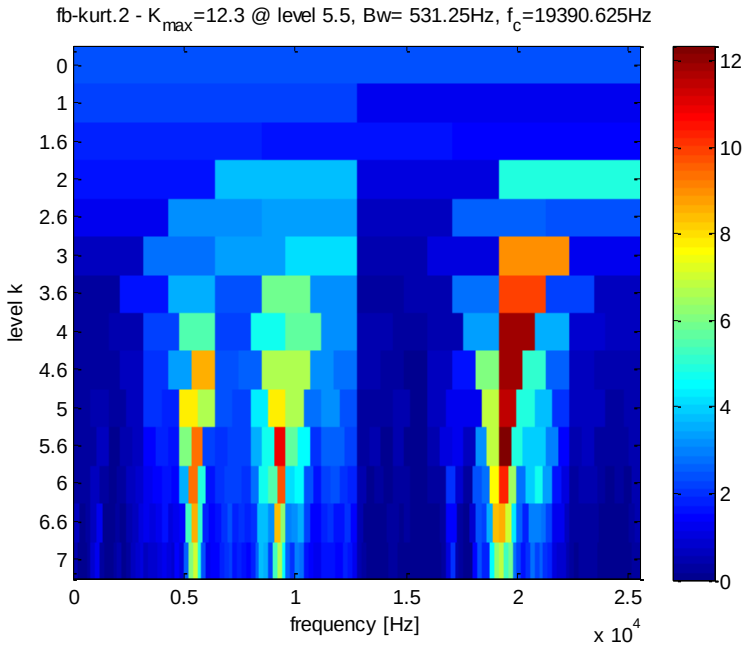

Figure 41: FK at variable speed (20 second ramp)

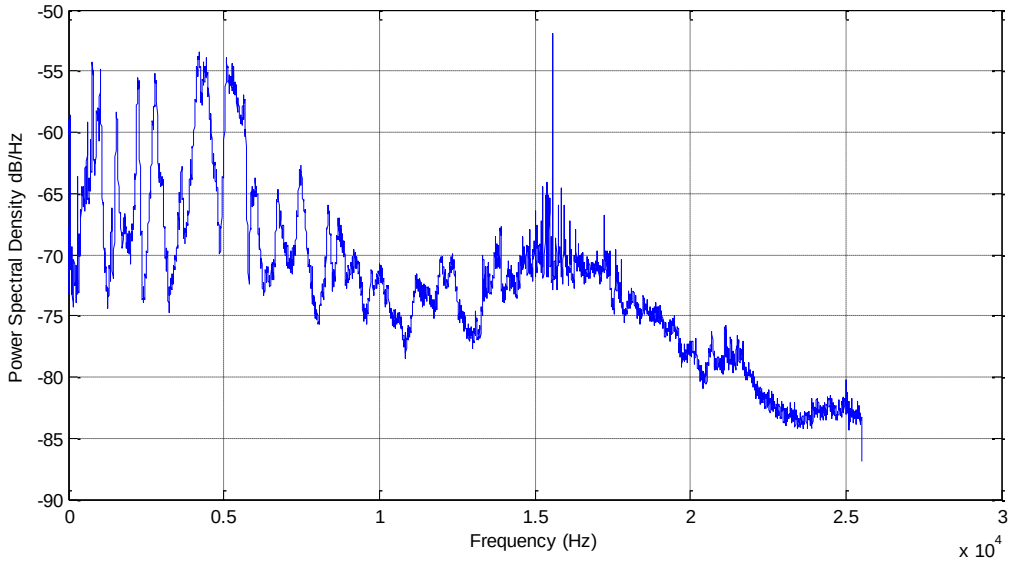

Figure 42: PSD of variable speed data (20 second ramp)

FK revealed the most impulsive band to be at $f_c = 19{,}390\ Hz$ with a bandwidth of $Bw = 531\ Hz$. In the case that the signal was filtered using the band suggested by FK in Figure 41, the following envelope spectrum results:

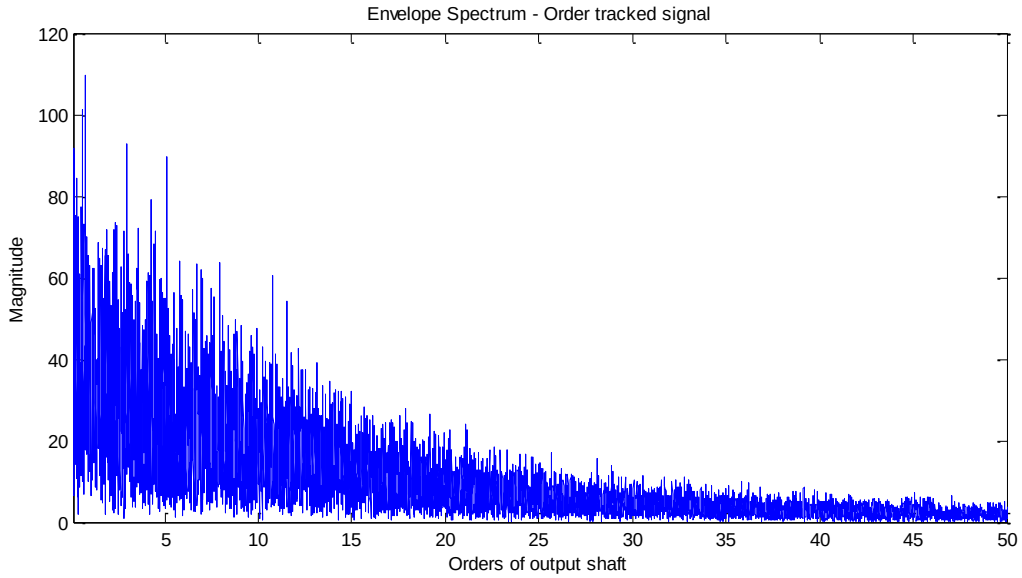

Figure 43: Envelope spectrum with bandpass filtering at variable speed (20 second ramp)

The result is an unclear envelope spectrum. The second most impulsive band found from FK in Figure 41 at the lower frequencies ($\sim$9,300 Hz) was also investigated and revealed the following envelope spectrum:

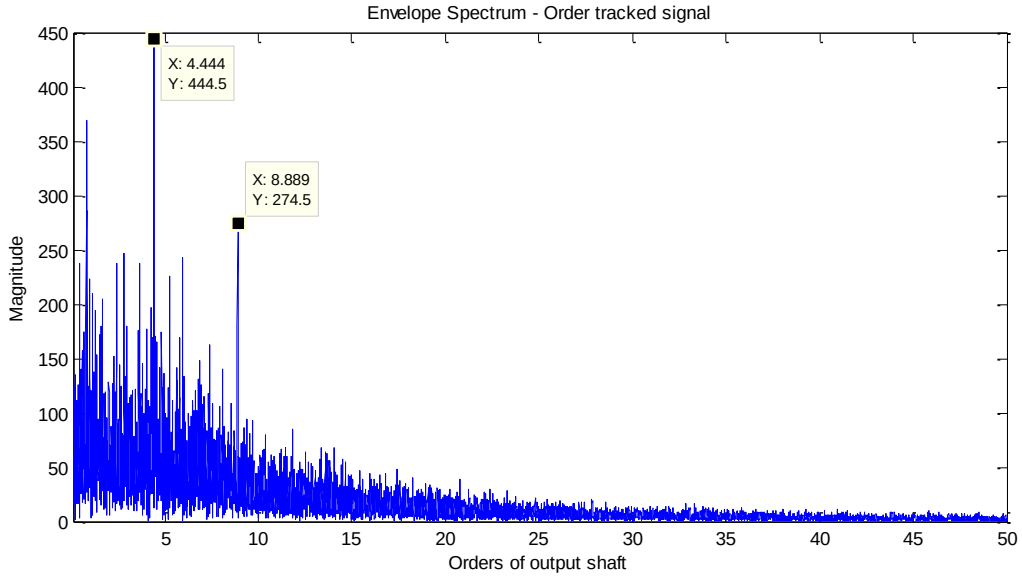

Figure 44: Envelope spectrum with bandpass filtering at variable speed 2 (20 second ramp)

In this case, the first two harmonics of 4.444 orders of output shaft were present once again. BPFI was not found and the use of the Fast Kurtogram did not prove beneficial. This

therefore raises the question of usefulness of the Fast Kurtogram for bandpass filtering in this application. Analysis on the remaining data obtained can confirm this finding.

Filtering with the band between 3,813 and 4,837 Hz from visual inspection of the PSD (Figure 45) provided a clearer envelope spectrum (Figure 46) than FK, but revealed the same harmonics of 4.444 orders of output shaft speed with a faint trace of 5.926 orders.

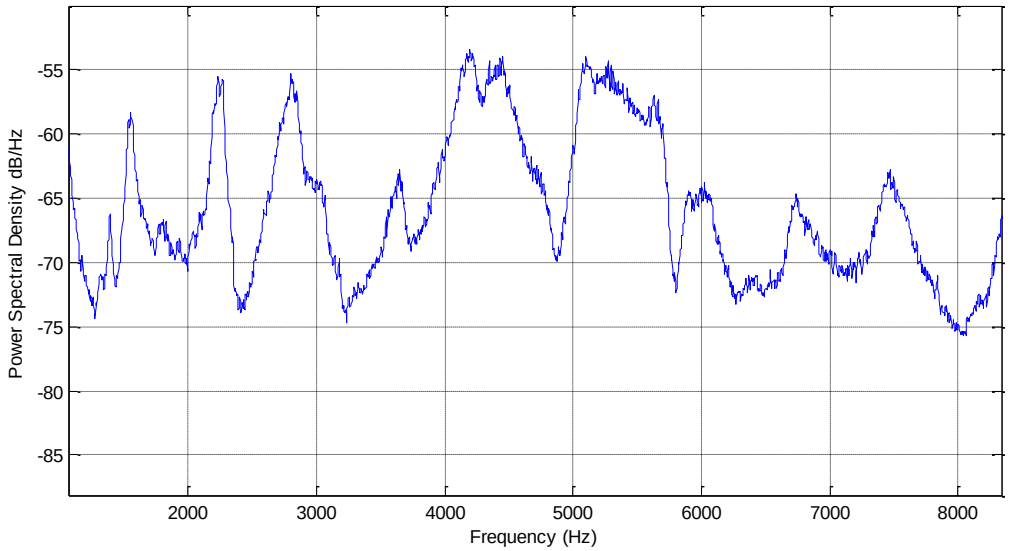

Figure 45: PSD of variable speed data (20 second ramp)

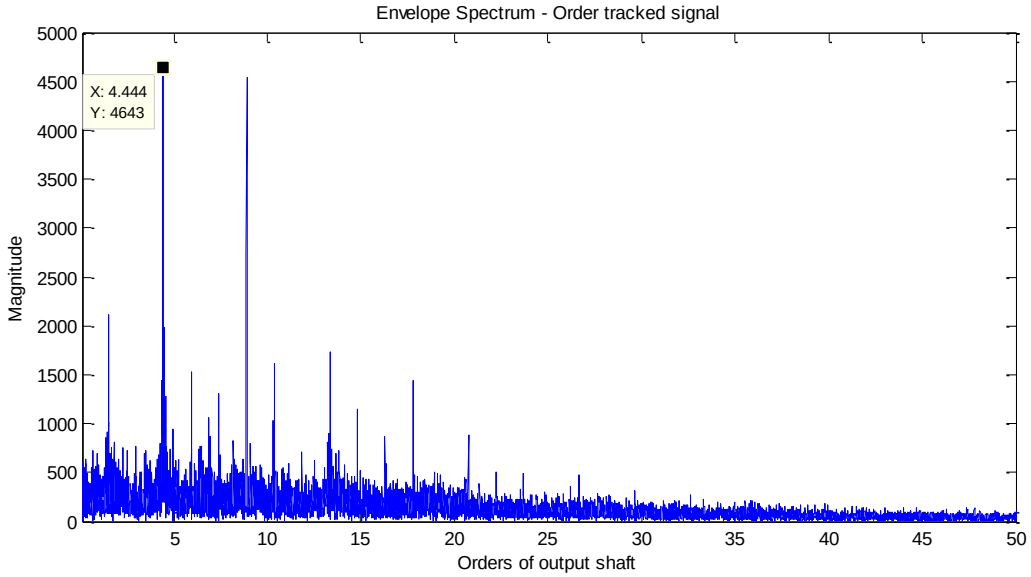

Figure 46: Envelope spectrum with manual bandpass filtering (20 second ramp)

Neither technique (FK or PSD) have uncovered the fault, although it could be said that manually filtering has somewhat exposed a periodic modulation with an unknown root cause.

4.2.1.2 Linear ramp-up over 10 seconds

In this test, the linear ramp-up occurred in a shorter timeframe, i.e. 10 seconds. FK and PSD plots are found below. While it is becoming clear FK is not suitable in this application, it is still shown to reveal the impulsive bands picked up for comparison with the other test cases.

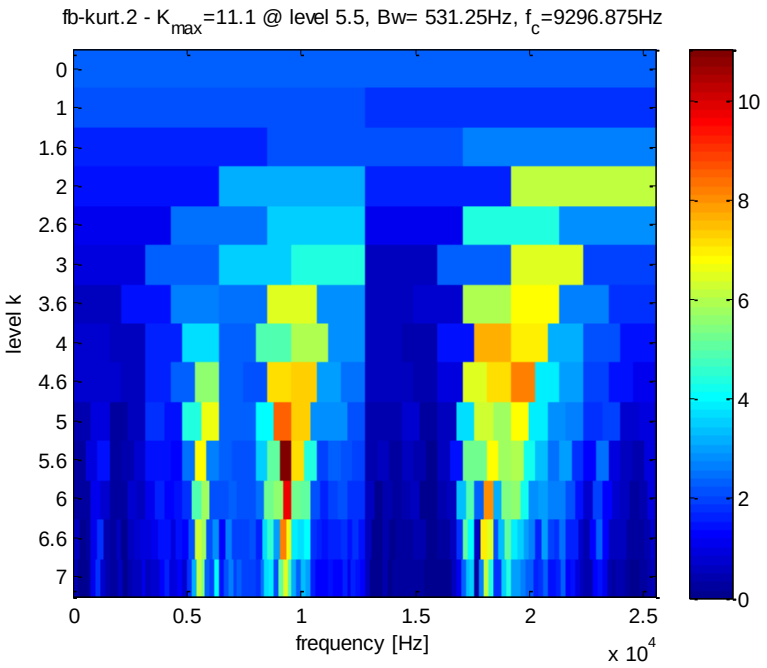

Figure 47: FK of variable speed (10 second ramp)

It can be seen that between the 20 second ramp-up and 10 second-ramp up FK that impulsive bands are found in approximately the same frequency ranges. A comparison in PSD from both cases is shown below. Different window lengths were used for each case for clarity.

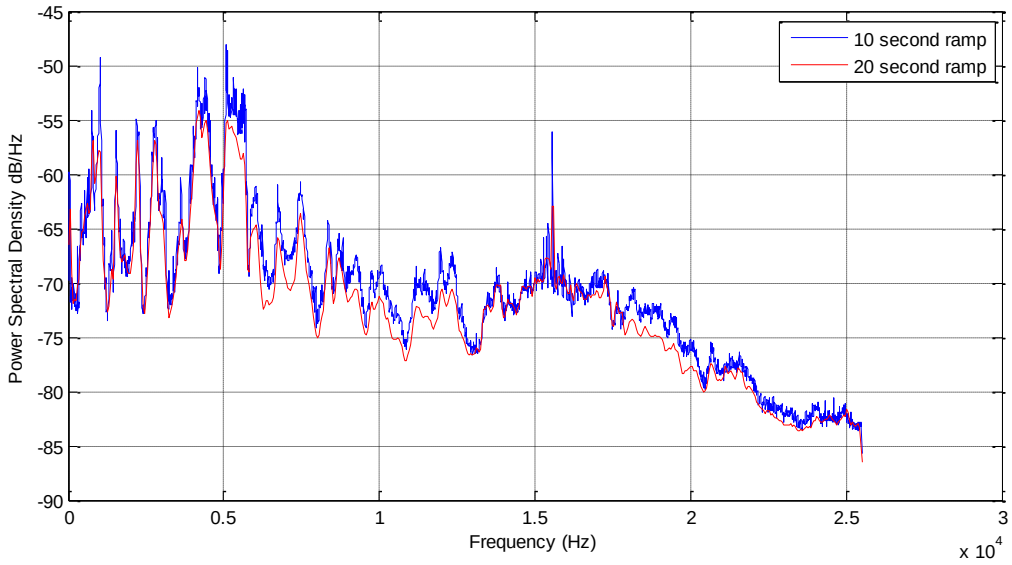

Figure 48: PSD comparison

The comparison reveals that both signals have approximately the same PSD. This allows the use of the same band as the previous case to allow better detection of the fault. The plots below reveal the difference obtained with and without (manual) bandpass filtering:

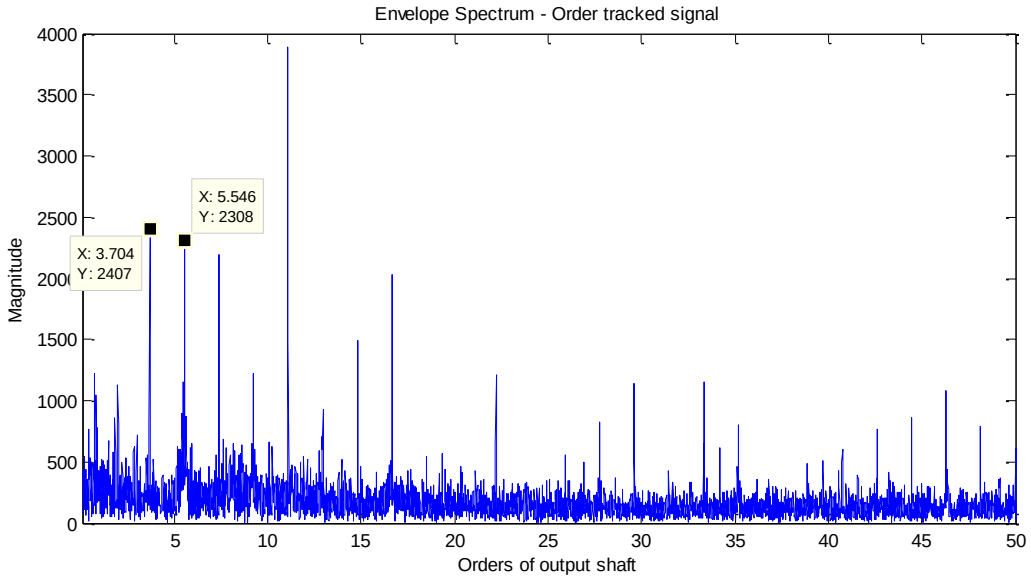

Figure 49: Envelope spectrum without bandpass filtering at variable speed (10 second ramp)

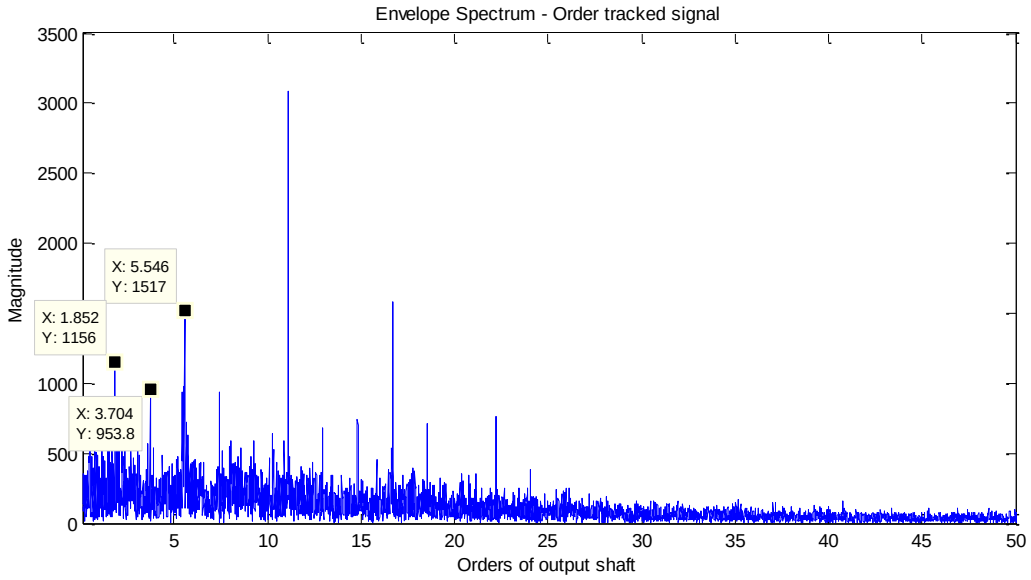

Figure 50: Envelope spectrum with manual bandpass filtering (10 second ramp)

The unfiltered signal revealed the harmonics of 5.546 orders of output shaft speed in this case and filtering using the same user selected band as the previous test has made the 3.704 orders of output shaft speed and its harmonics less prominent. In this instance, the orders changed from 5.926 to 5.546. There is reason to believe that this change is not a result of changing conditions that affects BPFI but rather electromagnetic interference as explained in Section 4.2.1.1.

4.2.1.3 Linear ramp-up over 5 seconds

For the remaining ramp-up test over a 5 second interval, the FK revealed the same impulsive bands as the latter case however the most impulsive band was now at $\sim 21\ kHz$. The PSD also returned the same basic shape as the two latter cases. The envelope spectrum of this data set also revealed clear harmonics of 5.556 orders of shaft speed and harmonics of 3.704 orders of output shaft speed once again with and without bandpass filtering.

The results of all the linear tests are discussed further in Section 4.3.

4.2.2 Test Set 2

In this section, the undulating speed profiles are analysed and discussed.

4.2.2.1 Undulating speed profile about Mean 1

The first test of an undulating speed profile was carried out about a mean of $15\,Hz$ nominal input shaft which varied by $\pm 20\%$ from 12 to $18\,Hz$. It should be noted the changes in frequency in this experiment were non-linear as compared to the earlier tests. The first 5 seconds of the variable speed portion of the signal was extracted and the raw signal waveform is shown below. This portion of the signal represents approximately a quarter cycle of a sinusoid increasing speed from the mean of $15\,Hz$ to maximum of $18\,Hz$ input shaft speed. It can be seen the magnitude is increasing with time.

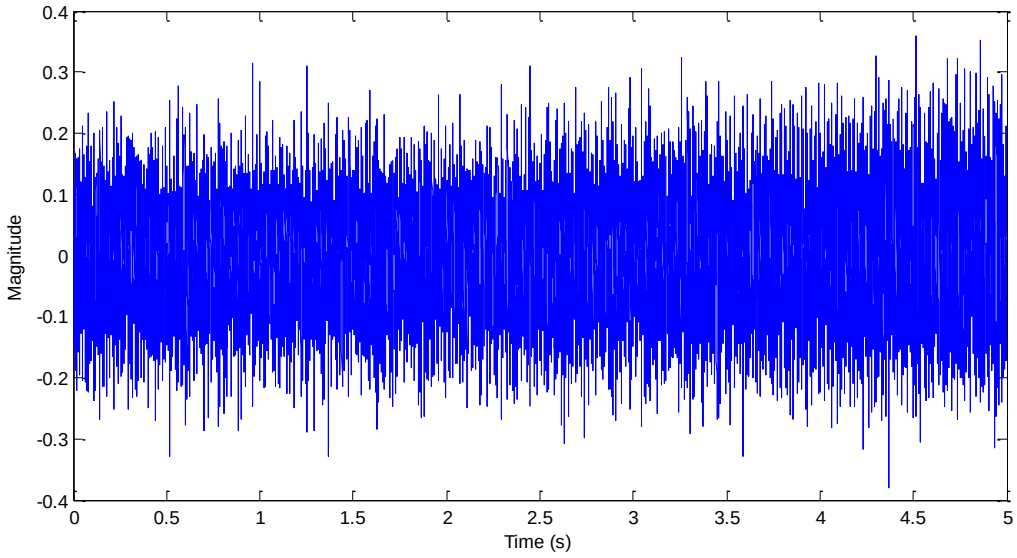

Figure 51: Waveform of variable speed (5 second extract)

Without bandpass filtering, order tracking and TSA were applied to reveal the envelope spectrum illustrated below. The possibility of the bearing fault is clear, starting at 5.556 orders of output shaft speed.

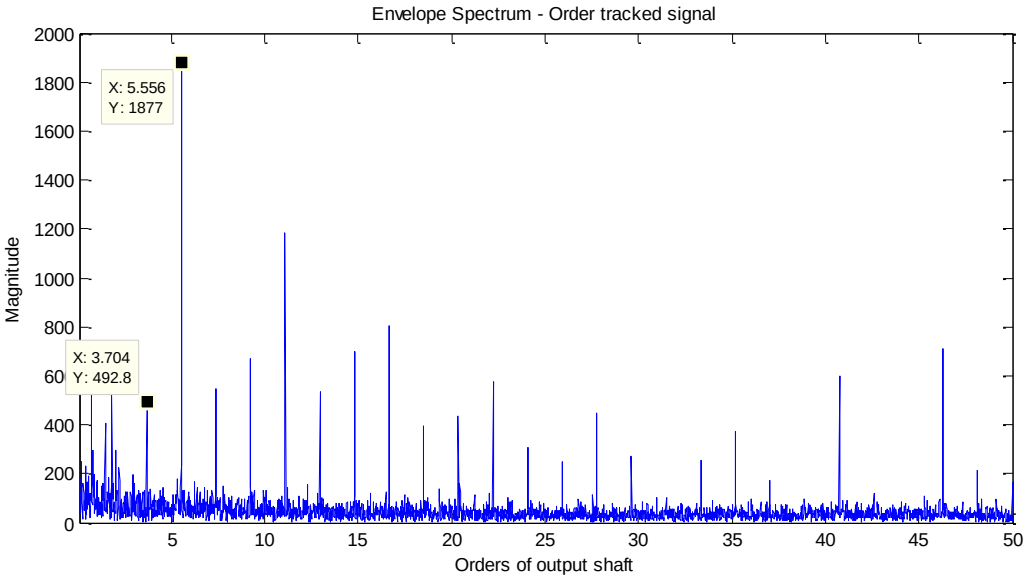

Figure 52: Envelope spectrum without bandpass filtering at variable speed (5 second extract)

While harmonics of possible fault frequency were clear, so too were harmonics of 1.852 orders of output shaft speed. Sidebands are expected to be seen at shaft speed however are not apparent. Following this result, a larger extract was taken to include approximately three quarters of a cycle of the input shaft frequency, as can be seen from the waveform below. This was to verify if the change in average shaft speed would influence the harmonics that seem to be evident in the constant speed data.

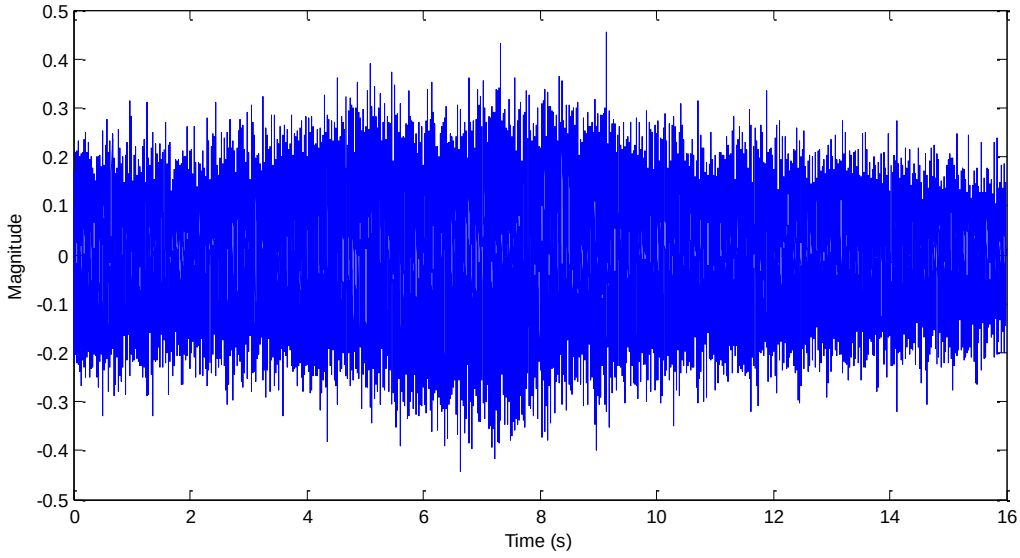

Figure 53: Waveform of variable speed (16 second extract)

FK revealed only one impulsive band at approximately 20 kHz.The PSD once again showed strong discrete frequencies at approximately 15 kHz. Bandpass filtering using FK did not yield useful results once again. The envelope spectrum of the unfiltered signal is shown below.

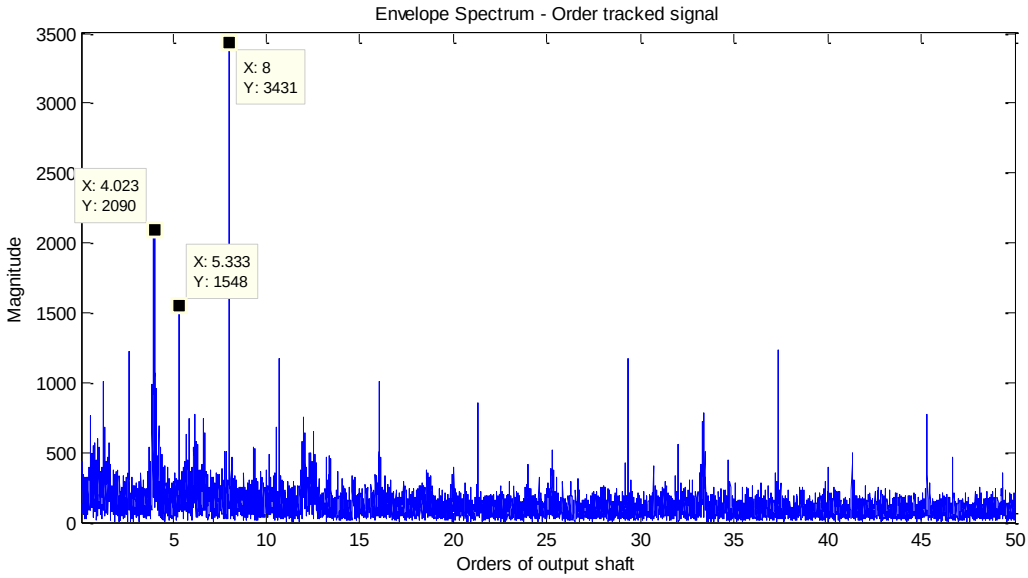

Figure 54: Envelope spectrum without bandpass filtering of variable speed (16 second extract)

Harmonics of 5.333 orders of output shaft speed can be clearly seen with clear peaks at 4 and 8 orders. A final attempted was made to investigate a change in harmonics with a larger extract of the recorded signal all over variable speed and revealed the same envelope spectrum with the same harmonics found in Figure 54 above.

4.2.2.2 Undulating speed profile about Mean 2

The second test of an undulating speed profile was carried out about a mean of 23 Hz nominal input shaft which varied by $\pm 20\%$ from 18 to 27 Hz. The average torque value recorded was 16 $N.m$. It should be noted the changes in frequency in this experiment were non-linear as compared to the linear ramp tests. The first 10 seconds of the variable speed portion of the signal was extracted and the raw signal waveform is shown below. It can be seen the magnitude is increasing and decreasing with time.

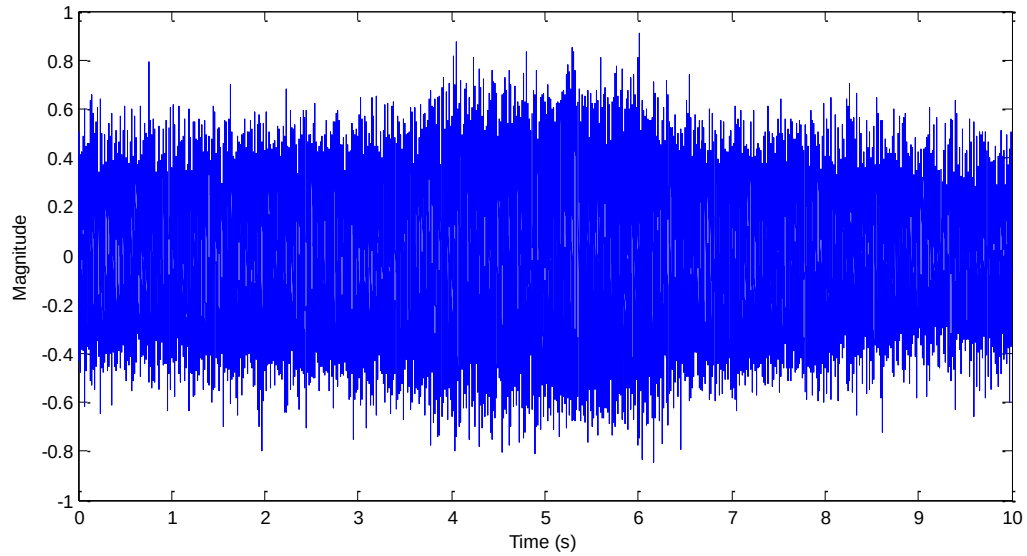

Figure 55: Waveform of variable speed (10 second extract)

As it was clearly established FK was not useful in determining the impulsive band containing the bearing fault and the PSD yielded better filtering results. Therefore, the order tracked and TSA applied techniques to extract the residual signal were carried out for the full band for the envelope spectrum found below.

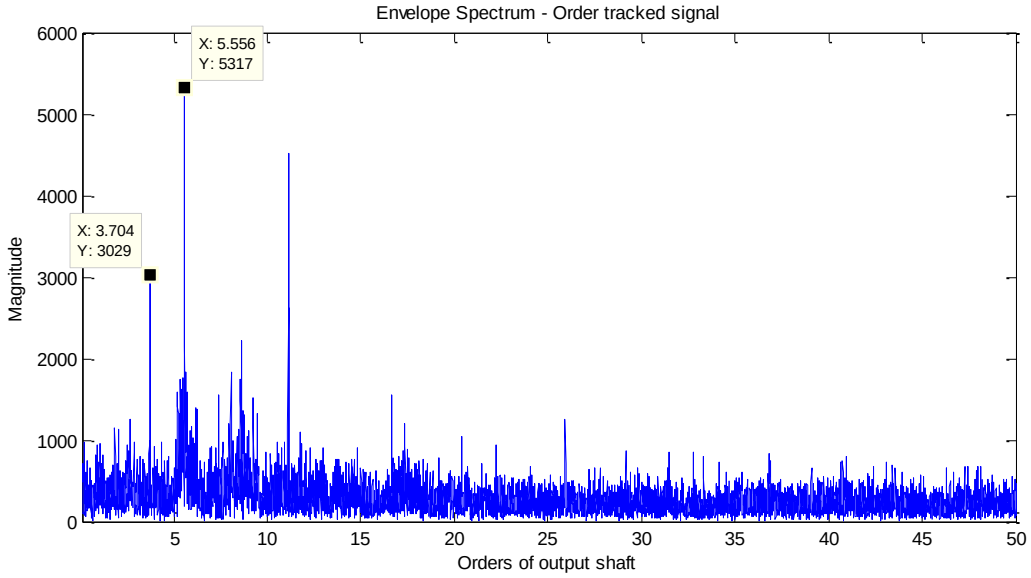

Figure 56: Envelope spectrum without bandpass filtering at variable speed (10 second extract)

Harmonics of 1.852 and 5.556 orders of output shaft speed were present once again. As discussed in the following section, it was thought this was not indicative of the fault.

4.3 Discussion of Spur Gearbox

The results obtained from the experiments could lead to the conclusion that the bearing fault (BPFI) was successfully found. However, the variations found in the results were evidence that the fault may not have been the cause of the prominent harmonics found in the envelope spectra. There are a few key considerations that would make the diagnosis of a bearing fault for this test rig inconclusive.

The first of these considerations is the expected modulation frequency. The modulation frequency is expected to be exactly 1.000 orders of output shaft speed. The strength of the impulse caused by the rolling elements striking the fault is dependent on the load borne by them and is modulated by the rate at which the fault is passing through the load zone [1]. In these experiments, the load recorded was considered low when compared to the rated load capacities of the bearings ($100\,N$ load on the bearings with a dynamic load rating of $5.85\,kN$) and the bearing fault frequency should have been modulated by the output shaft frequency since this is the shaft on which the bearing was located. Therefore, this consideration of load amount and modulation points to the possibility that the rolling elements were not interacting with the fault present on the inner race. The sidebands that were expected in the envelope spectrum at 1.000 orders of output shaft speed were never found but rather, harmonics of 1.852 orders.

Electromagnetic interference is known to play a role in the ability to successfully diagnose bearing faults [31]. The raw spectrum at constant speeds did not reveal large peaks at harmonics of supply frequency as compared to variable speed, however large discrete frequencies were visible in the power spectrum densities for the constant speed data. It is co-incidence that at $15\,Hz$ input shaft speed, BPFI is calculated to be close to $150\,Hz$ which makes it possible harmonics of supply frequency are interfering with the bearing fault frequency. However, when considering the load and modulation as stated above, this does not seem likely.

A simple way around this conundrum would be to obtain baseline data on the test rig without the presence of a defective gear and bearing to establish a clear comparison. Due to time constraints, the time required to assemble and disassemble the rig and eventual breakdown of the rig made this difficult to achieve.

It remains likely that the results obtained from these experiments were affected by electromagnetic interference as the only constant in time was the supply frequency. The mechanical and VFD frequencies were changing during the variable speed tests and may have been interacting with the supply frequency to reveal the results obtained. Future tests with outer race faults could also shed more light on this phenomenon as the outer race fault frequency would be different enough in terms of orders of output shaft to establish whether these results are due to interference.

The Fast Kurtogram in each of the data sets obtained did not prove useful. On each occasion, the impulsive bands of the signals were comparable but investigation of each impulsive band did not yield informative results. Rather, the use of PSD and manual selection of bands were more successful for filtering. With an externally mounted accelerometer, it is likely the data set contained impulsive signals that were caused by other components of the test rig. This has potential implications when dealing with diagnosis in industry as the FK could very well respond to signals that are not caused by faults in a system and therefore not reveal if faults were present.

Based on the inconclusive results of this experiment and inability to explore this phenomenon in more depth, further testing was carried out on the UNSW planetary gearbox testing rig. The results and discussion of the experiments carried out on the planetary gearbox are found in the next section.

4.4 Preliminary Analysis of Planetary Gearbox

In this section, the theoretical frequencies are calculated and compared with constant speed data to establish if the fault is diagnosable.

4.4.1 Theoretical Frequencies

The frequency that is relevant for this experiment is the Ball Pass Frequency for an Outer Race fault. The formula is given by equation (12):

$$BPFO = \frac{n}{2}\left\{(f_i - f_o)\left(1 - \frac{d}{D}cos\phi\right)\right\}$$

where f_o and f_i are the planet bearing outer race and inner race speeds; planet gear and carrier speeds respectively. The gear tooth numbers are known and listed in Table 5 (Section 3.3.1). The bearing dimensions are known and listed in Table 6 (Section 3.3.2). The gear tooth numbers allow the calculation of f_o and f_i using the following equations [32]:

Carrier frequency $f_i = f_c$:

$$f_c = f_{input}\left(-\frac{N_{pinion}}{N_{spur}}\right) = f_{input}\left(-\frac{42}{55}\right)$$

$$f_c = f_i = -0.7636 \times f_{input}$$

Absolute planet frequency $f_o = f_p$:

$$f_p = f_c\left(1 - \frac{N_R}{N_P}\right) = f_{input}\left(-\frac{42}{55}\right)\left(1 - \frac{80}{23}\right)$$

$$f_p = f_o = 1.8925 \times f_{input}$$

Substituting these values into equation (12) yields:

$$BPFO = \frac{11}{2}\left\{\left(1.8925 f_{input} - -0.7636 f_{input}\right)\left(1 - \frac{3}{19}\cos(0°)\right)\right\}$$

$$BPFO = 12.3019 \times f_{input}$$

The bearing fault frequency can be calculated using the above formula with the input frequency f_{input}. As previously mentioned, the AC motor used is 8 pole therefore the input frequency on the VFD must be divided by 4 to obtain f_{input}. Depending on the loading condition, slip may be more pronounced. This can be calculated using obvious peaks on the raw spectrum representing the gearmesh frequencies. As the number of teeth do not change, the actual input speed can be calculated and used to find the percentage slip and a more accurate number for BPFO when analysing the envelope spectrum. The gearmesh frequencies can be calculated using the following formulas [32]:

Spur gear mesh frequency (SGMF):

$$SGMF = f_{input} \times N_{pinion} = 42 \times f_{input}$$

Ring gear mesh frequency (RGMF):

$$RGMF = f_c \times N_R = 0.7636 \times 80 \times f_{input} = 61.0910 \times f_{input}$$

4.4.2 Constant Speed Data

The first experiment run was Test Set 1: a linear run-up test from a VFD input frequency of $15.74\,Hz$ to $23.00\,Hz$ where the increase in frequency took place over 30 seconds at constant acceleration. The gearbox operated at a constant frequency of $15.74\,Hz$ for the first 20 seconds after being brought to speed from zero, followed by the constant acceleration over a period of 30 seconds to a final input shaft frequency of $23\,Hz$ for the last 20 seconds before machine run-down to zero. This section outlines the analysis of the constant frequency input of $23\,Hz$ ($5.75\,Hz$ nominal input shaft frequency) using the post-processing steps outlined in Section 3.5. The following figure reveals the waveform of the signal at constant speed.

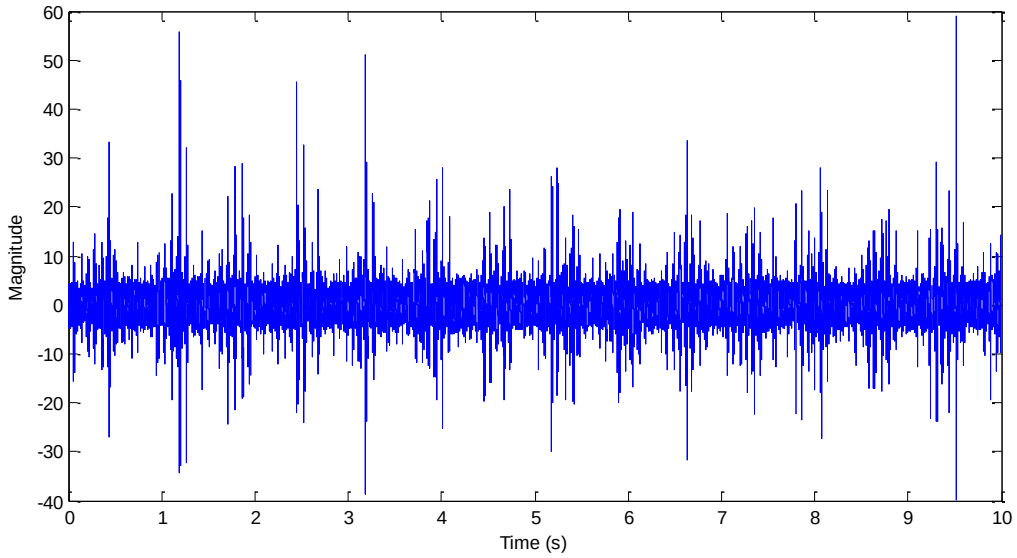

Figure 57: Waveform at constant speed

The raw waveform reveals some impulsiveness, unlike the spur gearbox, but further analysis is required to determine which component of the signal is responsible for the visible impulsiveness. The raw spectrum revealed the gearmesh frequencies and harmonics of gearmesh. No harmonics of supply frequency were found. The gear mesh frequency was used to calculate the actual input shaft frequency.

$$f_{input,actual} = 5.40\ Hz$$

This difference is a result of the induction motor slip, therefore all frequencies will be slightly different, including BPFO which will be slightly different due to bearing slip.

The envelope analysis revealed no clear fault without bandpass filtering. With filtering required to find the fault, the FK was used and is shown below.

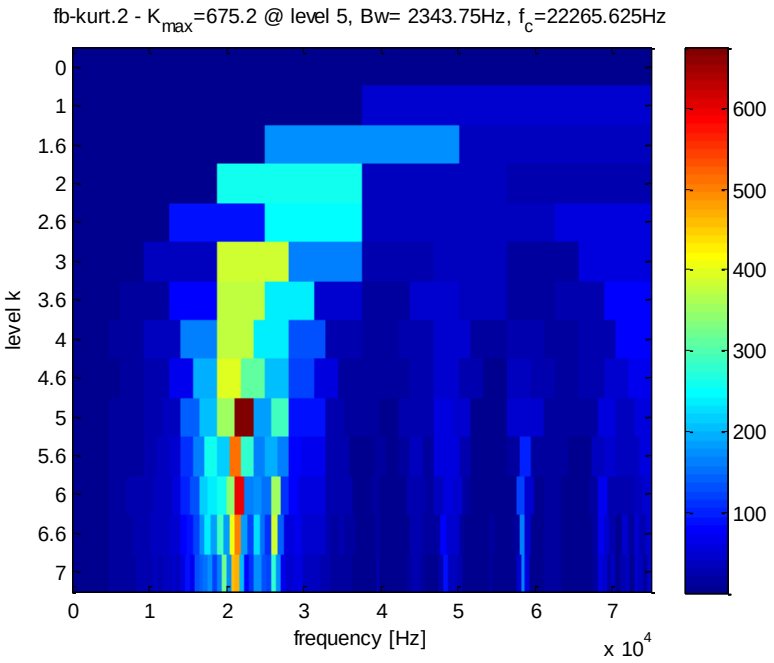

Figure 58: FK of constant speed signal

In an attempt to assess the suitability of FK in this application, the signal was filtered using the suggested band. The envelope spectrum below reveals the result.

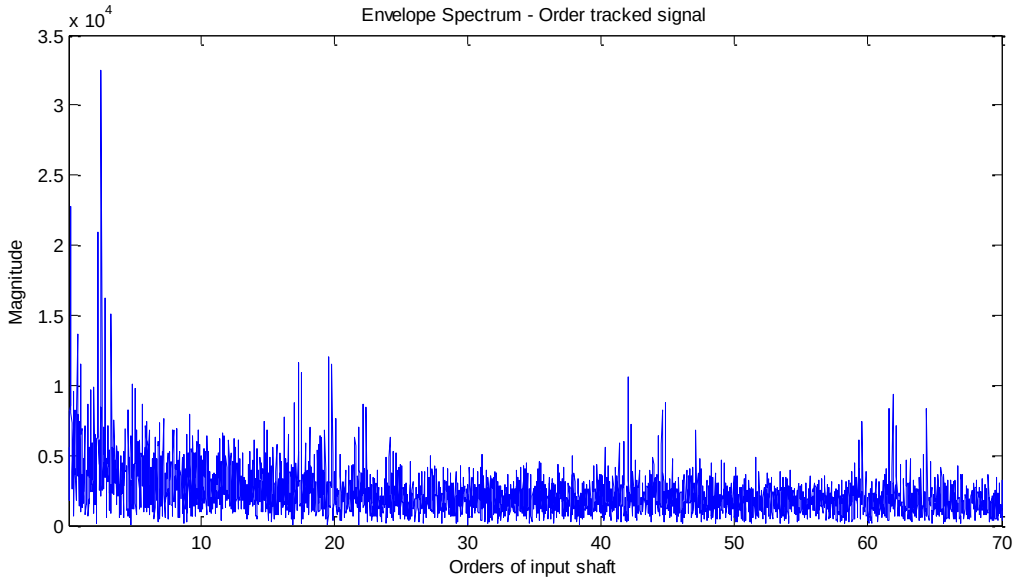

Figure 59: Envelope spectrum with bandpass filtering at constant speed

A clear peak is shown at output shaft ratio in terms of orders of input shaft speed with a value of 2.566. Aside from this finding, there are no other indications of a fault. Knowing that FK had limited use in the application of the spur gearbox as previously seen, the PSD was used

as a comparison and a seemingly more appropriate band was used for filtering. The PSD of the constant speed data is found below and reveals a clear resonance peak at approximately 49 kHz. This peak was used for filtering.

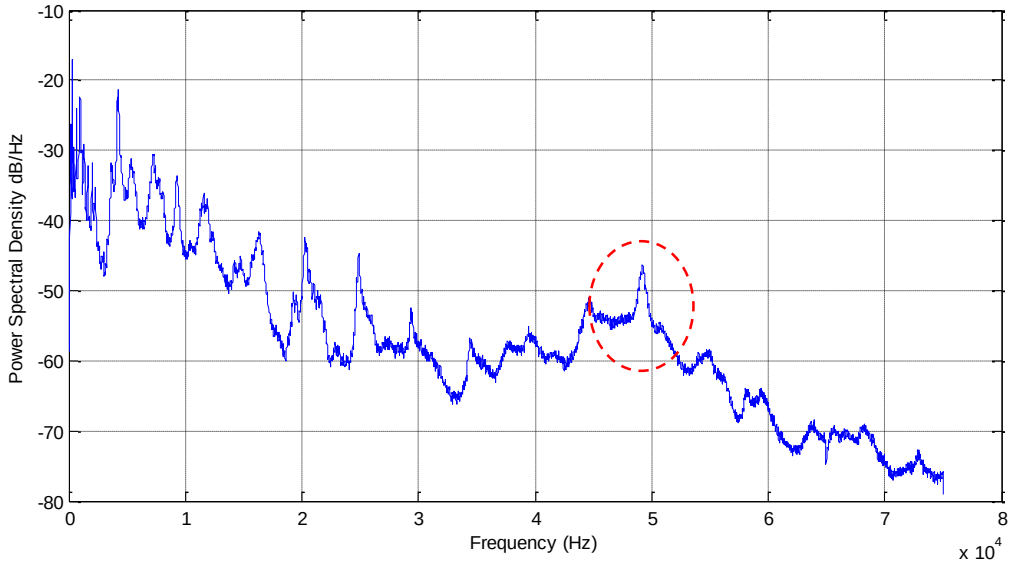

Figure 60: PSD of constant speed data

The envelope spectrum following this bandpass filtering was expected to contain peaks at BPFO harmonics. After applying order tracking, DRS and bandpass filtering, the resulting envelope spectrum illustrated below shows evidence of a fault.

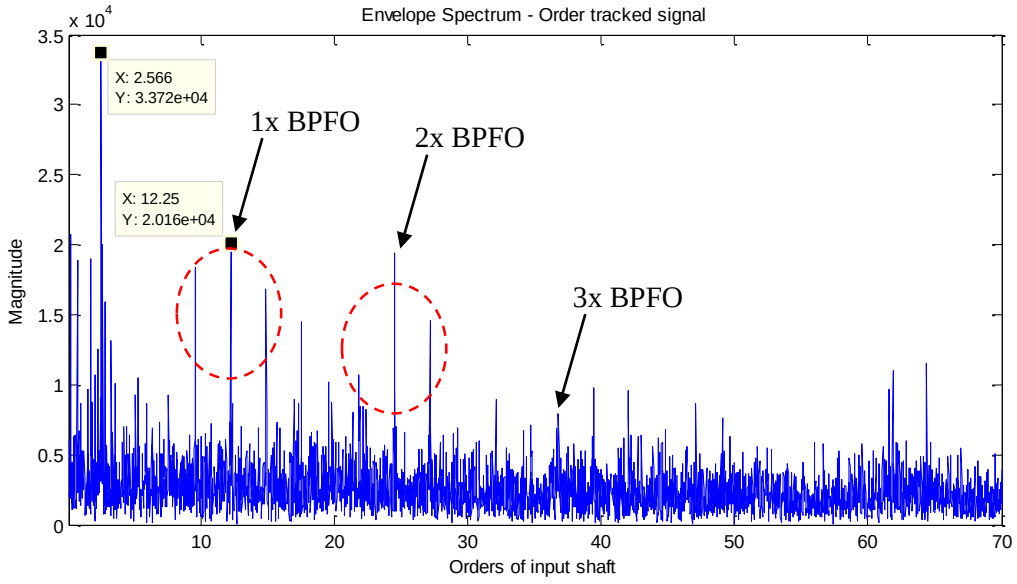

Figure 61: Envelope spectrum with manual bandpass filtering at constant speed

A strong peak of 2.566 can be found which is the ratio of output shaft in terms of orders of input shaft speed. The two next prominent peaks visible are found to be BPFO with clear sidebands (shown either side of BPFO harmonics) modulated at 2.656 which is the planet gear speed relative to the carrier ratio. This provides strong evidence of the bearing fault.

From the constant speed analysis carried out in this section, the bearing fault was and proves diagnosable. The next section explores the variable speed conditions of the experiments.

4.5 Variable Speed Analysis of Planetary Gearbox

This section analyses the variable speed portions of the signals obtained during experiments on the planetary gearbox. It should be noted the frequency of the motor in this experiment was controlled by a speed profile fed to the control system of the variable frequency drive. As a result, the frequencies did not deviate more than $\pm 0.2\,Hz$ from observation. The speed profiles were also accurate in that the linear portions were in fact constant acceleration sections and the undulating speed profile followed an exact sinusoid.

4.5.1 Test 1

In test 1, the linear ramp-up occurred over 30 seconds. Based on this relatively slow acceleration, a 20 second extract was taken and the waveform is found below. Impulsiveness is evident in the figure however the complexity of the signal with two distinct gearmesh frequencies must be further processed much like the constant speed analysis to reveal the fault.

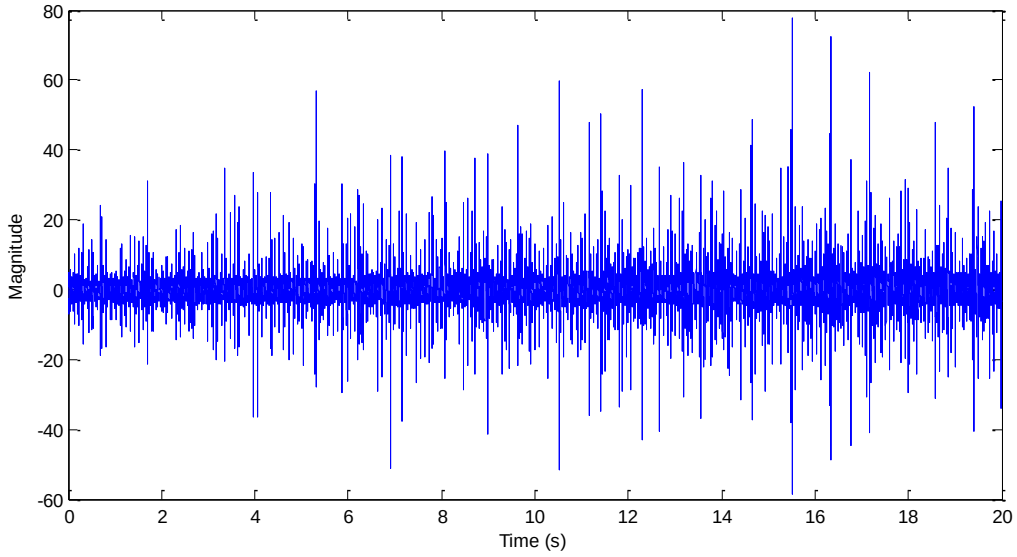

The raw spectrum of the data (below) reveals smearing and therefore cannot be used to find useful information. The post-processing techniques outlined in Section 3.5 must be applied.

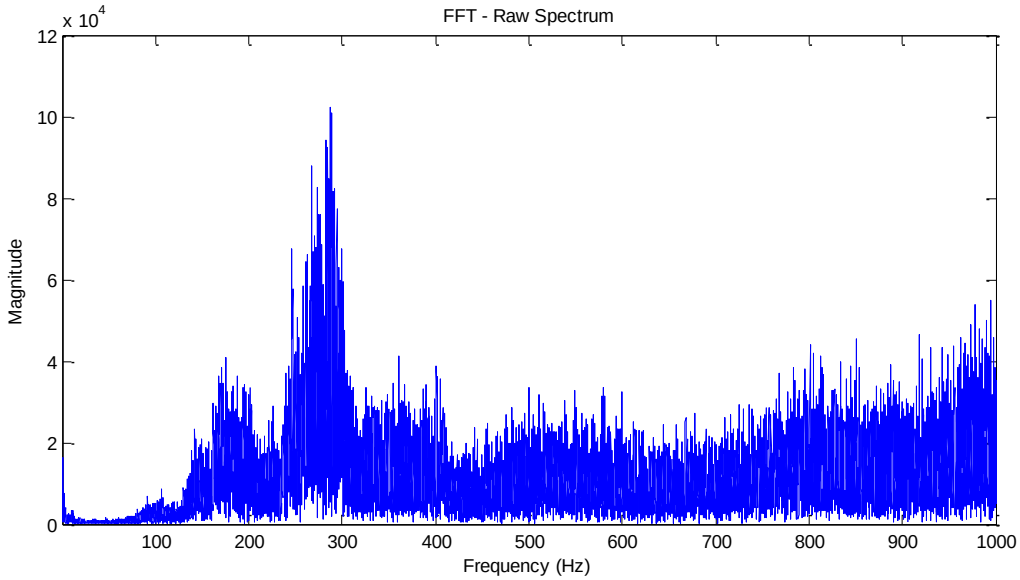

Figure 62: Raw spectrum of variable speed

The effect of electromagnetic interference was previously explored by Fan in [31] on this test rig. Unlike the spur gearbox spectrum at variable speed, there are no harmonics of supply frequency as this rig was modified such that wiring was shielded to prevent electromagnetic interference. The PSD revealed the same resonance peak (from Figure 60) that was used for filtering. This was followed by order tracking and then DRS to allow envelope analysis. The following figure reveals the envelope spectrum for variable speed.

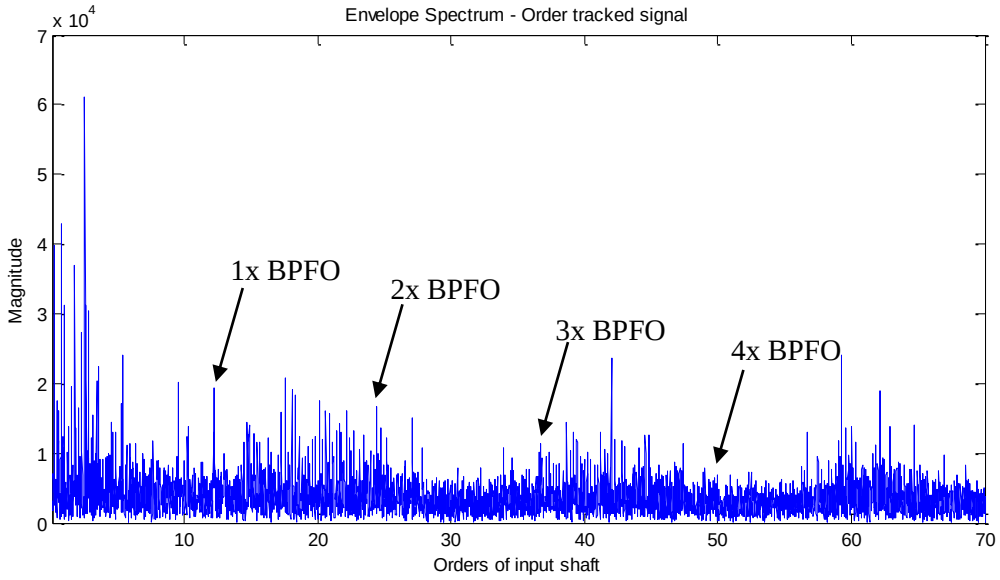

Figure 63: Envelope spectrum with bandpass filtering at variable speed (test 1)

The envelope spectrum is much less revealing with the same band used for the constant speed section. Other possible resonance peaks were explored in the PSD and checked for a clearer indication of the bearing fault but none yielded better results. There are a few factors that may be affecting the ability to detect the fault. The extract of the ramp was closer to the beginning of the ramp with a load of approximately $40\ N.m$ as opposed to the end where the load experienced increased to $60\ N.m$. The load was discussed to be an important factor in the ability to detect a fault as the absence of a load may cause the rolling elements to not interact with the fault. Using the last 20 seconds of the ramp with the same frequency band used above revealed the following:

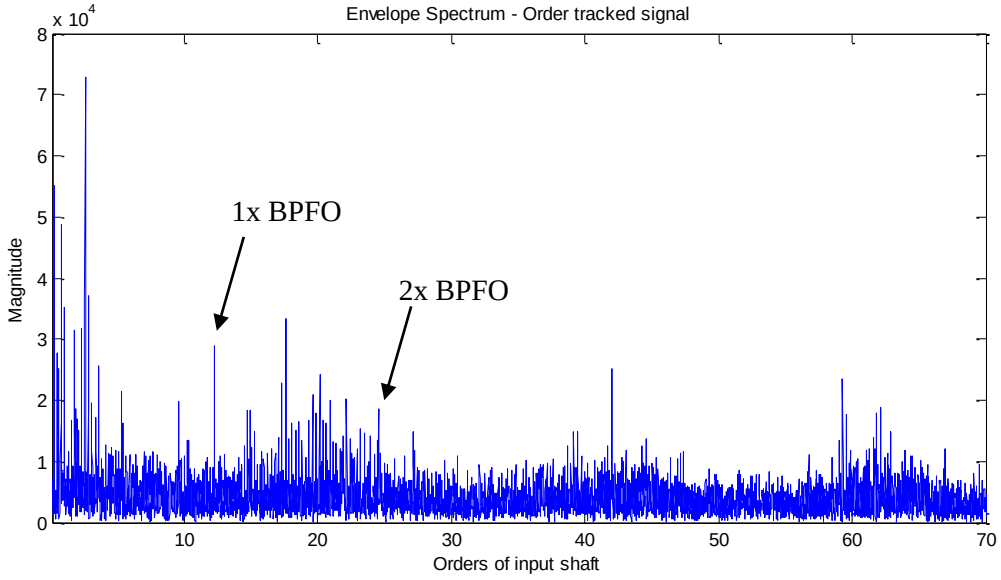

Figure 64: Envelope spectrum with bandpass filtering at variable speed (test 1, higher load section)

The result is a clearer first harmonic of BPFO with the presence of sidebands. This confirms the importance of the load in the diagnosis however the higher harmonics were not affected.

4.5.2 Test 2

The second test that was carried out featured a higher acceleration in the ramp-up portion of the signal. The same analysis was carried out to establish a clear envelope spectrum. A narrower resonance peak was found in the same frequency range from the PSD that was used for bandpass filtering. The resulting envelope spectrum is found below.

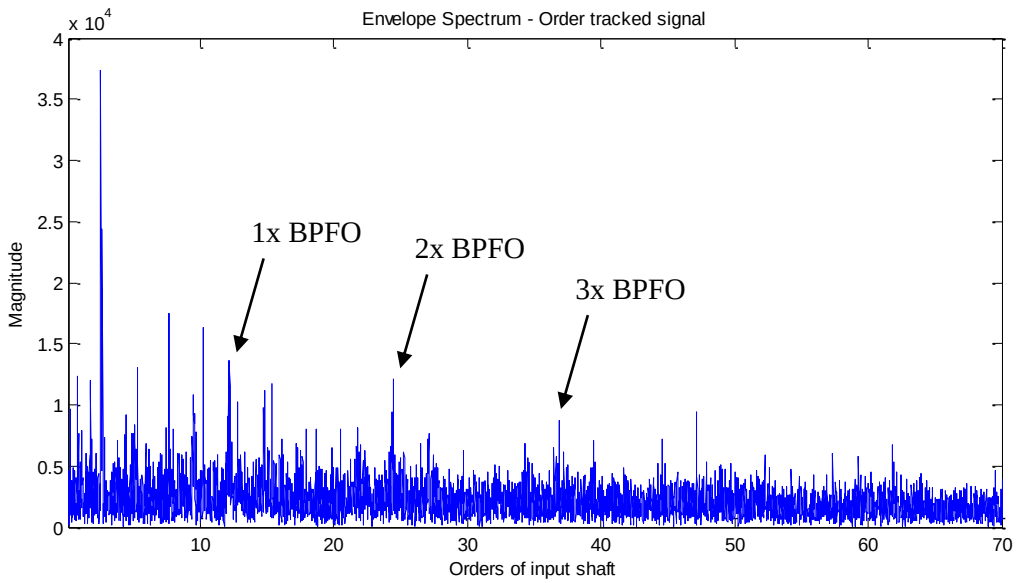

Figure 65: Envelope spectrum with bandpass filtering at variable speed (test 2)

The result of using the last 10 seconds of the ramp-up portion of the signal resulted in indications of BPFO as shown in the figure above. The more prominent peaks are harmonics of the output shaft in orders of input shaft speed. It appears in this test the harmonics of BPFO are more clear but do not have the presence of sidebands. The harmonics of output shaft speed are more dominating in this spectrum. The final test covers non-linear changes in speed to determine the suitability of the techniques further.

4.5.3 Test 3

The final test carried out features a sinusoidal change in input shaft frequency as seen by the frequency profile in Section 3.4.3. The load condition was such that at the highest frequency achieved during the test resulted in 60 $N.m$ experienced. The extracted portion of the signal was from the lowest to highest point of the cycle to feature a range of accelerations. The resulting waveform is shown below:

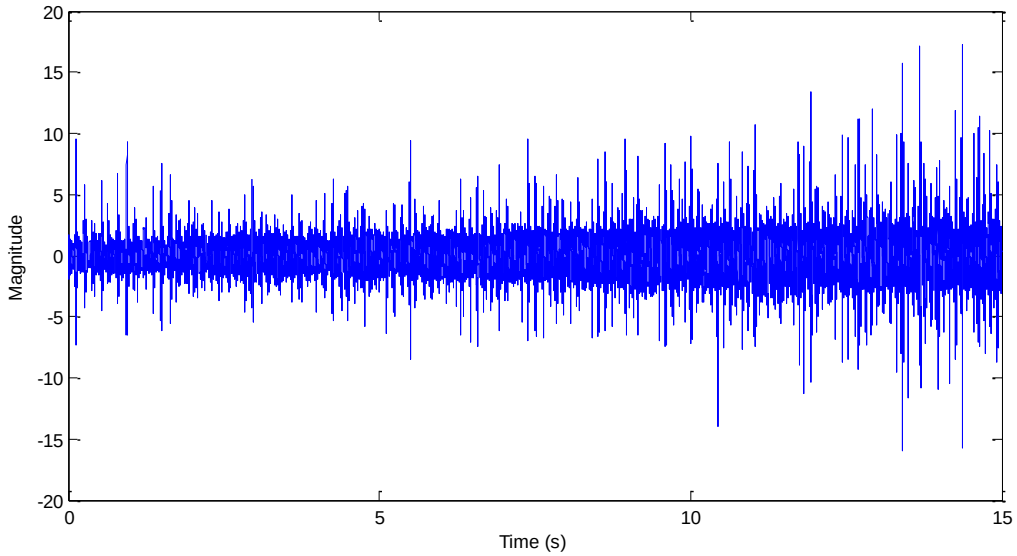

Figure 66: Waveform of variable speed during varying acceleration

The PSD revealed the same resonance peak in the range of $49\,kHz$ that was used for bandpass filtering. This was found to be the second most impulsive band in FK (both shown below).

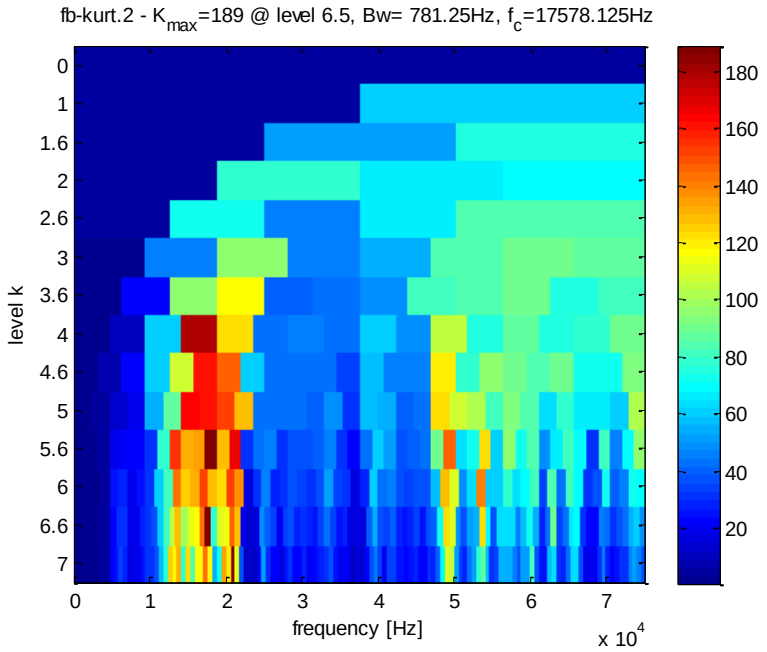

Figure 67: FK of variable speed during varying acceleration

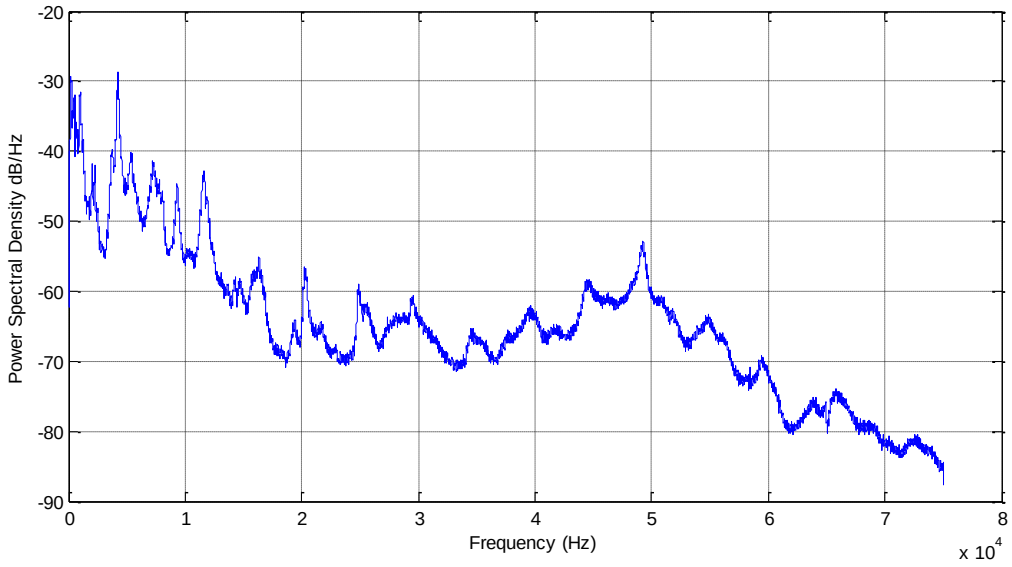

Figure 68: PSD of variable speed data during varying acceleration

The most impulsive band (as indicated by the FK) was at 17.5 kHz. Both these bands were investigated and resulted in the following envelope spectra:

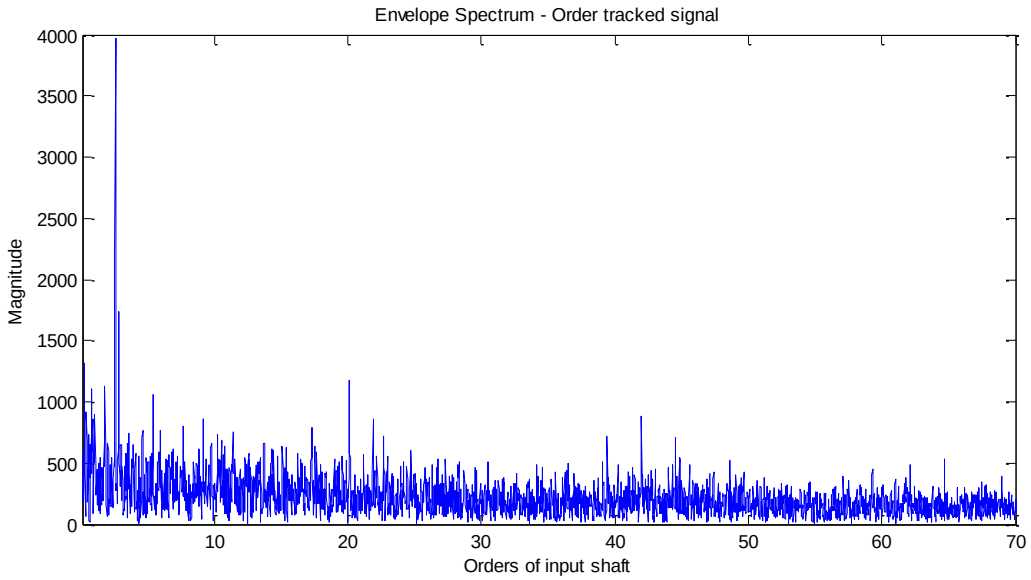

Figure 69: Envelope spectrum with bandpass filtering ($f_c = 17.5\ kHz$)

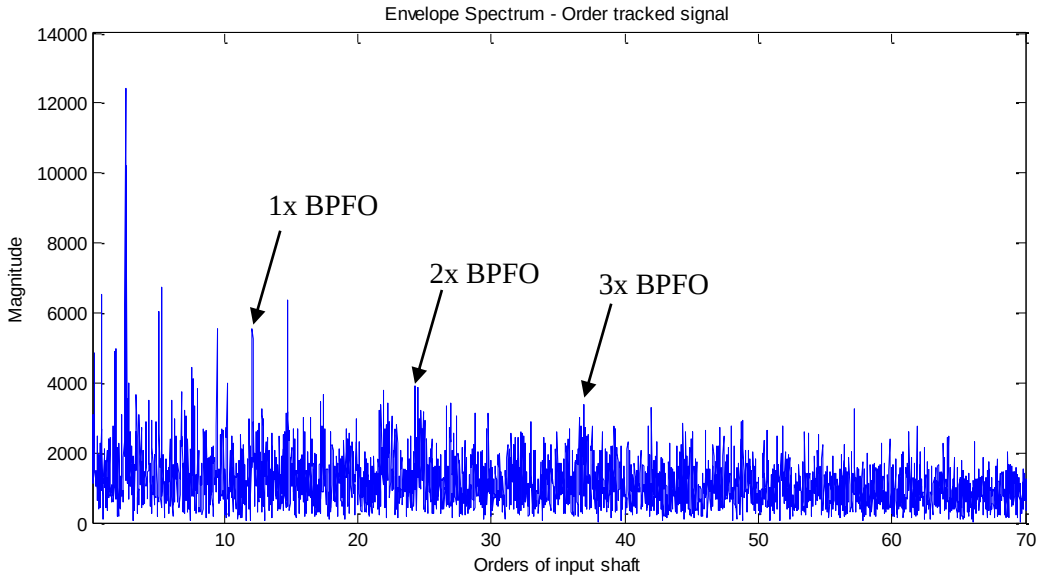

Figure 70: Envelope spectrum with bandpass filtering ($f_c = 49\ kHz$)

The band found by FK revealed no fault while the second most impulsive band revealed some indication of BPFO. The first harmonic of BPFO had sidebands at output shaft ratio in orders of input shaft speed however the higher harmonics of BPFO were not quite as prominent. The same analysis was carried out for a deceleration case from highest to lowest input shaft frequency as the load drop would have affect the result based on previous findings. The waveform can be seen below and decreases in magnitude with time.

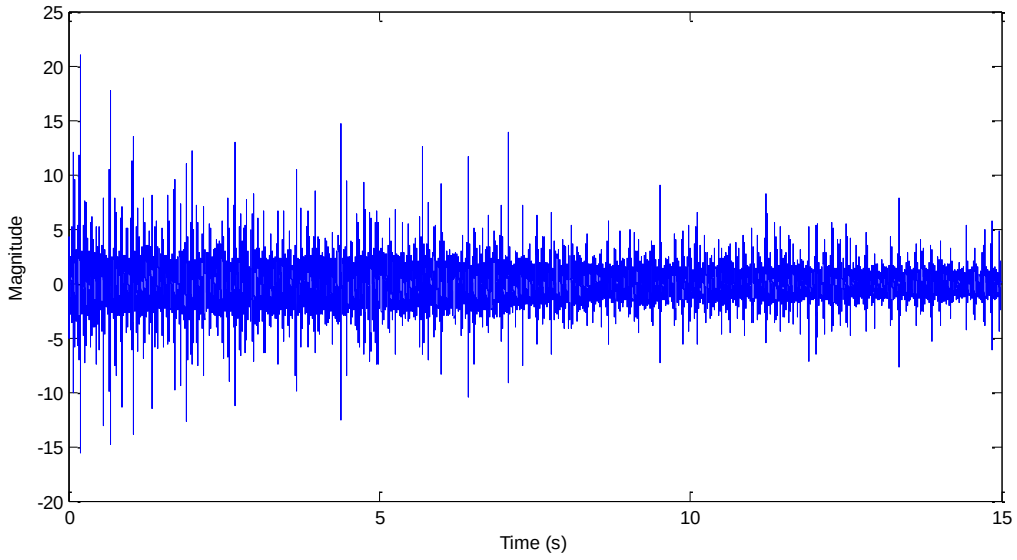

Figure 71: Waveform of variable speed during varying deceleration

FK and the PSD (shown below) revealed slight differences from the acceleration case.

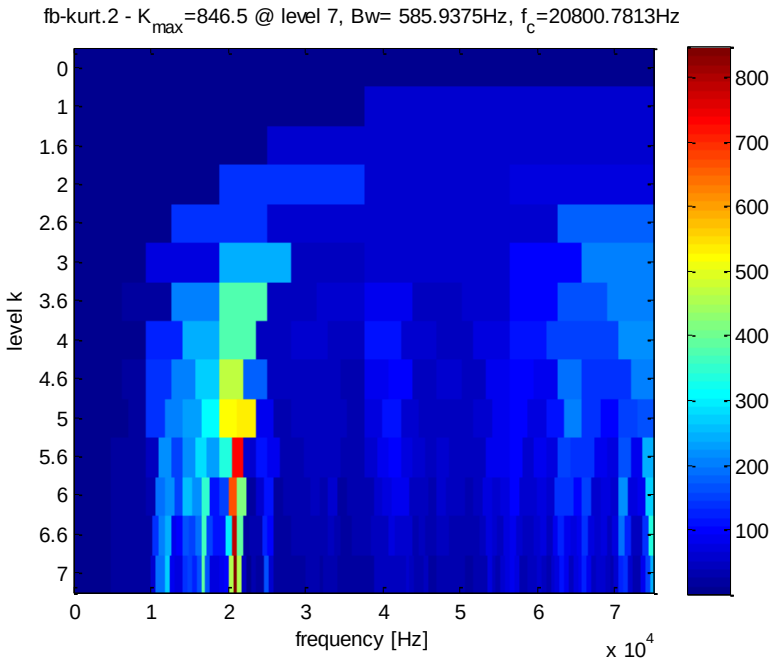

Figure 72: FK of variable speed during deceleration

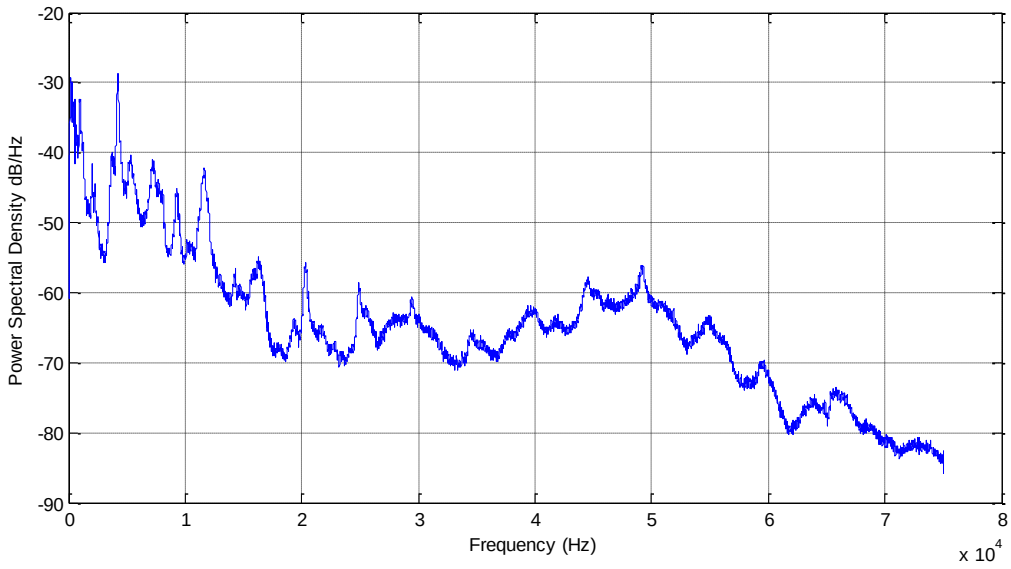

Figure 73: PSD of variable speed during deceleration

The most impulsive band found by FK is now at $f_c = 20.8\,kHz$ and the resonance peak previously used at $f_c = 49\,kHz$ is still present. These were both used to conduct envelope analysis and are found below.

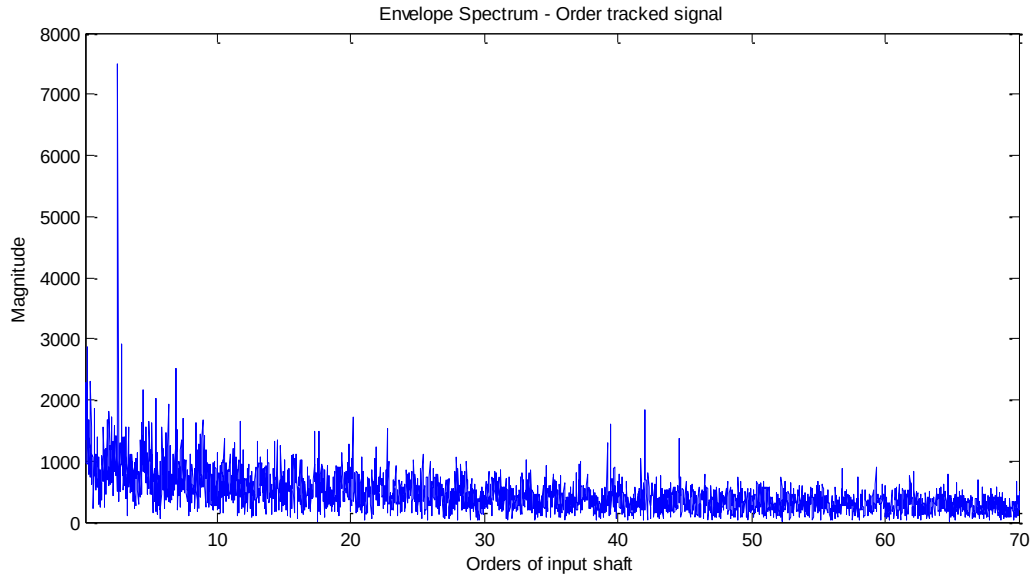

Figure 74: Envelope spectrum with bandpass filtering ($f_c = 20.8\ kHz$)

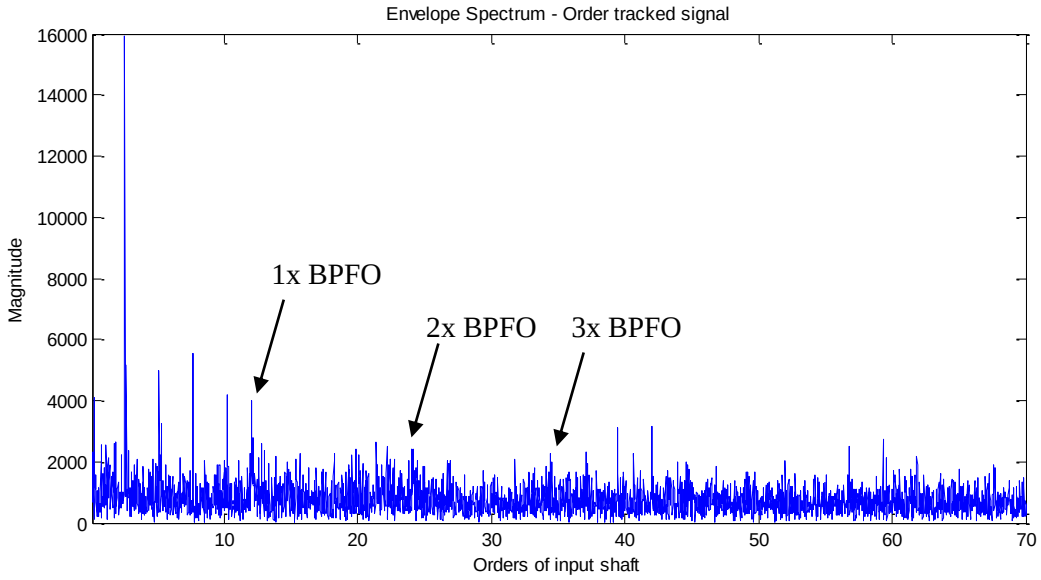

Figure 75: Envelope spectrum with bandpass filtering ($f_c = 49\ kHz$)

FK once again identified an impulsive band that was not caused by the bearing fault but rather some other component in the rig, therefore the resonance peak was one not excited by the bearing fault. Manual selection of the resonance peak from the PSD proved more successful than FK however only the first harmonic of BPFO was evident, with the more prominent peaks being harmonics of output shaft speed. The deceleration resulted in a large reduction in the load experienced on the bearings and could explain the drop off in magnitude seen in the envelope spectrum. The results found in this section are further discussed in the next section.

4.6 Discussion of Planetary Gearbox

It was observed on the torque indicator that the load experienced at the maximum frequency was higher when preceded by an acceleration from a lower frequency as opposed to decelerating from the point of maximum frequency down to lower frequencies. The load experienced was found to play a critical role in the ability to detect the bearing fault as seen by the ramp-up comparison and the acceleration and deceleration sections of the sinusoidal frequency variations. The harmonics of BPFO were always more obvious when more load was being applied on the bearing. Harmonics of output shaft speed in orders of input shaft speed were consistently found in the envelope spectra, which may indicate resonance was occurring from components associated with the output shaft. While $60\ N.m$ was close to the maximum load that could be applied using this experimental rig ($75\ N.m$ maximum), there exists the possibility that the torque indicator drifted over time since it was last calibrated and therefore be displaying incorrect load magnitudes for the experiments. The actual load applied may have been much lower than indicated.

The comparison between the Fast Kurtogram and PSD clearly showed the limited use of FK in this application. The impulsive band found was never successful in revealing the bearing fault. As stated by Antoni in [33], the most serious limitation of the kurtogram is that the technique is not able to identify whether the signal impulsivity is from a series of transients or, say, an isolated event. He continues to say that the value of kurtosis decreases as the repetition of a transient signal increases and the kurtogram is sensitive to impulsive noise which can cause misleading interpretations. This was certainly the case found in the two experiments carried out in this thesis.

The size of the fault used in this experiment was considered relatively large, however it was still difficult to gain a clear signal in the envelope spectrum under variable speed conditions. This may have been due to a smaller than expected load as previously stated, however if this was not the case, further testing would be required to determine the deterioration rate of a bearing with such a fault size as the difficulty of the diagnosis was evident in this case. Needless to say, bearing faults of a smaller size may have gone undetected in the same conditions and therefore a change in the diagnostic procedure used in this thesis may be required.

The external placement of the accelerometer in this experiment may also be limiting the ability of the sensor to pick up on the clear impulses generated from the bearing fault and therefore require the use of fault signal enhancement, such as MED. The transmission path of the signal may be causing distortion such that FK and PSD are not giving clear impulsive bands and results in the inability to select an appropriate band for filtering.

The diagnosis under constant speed was a confident one, as compared to the spur gearbox, since there was clear evidence of BPFO which was nowhere close to a harmonic of supply frequency, and more importantly, the sidebands provided evidence of modulation at the planet gear frequency relative to the carrier frequency ratio. This consideration was not found in the spur gearbox and solidifies the diagnosis for this gearbox.

Based on the successful result of the constant speed data, but the inability to obtain a clear signal under variable speed conditions, it can be said that provided there is sufficient load on the bearing and the accelerometer placement is such that the ability of the sensor to pick up the impulses from the fault is maximised, the diagnostic methods used for variable speed diagnosis were successful. Bandpass filtering is to be used as the first step, using FK or PSD, knowing that FK could have limited use and should be compared with the PSD, followed by order tracking to remove speed fluctuations, DRS and finally envelope analysis. In conditions where it is likely the transmission path is distorting the vibration signal, MED could be implemented as an extra step to maximise the chance of a successful diagnosis.

The next chapter summarises the results and analysis of the thesis and is followed by future work to be carried out to continue expanding the field of diagnostics under variable speed.

Chapter 5: Conclusion

The aim of this thesis was to expand the use of available techniques developed for rolling element bearings under variable speed conditions to establish reliable techniques that can be used under these conditions. This was done by the use of two different experimental rigs; a spur and planetary gearbox. A number of classic techniques were used and compared over a range of different speed profiles to determine their suitability in each experiment. Order tracking, Time Synchronous Averaging on the spur gearbox, Discrete/Random Separation on the planetary gearbox, Fast Kurtogram, Power Spectral Density and envelope analysis were used together in specific order to ascertain the known bearing faults in the test rigs.

The spur gearbox did not yield clear results and a case was made that electromagnetic interference played a role in the inability to find the fault using envelope analysis. Concurrently, the absence of sidebands at the expected modulation frequency also gave an indication that the resulting peaks in the envelope analysis were a result of something other than the bearing fault. The addition of a defective gear increased the complexity of the vibration signal however the use of TSA as a separation technique worked well to remove gear frequencies and did not hinder the process of finding the defective bearing, despite not successfully diagnosing the fault. The use of the Fast Kurtogram proved to be limited and did not provide a clear diagnosis in any of the studied cases. Rather, PSDs were used to locate resonance peaks for bandpass filtering. Finally, the relatively low load experienced by the bearing may have resulted in the rolling elements to never interact with the fault as there does exist a small amount of clearance from the rolling elements and inner/outer races.

The planetary gearbox experiment produced a successful result at constant speed, where clear indications of the bearing fault frequency were found along with sidebands at the expected modulation frequency. The Fast Kurtogram once again proved limited in use, with the technique never successfully providing an appropriate frequency band for filtering. The use of PSD was required to locate clear resonance peaks for filtering. The variable speed analysis of the experimental data proved to work well, despite the reduced clarity of the fault as compared to constant speed. This was attributed to the lower loads experienced at changing speeds and the possibility of incorrect load indications. The variable speed analysis procedure worked well and recommendations were made to improve the likelihood of a successful diagnosis.

Chapter 6: Future Work

Based on the results obtained in this thesis, there are a number of avenues to continue for testing with variable speed to further develop useful diagnostic techniques and procedures. This section discusses the future work that can be carried out to continue contributing to this field of research.

The spur gearbox breakdown prevented further testing as well as obtaining baseline data, therefore the first course of action with this experimental rig would be to carry out testing with no faults present to obtain a set of baseline data at various constant speeds and with variable speed profiles similar to the profiles used in this thesis. While the use of the potentiometer was acceptable and may have more closely resembled speed changes in normal gearboxes, it would be beneficial to have a setup much like the planetary gearbox where a voltage signal can be fed to the VFD for accurate speed profile and timing. The use of a larger outer race fault as compared to the $0.8\,mm$ inner race fault used could provide a clear differentiator from BPFI since this fault frequency was close to the supply frequency.

The outer race bearing fault used in the planetary gearbox experiment (at $1.6\,mm$) was sufficiently large and the gearbox featured no defective gears. However, the fault was not as clear as expected. A case was made that there was potential drift in the load indicator and therefore this would have to be addressed before further tests can be carried out. The next course of action would be to determine if smaller faults would be diagnosable in different conditions (speed and load) by incrementally reducing the bearing fault size from $1.6\,mm$ to $0.4\,mm$. The same speed profiles could be used to find the trend and determine the minimum fault size that can be found. This can also be done for an inner race fault with the same speed and loading conditions. Gear signals tend to mask bearing faults, therefore, the introduction of gear faults in the gearbox can be used to complicate the signal further. The suitability of the same techniques can be tested in new and more complex conditions. This would allow the determination of more robust diagnostic methods as industrial applications tend to be more complicated to analyse, whether because the signals may contain more noise or because of the inability to place sensors in key locations, reducing the impulsiveness found in a vibration signal as a result of the transmission path.

While the above are suggestions for experimental work, the area of analysis requiring improvement is band selection. The FK was a major problem encountered throughout the thesis for band selection. Future work in the analysis should target this shortfall by perhaps developing the use of spectral correlation as it is claimed to be a more efficient tool for detecting the presence of repetitive transients within a signal [33], or improve the Kurtogram to address its shortcomings. The development of a revised Kurtogram that imposes a repetitive structure on the pulses from the bearing fault would address this issue (which is being tackled to some extent at present by Antoni in [33]). Further work could also incorporate the use of fault signal enhancement such as MED to determine the extent to which band selection is essential before being able to find the bearing fault.

References

[1] R. B. Randall, *Vibration-based Condition Monitoring: Industrial, Aerospace and Automotive Applications*: John Wiley and Sons Ltd, 2011.

[2] R. G. Budynas and J. K. Nisbett, *Shigley's Mechanical Engineering Design*, 10 ed.: McGraw Hill Education, 2015.

[3] LionPrecision. (2012, 10/04/2016). *Spindle Measurement: RPM and Bandwidth*. Available: http://www.lionprecision.com/tech-library/technotes/cap-0033-SEA-RPMvsBandwidth.html

[4] S. A. McInerny and Y. Dai, "Basic Vibration Signal Processing for Bearing Fault Detection," *IEEE Transactions on Education,* vol. 46, pp. 149-156, 2003.

[5] V. N. Patel, N. Tandon, and R. K. Pandey, "Experimental Study for Vibration Behaviors of Locally Defective Deep Groove Ball Bearings under Dynamic Radial Load," *Advances in Acoustics and Vibration,* vol. 2014, p. 7, 2014.

[6] N. Tandon and A. Choudhury, "A Review of Vibration and Acoustic Measurement Methods for the Detection of Defects in Rolling Element Bearings," *Tribology International,* pp. 469-480, 1999.

[7] R. Ahmad and S. Kamaruddin, "An Overview of Time-Based and Condition-Based Maintenance In Industrial Application," *Computers & Industrial Engineering,* vol. 63, pp. 135-149, 2012.

[8] W. S. Siew, W. A. Smith, Z. Peng, and R. B. Randall, "Fault Severity Trending In Rolling Element Bearings," presented at the Acoustics 2015 Hunter Valley, 2015.

[9] S. Patidar and P. K. Soni, "An Overview on Vibration Analysis Techniques for the Diagnosis of Rolling Element Bearing Faults," *International Journal of Engineering Trends and Technology,* vol. 4, pp. 1804-1809, 2013.

[10] D.-H. Kwak, D.-H. Lee, J.-H. Ahn, and B.-H. Koh, "Fault Detection of Roller-Bearings Using Signal Processing and Optimization Algorithms," *Sensors,* pp. 283-298, 2013.

[11] R. B. Randall and J. Antoni, "Rolling element bearing diagnostics - A tutorial," *Mechanical Systems and Signal Processing,* pp. 485-520, 2011.

[12] H. Li, Y. Zhang, and H. Zheng, "Bearing fault detection and diagnosis based on order tracking and Teager-Huang transform," *Journal of Mechanical Science and Technology,* vol. 24, pp. 811-822, 2010.

[13] P. Borghesani, P. Pennacchi, R. B. Randall, and R. Ricci, "Order tracking for discrete-random separation in variable speed conditions," *Mechanical Systems and Signal Processing,* pp. 1-22, 2012.

[14] C. J. Stander and P. S. Heyns, "Transmission path phase compensation for gear monitoring under fluctuating load conditions," *Mechanical Systems and Signal Processing,* pp. 1511-1522, 2006.

[15] D. Ho and R. B. Randall, "Effects of time delay, order of FIR filter and convergence factor on self adaptive noise cancellation," presented at the Fifth International Congress on Sound and Vibration, Adelaide, South Australia, 1997.

[16] J. Antoni and R. B. Randall, "Unsupervised noise cancellation for vibration signals: part I - evaluation of adaptive algorithms," *Mechanical Systems and Signal Processing,* pp. 89-101, 2004.

[17] J. Antoni and R. B. Randall, "Unsupervised noise cancellation for vibration signals: part II - a novel frequency-domain algorithm," *Mechanical Systems and Signal Processing,* pp. 103-117, 2004.

[18] N. Sawalhi and R. B. Randall, "The Application of Spectral Kurtosis to Bearing Diagnostics," presented at the Proceedings of ACOUSTICS 2004, Gold Coast, Australia, 2004.
[19] J. Antoni and R. B. Randall, "The spectral kurtosis: application to the vibratory surveillance and diagnostics of rotating machines," *Mechanical Systems and Signal Processing*, vol. 2006, pp. 308-331, 2004.
[20] C. Ruiz-Carcel, E. Hernani-Ros, Y. Cao, and D. Mba, "Use of Spectral Kurtosis for Improving Signal to Noise Ratio of Acoustic Emission Signal from Defective Bearings," *Journal of Failure Analysis and Prevention*, pp. 363-371, 2014.
[21] J. Antoni, "Fast computation of the kurtogram for the detection of transient faults," *Mechanical Systems and Signal Processing*, vol. 21, pp. 108-124, 2005.
[22] Y. Lei, J. Lin, Z. He, and Y. Zi, "Application of an improved kurtogram method for fault diagnosis of rolling element bearings," *Mechanical Systems and Signal Processing*, vol. 2011, pp. 1738-1749, 2011.
[23] Y. Lei, J. Lin, M. J. Zuo, and Z. He, "Condition monitoring and fault diagnosis of planetary gearboxes: A review," *Measurement*, vol. 2014, pp. 292-305, 2013.
[24] W. A. Simith, Z. Fan, Z. Peng, H. Li, and R. B. Randall, "Optimised Spectral Kurtosis for bearing diagnostics under electromagnetic interference," *Mechanical Systems and Signal Processing*, vol. 2016, pp. 371-394, 2015.
[25] D. Zhao, J. Li, and W. Cheng, "Feature Extraction of Faulty Rolling Element Bearing under Variable Rotational Speed and Gear Interferences Conditions," *Shock and Vibration*, vol. 2015, 2015.
[26] J. Urbanek, T. Barszcz, and J. Antoni, "Time-frequency approach to extraction of selected second-order cyclostationary vibration components for varying operational conditions," *Measurement*, vol. 2013, pp. 1454-1463, 2013.
[27] R. Randall, W. Smith, and M. Coats, "Bearing diagnostics under widely varying speed conditions," n.d.
[28] N. Sawalhi and R. B. Randall, "Semi-Automated Bearing Diagnostics - Three Case Studies," presented at the COMADEM 2007, Portugal, 2007.
[29] P. Borghesani, R. Ricci, S. Chatterton, and P. Pennacchi, "A new procedure for using envelope analysis for rolling element bearing diagnostics in variable operating conditions," *Mechanical Systems and Signal Processing*, vol. 2013, pp. 23-25, 2013.
[30] R. Randall and W. Smith, "Use of the Teager Kaiser Energy Operator to estimate machine speed," presented at the European Conference of the Prognostics and Health Management Society 2014, Europe, 2014.
[31] Z. Fan, "Vibration-based condition monitoring in planetary gearbox via using an internal sensor," Master of Engineering, School of Mechanical & Manufacturing Engineering, The University of New South Wales, Sydney, 2015.
[32] K. H. Grote and E. K. Antonsson, *Springer Handbook of Mechanical Engineering*: Springer, 2009.
[33] J. Antoni, "The infogram: Entropic evidence of the signature of repetitive transients," *Mechanical Systems and Signal Processing*, vol. 74, pp. 73-94, 6/1/ 2016.

Appendix

The formulas used in the body of this thesis for gear ratio calculations were from [32]. The remaining gear ratio formulas can be found below also from [32].

Carrier frequency

$$f_c = f_{input}\left(-\frac{N_{PIN}}{N_{SPU}}\right)$$

Absolute planet frequency

$$f_p = f_c\left(1 - \frac{N_R}{N_P}\right)$$

Planet frequency relative to carrier

$$f_{p/c} = f_c\left(-\frac{N_R}{N_P}\right)$$

Absolute sun frequency

$$f_s = f_c\left(\frac{N_R}{N_S} + 1\right)$$

Sun frequency relative to carrier

$$f_{s/c} = f_c\left(\frac{N_R}{N_S}\right)$$

Spur gear mesh frequency

$$SGMF = f_{input} \times N_{PIN}$$

Ring gear mesh frequency

$$RGMF = f_c \times N_R$$

Planet pass frequency

$$PPF = f_c \times n$$